MODELING OF WIND INDUCED FATIGUE OF THIN-WALLED FOLDED PLATES

Osvaldo Rosario Galanes

A thesis submitted in partial fulfillment of the requirements for the degree of

MASTER OF SCIENCE
in
CIVIL ENGINEERING

UNIVERSITY OF PUERTO RICO
MAYAGÜEZ CAMPUS
2011

Approved by:

Luis A. Godoy, PhD President, Graduate Committee	Date
Ricardo R. López, PhD Member, Graduate Committee	Date
Ali Saffar, PhD Member, Graduate Committee	Date
Néstor Pérez, PhD Representative of Graduate Studies	Date
Ismael Pagán Trinidad, M.S. Chairperson of the Department	Date

Abstract

During high wind events thin-walled folded plates such as roof claddings suffer extensive damage due to fatigue failure at their screwed connections. Currently, damage prediction is based on fragility curves and semi-empirical models where there is no direct relation between loads and failure parameters. In this research a finite element model and fatigue criteria were validated in correlating a wind loading protocol to a specific fatigue failure mechanism. The 3D fatigue process was reduced to a one-dimensional problem by using one or two strain and stress parameters from the finite element model. These parameters were used on a fatigue stress-based and strain-based criteria to establish a fatigue failure mechanism. The fatigue life, and crack directions were predicted as a function of loading parameters and specific cladding configuration. As a result a roofing assembly can be evaluated and rated to withstand a specific wind resistance according to a specific loading protocol.

Resumen

Los techos y cubiertas de placas de pared delgada de lámina metálica sufren daños considerables debido a fallas por fatiga en las conexiones atornilladas durante eventos de viento. Actualmente la predicción de daño está basada en curvas de fragilidad y modelos semi empíricos en donde no existe una relación directa entre carga y parámetros de falla. En esta investigación se validó un modelo de elementos finitos y un criterio de fatiga que correlacionan un protocolo de cargas de viento a un mecanismo de falla por fatiga. El proceso tridimensional se redujo a un problema unidimensional utilizando uno o dos parámetros de esfuerzo y deformación del modelo de elementos finitos. Estos parámetros se usaron en un criterio de fatiga basado en esfuerzos y deformaciones para establecer un mecanismo de daño por fatiga. La vida de fatiga y las direcciones de propagación de las grietas se predijeron en función de los parámetros de carga y la configuración especifica estudiada. Como resultado una cubierta de techo puede ser evaluada y calificada para resistir una carga de viento en específico de acuerdo a un protocolo de carga.

Acknowledgments

In first place I want to thank my advisor, Dr. Luis A. Godoy, for inspiring me to see beyond the purely academic limits of the classroom into the art of visualizing reality through the mathematical equations that give a perfect physical meaning to our world. I also want to thank Dr. Ricardo López and Dr. Ali Saffar for guiding me throughout the process and getting me closer to achieving my goal. Dr. Marcelo Suárez also recommended important references for this research. Finally I am very grateful to my family and special people that supported me throughout this investigation. Ultimately I am grateful to God for all of my achievements and all of the great minds that motivated me to keep thinking.

Table of Contents

List of Tables

List of Figures

List of Appendices

List of Symbols

$[H]$ strain-curvature compatibility matrix

$[J]$ Jacobian matrix

$[k]$ element stiffness matrix

$[\mu]$ matrix of directional cosines

b fatigue strength exponent

B spatial derivative of field variable

c fatigue ductility exponent

d distance from edge of screw hole

E modulus of elasticity

e percentage of error

F fatigue damage

h element size

N shape function

N_f number of cycles to failure

N_M number of cycles to failure as defined by Morrow

N_G number of cycles to failure as defined by Goodman

N_{SWT} number of cycles to failure as defined by Smith, Watson and Topper

n number of cycles

O order of error

P wind load

$P_{\max}$ previously applied maximum load

$P_{\min}$ minimum sublevel load

$P_{sub\max}$ maximum sublevel load

R ratio of minimum stress to maximum stress

s sample standard deviation

u, v, w displacements

α, β nodal rotational degrees of freedom

γ shear strain

ε normal strain

ε_a strain amplitude

$\varepsilon_{\max}$ maximum principal strain

ε_y yield strain

ε'_f fatigue ductility coefficient

$\Delta\varepsilon_{eq}$ equivalent strain range

$\Delta\varepsilon_{\max}$ maximum principal strain range

μ sample mean

σ_a stress amplitude

σ_m mean stress

$\sigma_{\max}$ maximum stress

$\sigma_{\max\, p}$ maximum principal stress

$\sigma_{\max\, prev}$ maximum previously applied maximum stress

σ_u ultimate tensile strength

σ'_f fatigue strength coefficient

ν Poisson’s ratio

ϕ field quantity

ξ, η, ζ element local coordinates

Chapter 1: Introduction

1.1 Motivation

The need to understand wind damage induced failure on roof cladding systems has come a long way since the advent of new materials and building practices. The recent development of more durable high resistance thin walled structural components imposes a challenge in the design of structures for high winds. It is necessary that thin walled structures are designed to withstand the impact that such events can cause as huge economical losses have been reported throughout the industry. Knowledge of how these structural components fail during high wind events will provide new insights on how to design more efficiently and as a result minimize damage and economical losses as well as provide a sense of security.

There are several reasons that support further investigation on the behavior of these thin walled structural components during damaging wind storms. The first aspect is the difficulty in determining load fluctuations in time associated with these events. Although this research is not centered in determining loading variations in history, the nature of the load can significantly contribute to the complexity of the problem. Other challenges can arise if non-linear effects are considered on the static model. Once stress and strain components are determined from the static model, a new challenge arises in establishing successful fatigue criteria. There are further complications if one considers the phenomenon of three-dimensional fatigue and the wide margin of error attributable in making accurate predictions on the fatigue life. All of these factors introduce significant difficulties that establish a need to better understand the process associated with fatigue failure of thin walled structural components.

Although recent investigations have attempted to correlate static loading on steel claddings to wind induced failure, there is still a need to find a successful fatigue criterion that takes into account load fluctuations and cladding resistance to fatigue damage, based on analysis and understanding of the principles of stress and strain prediction as well as fatigue life. Knowledge of fatigue fracture parameters of different kinds of steels is now available in order to predict fatigue failure based on previously established criteria. This knowledge can be used in conjunction with finite element modeling and analysis of the stresses caused by the applied pressures and forces in order to predict capacity and hence failure.

1.2 Significance of the Present Study

Thin-walled roof claddings and structural components suffer the most when exposed to high winds due to their low weight to area ratio. The difference in pressure caused by wind can impose significant reaction loads on their screwed connections, causing high stress concentrations around them. Since industrial structures made out of these components are generally of low cost as compared to other building types, they often present deficiencies in design, which then imposes an imminent threat during wind events that occur mainly on tropical regions. Flying pieces of roof cladding can pose a threat to nearby property, as has been the case in numerous storms and hurricanes in the past.

As new insight is gained from the fatigue behavior of these structural components due to wind, previously established fatigue criteria can be used to predict and prevent failure of these systems. The present research attempts to correlate fatigue criteria to wind induced fatigue damage of thin walled steel components by linking current knowledge about fatigue failure and its application to thin walled steel claddings.

1.3 Scope of the Research

This investigation is limited to the behavior of thin-walled folded plates under fluctuating lateral loads. A specific geometric configuration of trapezoidal steel claddings is considered in this thesis, in which stress concentrations are considered in a localized zone. Other geometric configurations are not considered as the fatigue process is assumed to take place within a small, localized region. The research is only based on computational modeling and not on full-scale experimental studies, but results obtained have been compared to experimental results obtained by previous investigators in order to validate the analytical model. The present modeling employs a shell finite element in which elastic as well as plastic deformations are considered. From the finite element results, the analysis of multiaxial constitutive parameters aid in reducing the multiaxial state of stress and strain from a three dimensional fatigue problem into a one or two dimensional problem. Evaluation of fatigue criteria focuses on low-cycle fatigue and on criteria were fatigue parameters are already established for different kinds of steels. Out of all the possible loading configurations attributable to wind, a specific loading protocol is used to establish damage parameters caused by fatigue failure.

1.4 Objectives

The primary goal of this research is to provide a plausible explanation for describing the failure mechanism of thin-walled folded plates caused by fatigue damage associated to wind fluctuations. In order to achieve this goal, several specific objectives are proposed in this research:

1. To develop a two-scale model to evaluate stress fields in the local area of the connections in a folded plate under static lateral pressures.
2. To identify appropriate existing fatigue models to represent 3-D fatigue processes in thin-walled components.
3. To implement existing loading protocols used in fatigue testing into fatigue analysis.
4. To provide explanations of fatigue mechanisms in folded plates based on computer modeling and parametric studies.

Chapter 2: Literature Review

2.1 Previous Publications

It is common to observe wind induced damage of roof and wall steel cladding systems in the tropics and other high wind prone regions. The Canadian Standards Association (2004) developed a standard test method for the dynamic wind uplift resistance of mechanically attached membrane-roofing systems. The test method employs a wind loading protocol based on design wind pressures in accordance with local building codes. The dynamic protocol has five rating levels (identified as A to E) to evaluate a roof assembly for a specific wind resistance. Each level consists of eight load sequences with different pressure ranges representing different wind conditions (Baskaran *et al.* 2006). The structure is then rated based on how many levels it is able to withstand before failing. Several investigators have implemented this sequence in the full-scale testing of cladding systems (Avilés 2006; García 2007; García 2008). Avilés (2006) proposed to modify the original Canadian loading protocol by multiplying the total number of cycles by five. The new SIDGERS-5 loading protocol would allow any given roofing assembly to be rated in terms of the original rating system but being able to withstand five times the damage.

Research has been made in order to predict fatigue failure damage in steel cladding systems using empirical methods and fragility curves (Lee and Rosowsky 2004; García 2007; García 2008). García (2007) performed a series of tests on wood-zinc components in order to obtain the performance of a wood-zinc structure with a specific configuration. In his research, he sampled a variety of common configurations throughout

Puerto Rico and evaluated each configuration in terms of wind speed performance. He then calculated the roof performance index defined as the ratio of resistance to capacity based on the damage of individual components. Fragility curves are then obtained by plotting the probability of exceeding a given damage state versus wind speed. Based on the studies performed by García (2007), a specific structure can be rated to withstand a specific level of performance based on how well it is constructed. A contribution of this research is evaluating the performance of wood-zinc structures based on wind speed and construction practices, and to prove that these kinds of structures are able to withstand hurricane force winds if properly constructed. García (2008) based his research on what is called Component Based Fragility. In this approach, the individual capacities of each connection on a structure are found and compared to individual demands. According to a specific wind speed, the percent of capacities that are not able to withstand the demands are then found and a structure is then rated based on a specific level of damage. The probability of exceeding a given level of damage is then plotted versus wind speed and fragility curves are obtained. The main difference from García (2007) is that García (2008) studied construction practices used mainly on industrial buildings. In his research he performed full-scale tests of structural components, which are most vulnerable on these kinds of buildings, namely roof and wall steel claddings. Among empirical methods, Avilés (2006) performed similar tests on steel claddings and plotted the load versus number of cycles on a logarithmic scale in order to obtain a relationship for the fatigue life equation.

Recent investigations in Australia have adopted analytical approaches using large-scale experimental models and finite element analysis models of cladding systems. Such investigations were successful in determining a strain criterion and design formula for static pull-through failures in crest-fixed steel claddings (Mahaarachchi and Mahendran 2008, 2009).

Although there is a wealth of information about wind induced failure of steel cladding systems, research is still needed to account for building practices in the US and Puerto Rico. Almost all analytical models dealing with steel cladding systems are aimed at Australian construction practices. The differences between Australian, European, and American construction practices has been highlighted as follows: "European and American recommendations for steel claddings cannot be used as compared with Australian steel claddings, they are made of thicker, deeper and softer steel cladding fastened at valleys while Australian steel claddings are commonly made of thin, high strength steel G550 and are crest-fixed" (Mahaarachchi and Mahendran 2009). A new approach is needed that considers valley-fixed steel claddings and fatigue loading in developing a working analytical model.

The process of fatigue failure of thin-wall folded plates is governed by several factors discussed earlier. Before treating the process of fatigue failure of thin-wall folded plates, which is mostly considered based on observations and for which an analytical basis is not fairly grounded in the literature, it is first necessary to understand the behavior under static load. The static load case is well documented. Observations and analytical models have described static failure. The static analysis of an industrial building should consider the structural component that is most vulnerable to fatigue damage. These components are the thin metal roof claddings (Morgan and Beck 1977). Other studies have shown that among these components, stress concentrations around the connections are responsible for low cycle fatigue failure (Beck and Stevens 1979), (Cook 1990), and Mahendran (1990a, b, 1995). An investigation of the static load case was made when "An inspection of steel roofs made of trapezoidal steel sheeting (Reardon and Mahendran 1988) has shown that roofing has been split in the transverse direction under the screw heads due to the over tightening of screw fasteners either accidentally or by poor workmanship." It is also postulated: "the splitting phenomenon does not depend on the fastener location and is essentially a localized effect" (Mahendran and Mahaarachchi 2004). In previous studies, Mahaarachchi and Mahendran (2000) showed that splitting starts when "the longitudinal membrane tensile strain is greater that 60% of the total tensile strain at the edge of the fastener holes, and the total tensile strain is equal to the measured failure strain from tensile coupon tests of steel." (Mahendran and Mahaarachchi 2004). Later studies (Mahaarachchi and Mahendran 2008) extensively evaluated the splitting resistance of steel claddings of different geometrical shapes and material properties and postulated a strain criterion based on their previous findings. A need for a strain criterion for the pull-through failure of steel claddings was made evident when "the finite element analyses could not predict the failure loads as elastic-perfect plastic material behavior with infinite ductility is assumed without any allowance for splitting since the local pull-through failures in the less ductile steel claddings are initiated by transverse splitting at the fastener hole." (Mahaarachchi and Mahendran 2008). This study also shows that although "tensile testing of steel coupons showed that it has very little strain hardening and failure strain is only about 2%," type B roofing sustained considerable "local plastic deformations without any load increase" and could sustain even greater loads after plastic deformation in contrast with type A roofing which sustained no load increase after plastic deformation. (Mahaarachchi and Mahendran 2008). This shows that element geometry plays a critical role in the static behavior of plates. They also evaluated design equations based on their findings.

With knowledge of the static failure of plates in mind, it is now necessary to establish a relationship between static failure and fatigue failure of plates. After Hurricane Tracey struck parts of Australia, research was made in order to discover the nature of the extensive damage caused by fatigue failure. “Morgan and Beck (1977) showed that the thin crest-fixed metal roof claddings suffered a fatigue failure of the sheeting in the vicinity of the fasteners under the action of sustained fluctuating wind loading.” (Mahendran 1995). A physical description of the low cycle fatigue failure of roof claddings and experimental results are given by Mahendran (1990a, b). “Field investigations and laboratory tests identified fatigue failure near the roof fasteners as the sole reason for the severe roofing damage (Beck and Stevens 1979).” (Xu 1995). Once it was determined that fatigue was essentially a localized effect subsequent research was aimed on small-scale tests. Mahendran and Mahaarachchi (2002) conducted small-scale constant amplitude load tests of steel cladding connections and compared the results to the static failure loads. They developed simple equations relating the static failure load to constant amplitude loads. They also performed multilevel cyclic test and proposed a modification factor to be used on Miner’s law in order to predict fatigue damage for variable amplitude loading. Although equations exists that relate static failure loads to fatigue damage loads, these equations are only applicable to a limited number of steel cladding configurations and materials. In order to be able to predict fatigue damage in all possible cases it is necessary to establish a solid theoretical basis that accounts for the fatigue properties of different materials and is based on analytical models of the stresses and strains that are responsible for fatigue failure. Research is needed in relating existing fatigue criteria to fatigue damage observed on steel claddings.

Emphasis is now given to different criteria in multiaxial fatigue. Several models have been established for describing multiaxial fatigue. There are stress based models, strain based models, and energy based models. "Brown and Miller (1982) reviewed much of the available multiaxial low-cycle fatigue literature with particular emphasis on the formation and early growth of cracks. Unlike octahedral shear stress, which in some cases has been shown to be effective when correlating high-cycle fatigue failure, octahedral shear strain and maximum shear strain are not effective in describing low-cycle fatigue. Brown and Miller concluded that two strain parameters are needed to describe the fatigue process. They proposed that both the cyclic shear and normal strain on the plane of maximum shear must be considered. Brown and Miller also provided a comprehensive review of the literature in terms of strain. They considered the nucleation and growth of fatigue cracks and suggested the terms Case A and Case B cracks." (Socie and Marquis 2000). They proposed separate criteria for each type of cracking which depend on loading configuration. In contrast with static failure of claddings in which failure was a function of only one parameter (membrane tensile strain), fatigue failure of claddings is a function of two parameters (cyclic shear and normal strain).

Sufficient information has been gathered regarding the static failure of crest-fixed steel claddings and experiments have been made regarding fatigue failure of crest-fixed steel claddings but a connection is still missing between static failure parameters and fatigue failure observations. A successful fatigue model should be stated in terms of the stress and strain tensor at a given point in the structure as compared to previous models which are stated in terms of static failure load at the connection for a given geometric configuration and material. Also valley-fixed claddings, which are common in the US and Puerto Rico, need to be treated. The scope of this research is to incorporate different geometric configurations into a simple model that could be used in the prediction of the fatigue life.

Chapter 3: Methodology

3.1 Introduction

There are several methods for the assessment of wind induced fatigue damage on structural components. The method to be used in each case depends on the purpose for which the data will be used. Methods can be classified as empirical, semi-empirical or analytical. Empirical methods, such as full scale testing, can be used to give a direct correlation between wind speed and total damage on a structure.

Figure 1 Wind pressure simulation by means of air bags in the experiments by García, 2008, pp. 62.

One such method is based on full-scale wind pressure simulation, as shown in Figure 1. In order to perform the analysis and design of structural components based on existing knowledge on the processes that cause the failure of these components, such as fatigue damage, analytical and semi-empirical methods can provide a much faster and cheaper solution without the need for expensive and time consuming experimentation.

The method used on this research is based on computational structural analysis solved by finite element methods and its application to the prediction of fatigue damage based on total life approaches. The use of this method only requires available fatigue data used to fit the fatigue models. The results obtained are compared to experimental data on the same structural component obtained from García (2008) in order to validate the analytical model.

3.2 Overall Methodology

Some detail is given concerning modeling screwed connections. Among thin metal roof cladding configurations, a two-span simply supported configuration is considered to be representative because it simulates a uniform wind uplift pressure and screw reactions can be estimated (Mahendran and Tang 1998). A type B wide rib cladding has been selected in this thesis as laboratory failure is well documented for this type of configuration (García 2008). The finite element software Abaqus Standard (2008) enables the user to create shell sections using CAD drawing utilities, which permits to construct the model from geometric properties. Other aspects, such as creating elastic-perfectly plastic material definitions and linear and non-linear geometry analysis, are necessary features in order to represent the complex behavior of the structural component subject to lateral wind pressures.

The method for evaluating the fatigue life of the structure proposed can be resumed by two main activities. The first set of activities is to model the static phenomenon in the structure caused by the proposed wind load. The wind load is first modeled by a loading protocol established by the Canadian Standards Association and this load is reduced to a static load *P*, which acts upon the structure. The finite element analysis program Abaqus is used to calculate the stress and strain tensors, which are needed for the fatigue model. The second set of activities is to model the repetitive fatigue effect of this load on the structure. Although the structure is initially assumed to behave in a static manner, a dynamic load fluctuation is the cause investigated for fatigue damage. Existing multiaxial fatigue criteria are evaluated considering the strain tensor obtained from the finite element model and from available fatigue parameters for the material considered. Finally the fatigue life obtained from the fatigue criteria is compared with existing experimental data.

3.3 Finite Element Mesh and Type of Elements

Element description

In general, elements can be of any shape on which ξ, η, and ζ define local straight coordinates, which are used in the formulation of isoparametric elements. The need to transform from rectangular elements to an element of a more general shape is necessary in the formulation of curved shell elements. Refinement of the mesh is needed in order to mesh the zones near connections where stress concentration as well as geometry requires

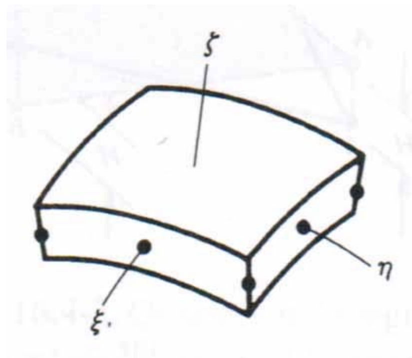

Figure 2 Eight node shell element (S8R) and local coordinate system adopted.

refined and special element shapes such as the triangular STRI65 element. Mindlin shell formulation (Cook, Malkus, Plesha, Witt 2002) is used to describe field quantities on elements. Shell normal displacements are interpolated as variables that are independent of cross-sectional rotation, whereas the curvatures depend on rotation and change in rotation. Consequently transverse shear strain is calculated as the mid-surface slope minus cross-sectional rotation. Nodal degrees of freedom include three translations and three rotations, totaling six degrees of freedom per node in accordance with thick shell formulation. For nonlinear geometry analysis and large displacements, the bending and membrane stiffness are coupled on the element stiffness matrix. Quadratic interpolation of geometry and field quantity is used on eight node elements. The Abaqus element library uses Mindlin formulation as standard for eight node elements with six degrees of freedom per node. A simpler formulation ignoring transverse shear strain could have been used given that element thickness can be regarded as thin. Element shape functions and displacements can be defined as in equations 1 and 2 as suggested by Cook, Malkus, Plesha, and Witt (2002).

$$N_1 = \frac{1}{4}(1-\xi)(1-\eta) - \frac{1}{2}(N_8 + N_5) \qquad N_5 = \frac{1}{2}(1-\xi^2)(1-\eta)$$

$$N_2 = \frac{1}{4}(1+\xi)(1-\eta) - \frac{1}{2}(N_5 + N_6) \qquad N_6 = \frac{1}{2}(1+\xi\ )(1-\eta^2)$$

$$N_3 = \frac{1}{4}(1+\xi)(1+\eta) - \frac{1}{2}(N_6 + N_7) \qquad N_7 = \frac{1}{2}(1-\xi^2)(1+\eta) \qquad \text{(eq. 1)}$$

$$N_4 = \frac{1}{4}(1-\xi)(1+\eta) - \frac{1}{2}(N_7 + N_8) \qquad N_8 = \frac{1}{2}(1-\xi\ )(1-\eta^2)$$

Displacements $\{\boldsymbol{u}\}$ over an element are defined by shape function interpolation as given by equation 2.

$$\begin{Bmatrix} u \\ v \\ w \end{Bmatrix} = \sum N_i \left(\begin{Bmatrix} u_i \\ v_i \\ w_i \end{Bmatrix} + \zeta \frac{t_i}{2} [\mu_i] \begin{Bmatrix} \alpha_i \\ \beta_i \end{Bmatrix} \right) \qquad \text{(eq. 2)}$$

Element geometry can be interpolated in a similar fashion where $[\boldsymbol{\mu}_i]$ is a matrix of directional cosines defining element shape, α and β are nodal rotational degrees of freedom, and i refers to the node number going from one through eight. It can be shown that:

$$\lfloor \varepsilon_x \quad \varepsilon_y \quad \varepsilon_z \quad \gamma_{xy} \quad \gamma_{yz} \quad \gamma_{zx} \rfloor^T = \sum [B_i] \lfloor u_i \quad v_i \quad w_i \rfloor^T \qquad \text{(eq. 3)}$$

after making appropriate coordinate transformations, where [**B**] is the strain-displacement matrix dependent on the derivatives of [**N**] with respect to global coordinates *x, y,* and *z*.

According to the Mindlin-shell formulation, matrix [**B**] is defined as:

$$[B]=[H]\begin{bmatrix} J^{-1} & 0 & 0 \\ 0 & J^{-1} & 0 \\ 0 & 0 & J^{-1} \end{bmatrix}\sum\begin{bmatrix} N_{i,\xi} & 0 & 0 & -\zeta t_i N_{i,\xi} l_{2i}/2 & \zeta t_i N_{i,\xi} l_{1i}/2 \\ N_{i,\eta} & 0 & 0 & -\zeta t_i N_{i,\eta} l_{2i}/2 & \zeta t_i N_{i,\eta} l_{1i}/2 \\ 0 & 0 & 0 & -t_i N_i l_{2i}/2 & t_i N_i l_{1i}/2 \\ 0 & N_{i,\xi} & 0 & -\zeta t_i N_{i,\xi} m_{2i}/2 & \zeta t_i N_{i,\xi} m_{1i}/2 \\ \vdots & \vdots & \vdots & \vdots & \vdots \\ 0 & 0 & 0 & -t_i N_i n_{2i}/2 & t_i N_i n_{1i}/2 \end{bmatrix}\begin{Bmatrix} u_i \\ v_i \\ w_i \\ \alpha_i \\ \beta_i \end{Bmatrix}$$

(eq. 4)

where *l, m,* and *n* are directional cosines contained on [$\boldsymbol{\mu}_i$], and [**H**] and [**J**] are defined in the form:

$$[\mathbf{J}] = \begin{bmatrix} x,_\xi & y,_\xi & z,_\xi \\ x,_\eta & y,_\eta & z,_\eta \\ x,_\zeta & y,_\zeta & z,_\zeta \end{bmatrix} = \sum_i \begin{bmatrix} N_{i,\xi} x_i & N_{i,\xi} y_i & N_{i,\xi} z_i \\ N_{i,\eta} x_i & N_{i,\eta} y_i & N_{i,\eta} z_i \\ N_{i,\zeta} x_i & N_{i,\zeta} y_i & N_{i,\zeta} z_i \end{bmatrix}$$

$$[H]=\begin{bmatrix} 1 & 0 & 0 & 0 & 0 & 0 & 0 & 0 & 0 \\ 0 & 0 & 0 & 0 & 1 & 0 & 0 & 0 & 0 \\ 0 & 0 & 0 & 0 & 0 & 0 & 0 & 0 & 1 \\ 0 & 1 & 0 & 1 & 0 & 0 & 0 & 0 & 0 \\ 0 & 0 & 0 & 0 & 0 & 1 & 0 & 1 & 0 \\ 0 & 0 & 1 & 0 & 0 & 0 & 1 & 0 & 0 \end{bmatrix} \qquad \text{(eq. 5)}$$

The element stiffness matrix [*k*] is defined as:

$$[k]=\int_{-1}^{1}\int_{-1}^{1}\int_{-1}^{1}[B]^T[E][B]\det[J]\,d\xi\, d\eta\, d\zeta \qquad \text{(eq. 6)}$$

where [*E*] is the material property matrix defined for plane stress and homogeneous material by making the appropriate coordinate transformation for an equivalent state of stress and strain on local coordinates ξ, η, and ζ.

3.4 Static Model

In the first part of this research, a finite element model of the proposed structure is constructed to identify the stresses and strains caused by the proposed wind pressure.

Geometry definition

The structure geometry is defined as a 3D shell with thickness varying from 0.0299in. (0.759mm) to 0.0478in. (1.214mm) as defined in Figure 3b and Appendix A. Three basic cases are considered in the proposed geometry: screwed connections in valleys, screwed connections in crests and washer reinforced connections in valleys as shown in figures 3c and 3d. Because of symmetry considerations, only one fourth of the cladding defined in Figure 3b is represented in the finite element model as shown in Figure 3a. The blue lines in Figure 3 represent partitions for the load and element distribution, and the red lines represent axes of symmetry. Center holes at the right of Figure 3a are defined by creating a circular extrusion cut with radius defined as the inner radius in Figure 4. Table 1 lists the different configurations modeled.

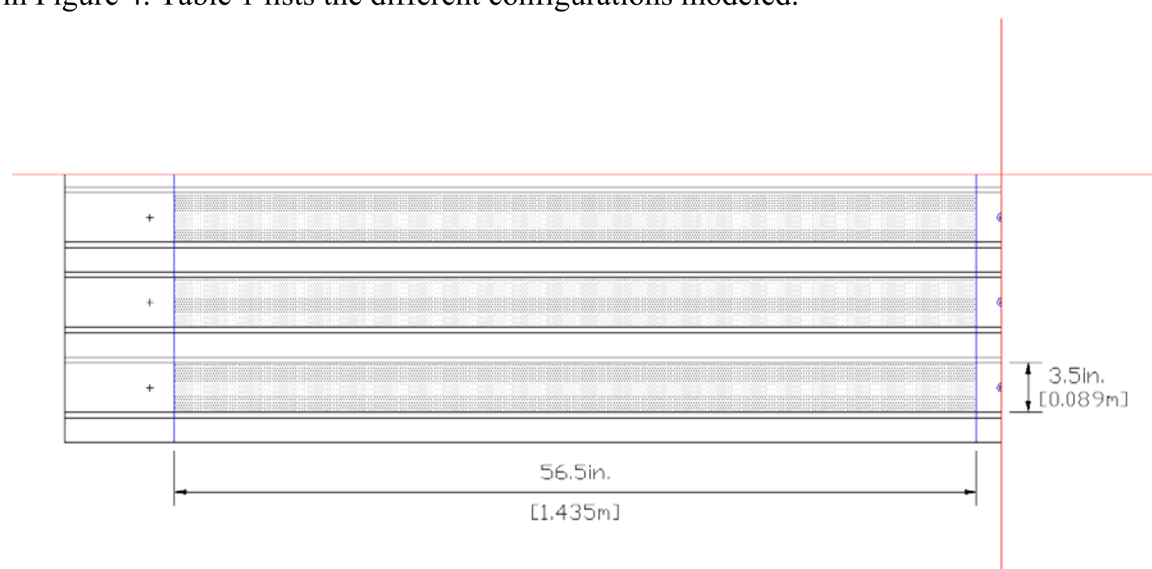

Figure 3a Geometry model

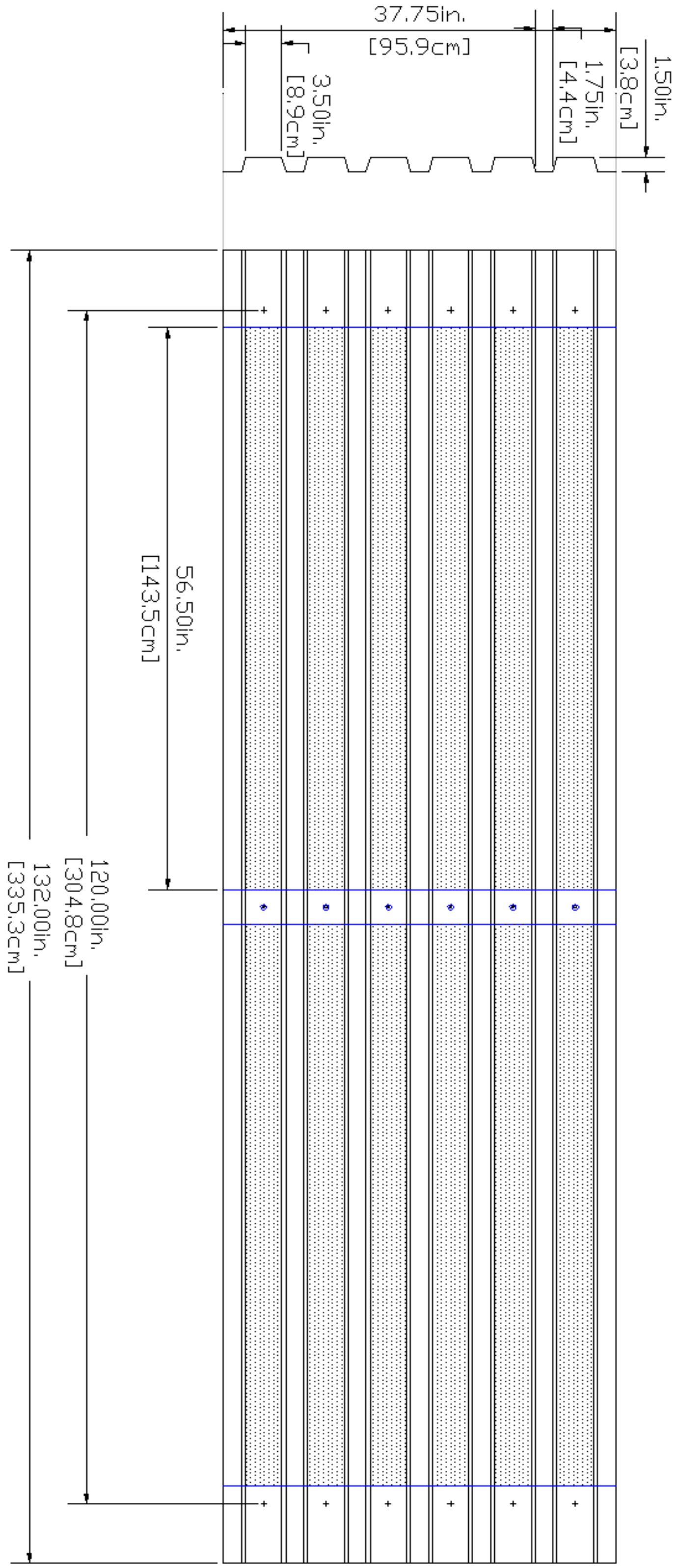

Figure 3b Geometry definition

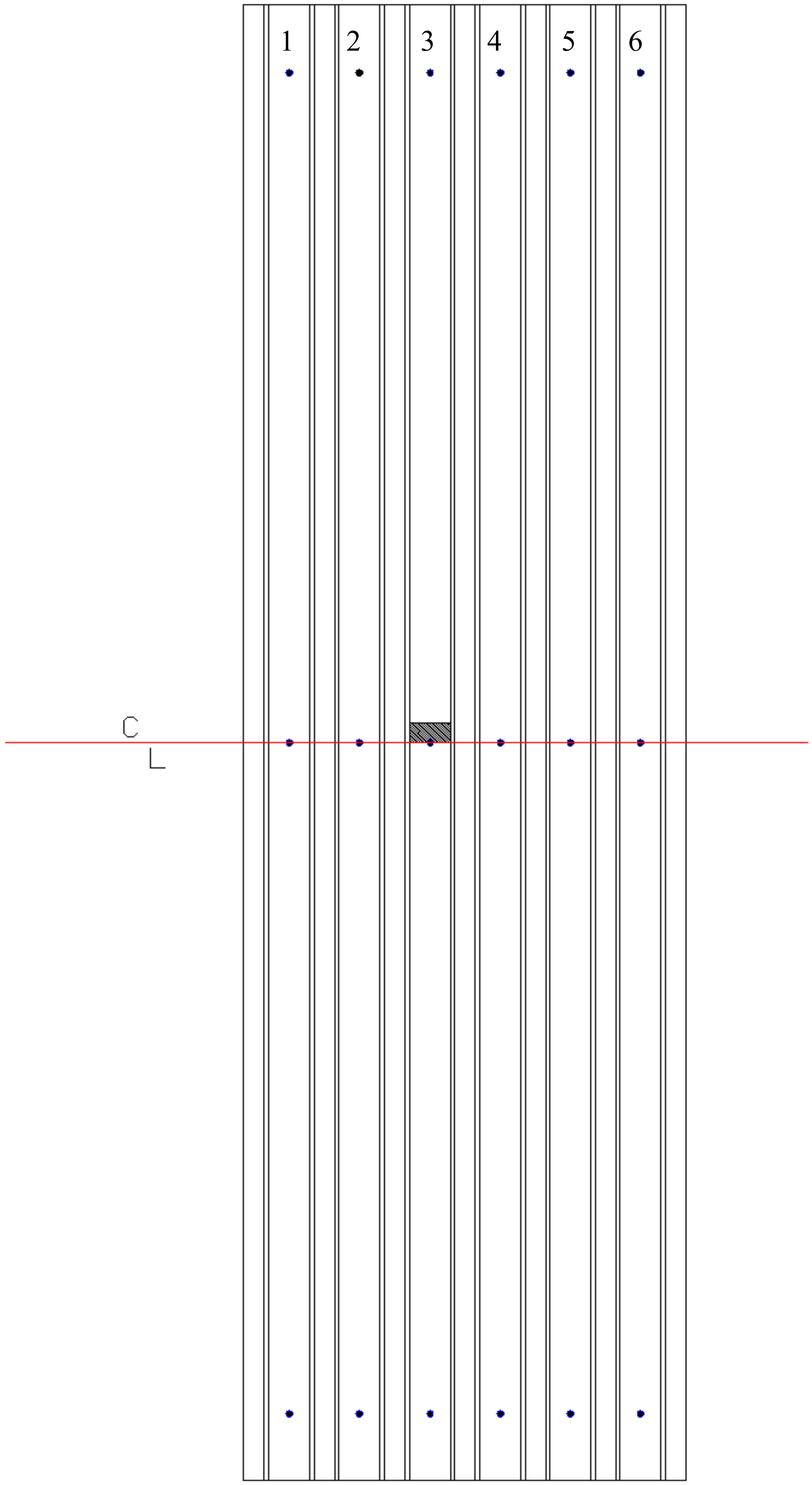

Figure 3c Type B (WR) cladding with screwed connections at valleys

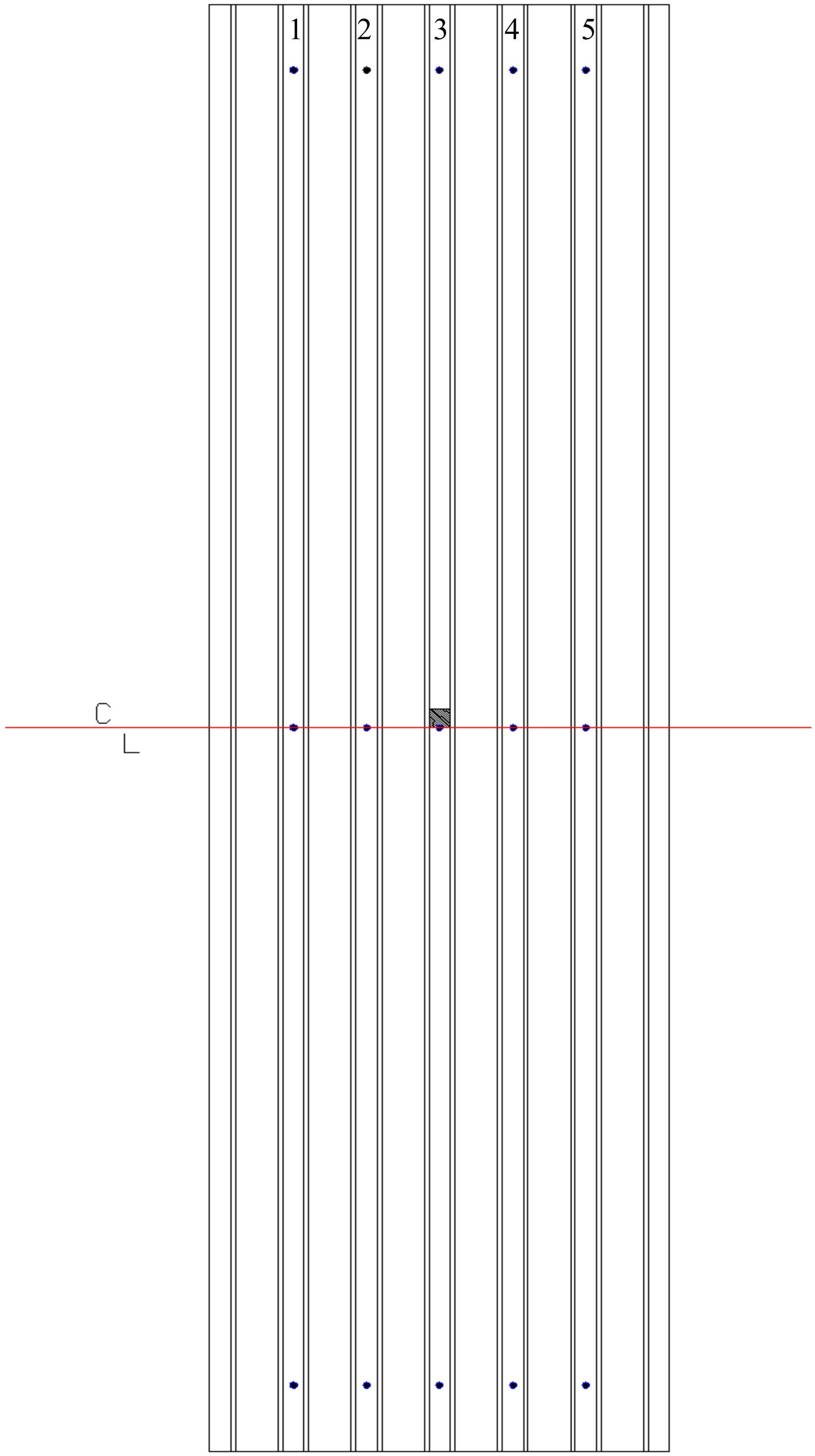

Figure 3d Type B (WR) cladding with screwed connections at crests

Table 1 Configuration definition

Model	Config.* #	Deck Gauge	Screw Locations (Figs. 3c-d)	Load P (kip)
1	3	22	1-2-3-4-5-6 (valleys)	2.0
2	4	22	1-3-4-6 (valleys)	1.0
3	5	22	1-2-3-4-5-6 (valleys-washer)	2.0
4	6	22	1-3-4-6 (valleys-washer)	2.0
5	13	18	1-3-4-6 (valleys)	1.5
6	15	20	1-3-4-6 (valleys)	1.5
7	17	20	1-3-4-6 (valleys-washer)	1.5
8	18	18	1-3-4-6 (valleys-washer)	2.5
9	19	18	1-2-3-4-5 (crests)	1.0
10	20	20	1-3-5 (crests)	1.2
11	21	22	1-3-5 (crests)	1.2
12	24	18	1-3-5 (crests)	1.2

*García (2008)

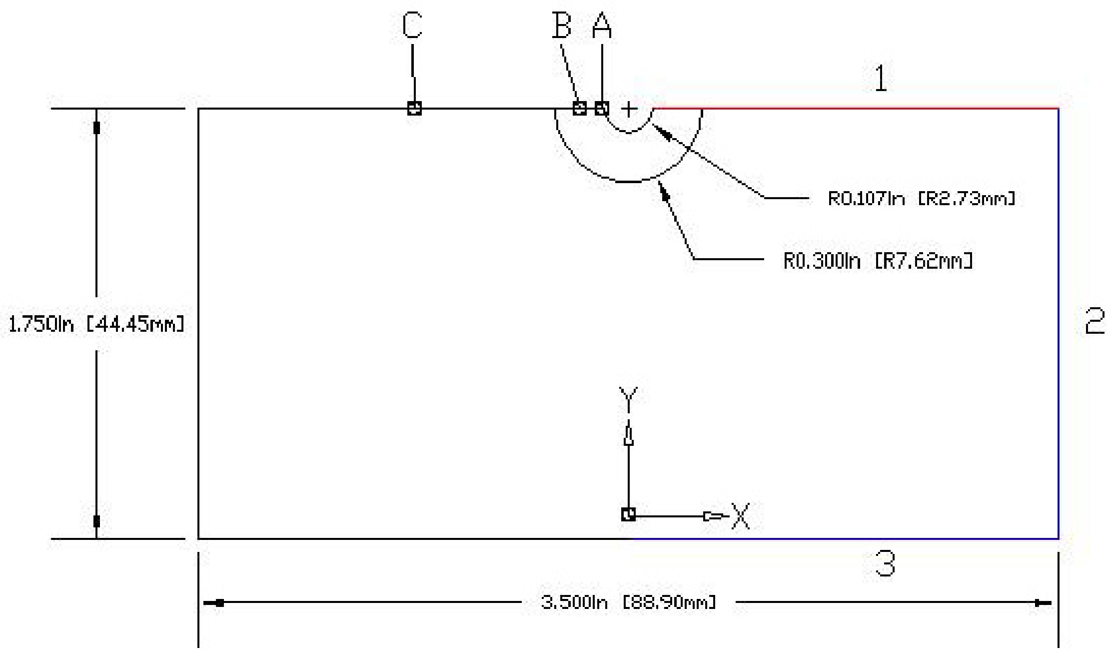

Figure 4a Detail of a center connection from shaded region in Figure 3c

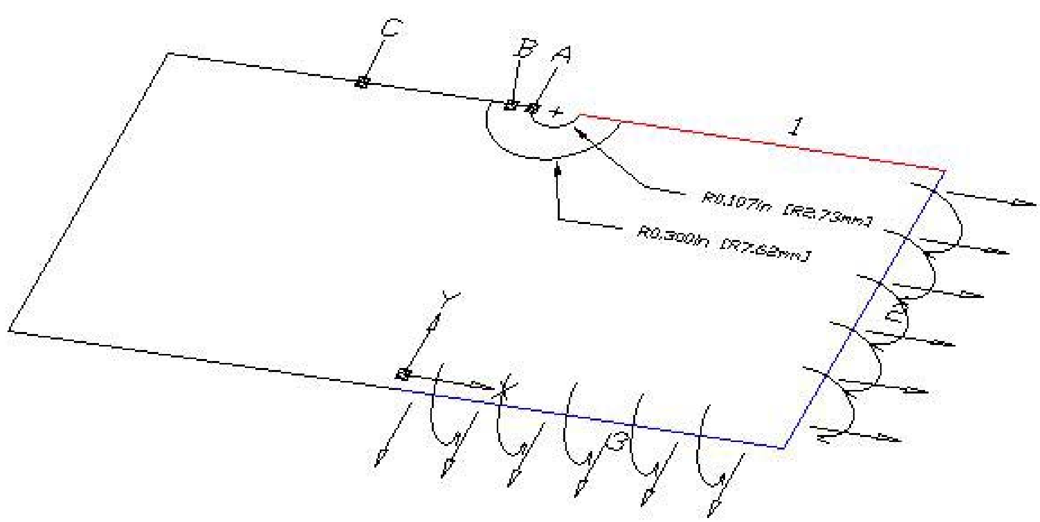

Figure 4b Direction of moments and forces acting on the section

Material and analysis

Type BWR decks used in experimental study (García 2008) are roll formed from hot-dipped galvanized steel conforming to ASTM specification A653. Results are computed for two different material definitions. In the first one, the material is defined as elastic-perfectly plastic, with modulus of elasticity E = 29,000ksi (200Gpa), Poissons ratio v = 0.3, and yield stress of 33ksi (228Mpa). In the second one, a third linear strain-hardening zone is added with hardening modulus of 2Gpa after a strain of 0.02 and extending to a failure strain of 0.20 and true fracture stress of 590 Mpa as shown in Figure 5. The point at which the strain-hardening region begins is taken to be 15 to 20 times the maximum elastic strain (Salmon, Johnson, Malhas 2009). Although realistic material behavior has a proportional limit lower than the yield strength, the flow stress starts at 2% strain, which is in good agreement with the elastic-perfectly plastic assumption (ASTM-A653 2009).

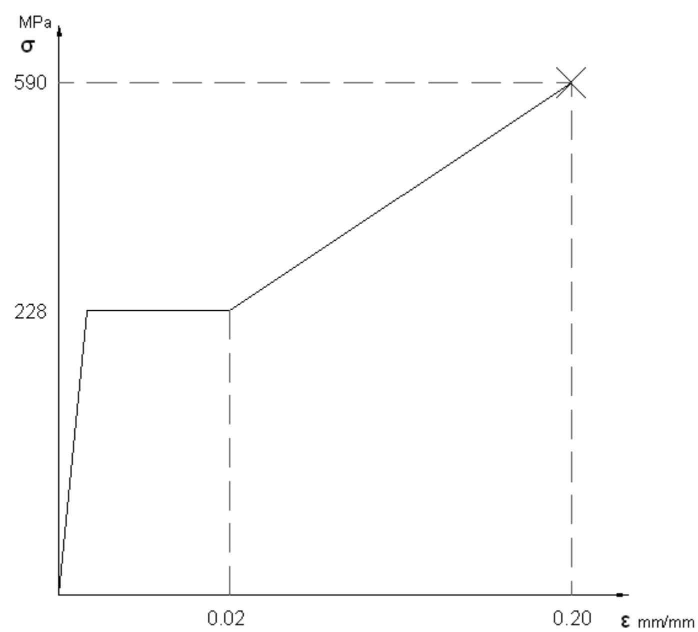

Figure 5 Strain hardening material definition

In the linear analysis the material is defined as elastic and linear in geometry. Non-linearity in geometry is used to account for large displacements and geometric non-linearity effects in the non-linear analysis.

Loads and boundary conditions

As an approximation, the total pressure is defined by means of an equivalent overall force applied to the complete panel, *P*, divided by the total area of the valleys where the pressure is assumed to act (3.5 x 56.5 x 12 = 2373 in^2) (1.531 m^2), as shown in the shaded region in Figure 3b. It is believed that this force evaluation is consistent with previous experimental studies, in which air bag pressure was applied at the valleys (García 2008). Screw holes are defined only on the center where the plate screws take most of the load, which is where the plate fails. The remaining screw holes are not defined on the plate and displacement restrictions on the three axes are defined as boundary conditions on a point where the center of the hole would be located. Refinement of the geometry of the plate near the holes with less load than the center holes is not considered to be necessary because stress and strain variations near the hole do not affect the stress fields on the other holes. At the center holes, displacement restrictions on the axis of the load are defined on the circumference of the circle defining the partition of the part around the hole (outer radius defined in Figure 4). This circumference defines the circumference of the screw head, which is responsible for the lateral reaction force per unit length in the plate. On washer reinforced connections this circumference defines the circumference of the washer which has a radius of 0.75 in.

(19.1mm). On the remaining screws, the reaction force is assumed to be a point load. Symmetry boundary conditions are defined as red lines in Figure 3.

3.5 Modeling Screwed Connections

In the previous section two different models were used on the same screwed connection. The type of model depends on the accuracy that is required for the field quantity near the connection. In the first less accurate model, the reaction force from the screw was simply modeled as a point load. Although point loads are easy to work with they are the source of singular fields in a structural response and prevent accurate representation of the field quantities. Point loads acting on a plate does not cause discontinuities in the displacement field but produce discontinuities in the stress field, which is a derivative of the displacement field. For the center connections, where the stress and strain fields need to be calculated, more accurate representations of loads and geometry are needed.

A better representation of the screw would involve an additional finite element model of the screw including different material properties and interaction between materials, such as contact stresses and friction forces. For the present case friction forces are neglected taking in consideration that the screws are not completely tight and the reaction force is assumed to be carried through the circumference of the screw head or washer by imposing displacement restrictions normal to the undeformed perimeter on a circle defining the circumference of the screw head or washer. Deformations in the other two directions in the plane of the plate are permitted as well as lateral deformation normal to the plate under the screw head or washer. In this way membrane action of the plate under the screw head or washer, where stress concentration is caused by the screw hole, is modeled as well as bending action caused by the screw head or washer. Additional modeling of the screw is not carried out because failure occurs on the steel cladding and not on the screw itself.

Finite element mesh

Quadratic quadrilateral-dominated elements having a random distribution are defined in order to make a transition from the circular geometry of the hole to the rectangular geometry of the span, as shown in Figure 6.

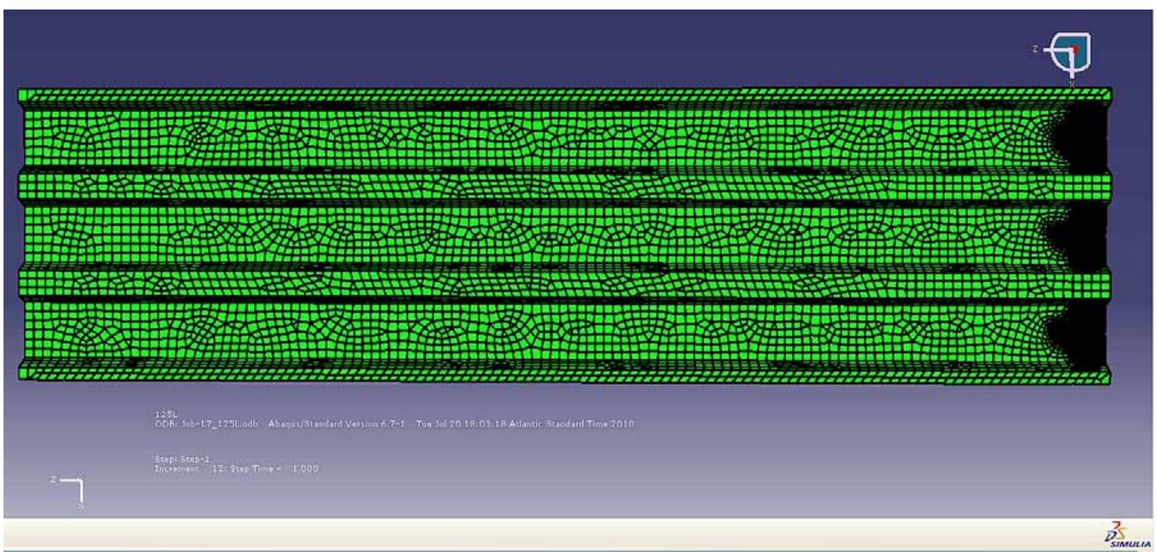

Figure 6a Complete mesh for ¼ of the cladding shown in Figure 3a corresponding to ϕ_5

The random distribution is necessary where changes in geometry do not allow a strictly defined mesh pattern. A more refined distribution is assigned to a square region of 88.9mm (3.5in) defined in Figure 4 surrounding the center screwed connections. The general trend of the mesh being more refined closer to the center holes is made to take into account the stress concentration near the holes, as suggested by previous studies (Mahendran and Mahaarachchi 2004). Refinement of the mesh is carried out by increasing the total number of elements on the partition and then on the squared regions along the center holes. Five mesh refinements are considered by increasing the total number of elements from 1,082; 7,715; 12,827; 20,742 and 30,929 corresponding to ϕ_1, ϕ_2, ϕ_3, ϕ_4, and ϕ_5 respectively. STRI65 and S8R shell elements from the ABAQUS element library are used.

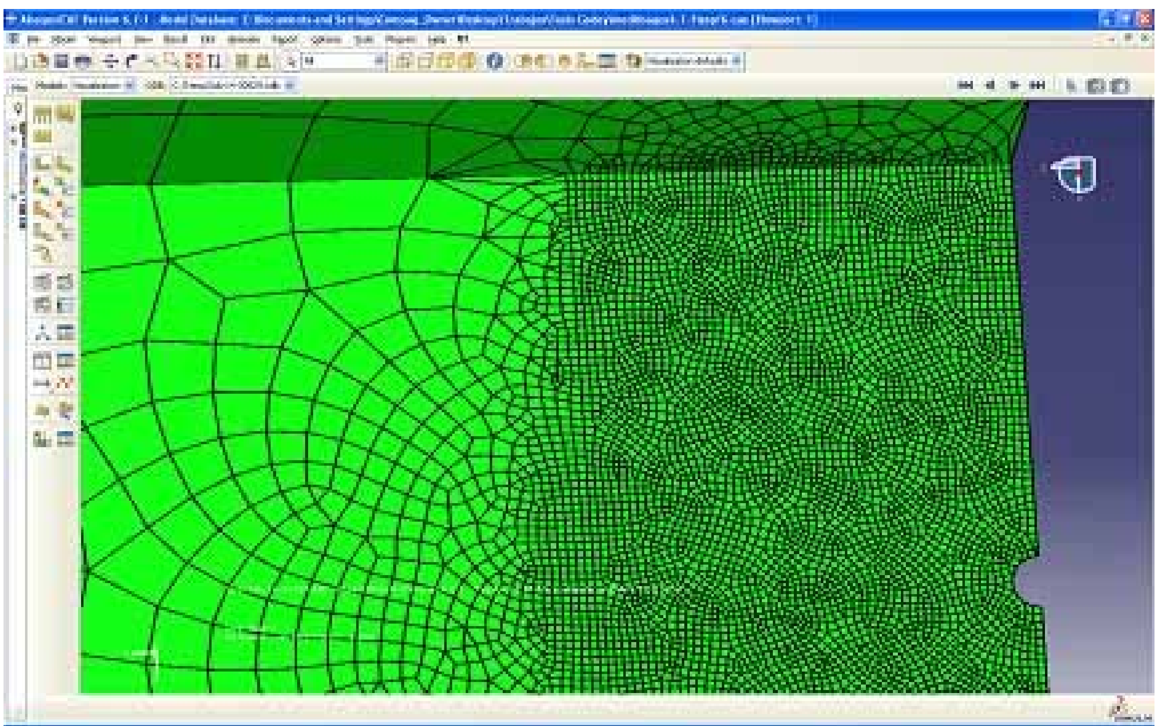

Figure 6b Mesh transition from a typical center screwed connection

Convergence and Error

In order to test for convergence and discretization error, five different meshes are used in which an irregular refinement is made by adding more elements. Values of displacement and strain are evaluated at three different points within the mesh.

The approximate element size *h* is plotted in figures 7 and 8 against the field quantity, which can be a displacement or one of its derivatives, such as a strain. Because the element distribution is not structured and subsequent mesh refinements do not preserve the original nodal positions, monotonic convergence is not guaranteed to occur. As the element size *h* decreases and approaches zero corresponding to an infinitely refined mesh, it is expected that the field quantity should approach the exact value. An approximate estimate may be calculated by the least squares method as the *y*-intercept in figures 7 and 8 corresponding to an element of size zero. Given the approximation of the exact value and the value obtained by a mesh with element size *h*, an estimate of the percentage of error has been calculated in Table 2.

Points A, B and C are located near the center screw holes on the bottom face, as shown in Figure 4. Strains at points A and B were found to have a larger error than at point C, given that they are located closer to the hole where the gradient in the field quantity is larger. As expected, strains were found to have larger error than displacements. The trend of greater error in strains than in displacements is explained by the fact that strains depend on a higher derivative of the field quantity than displacements and thus converge at a lower rate.

Although mesh refinement has been performed, the results of figures 7 and 8 do not indicate convergence in a direct way.

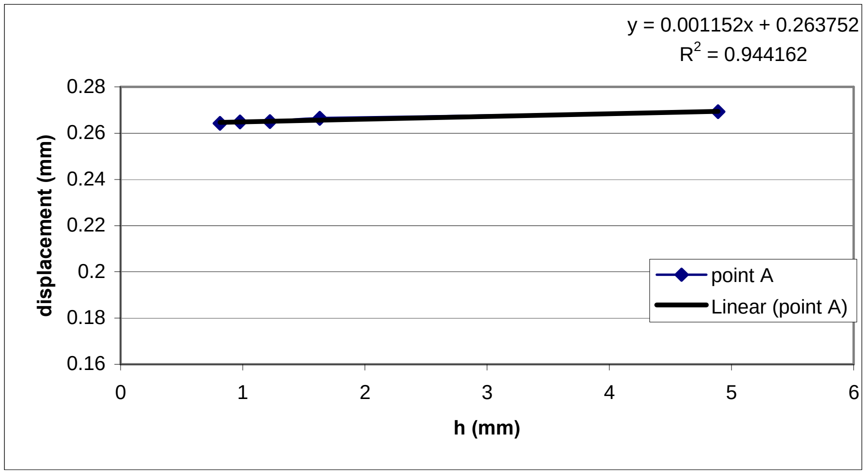

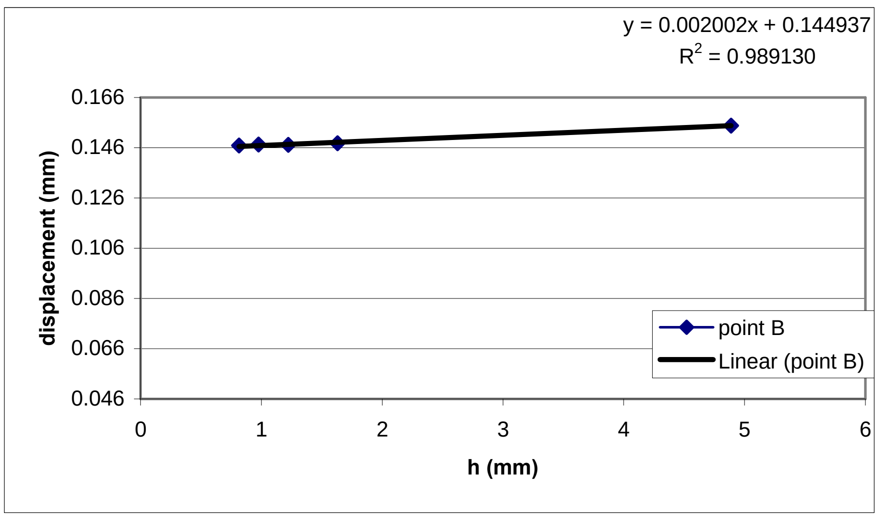

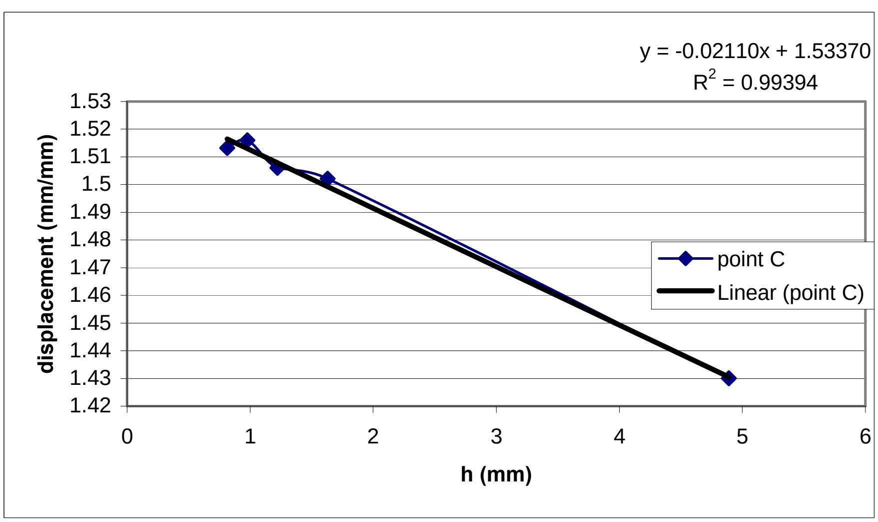

Figure 7 Displacement convergence

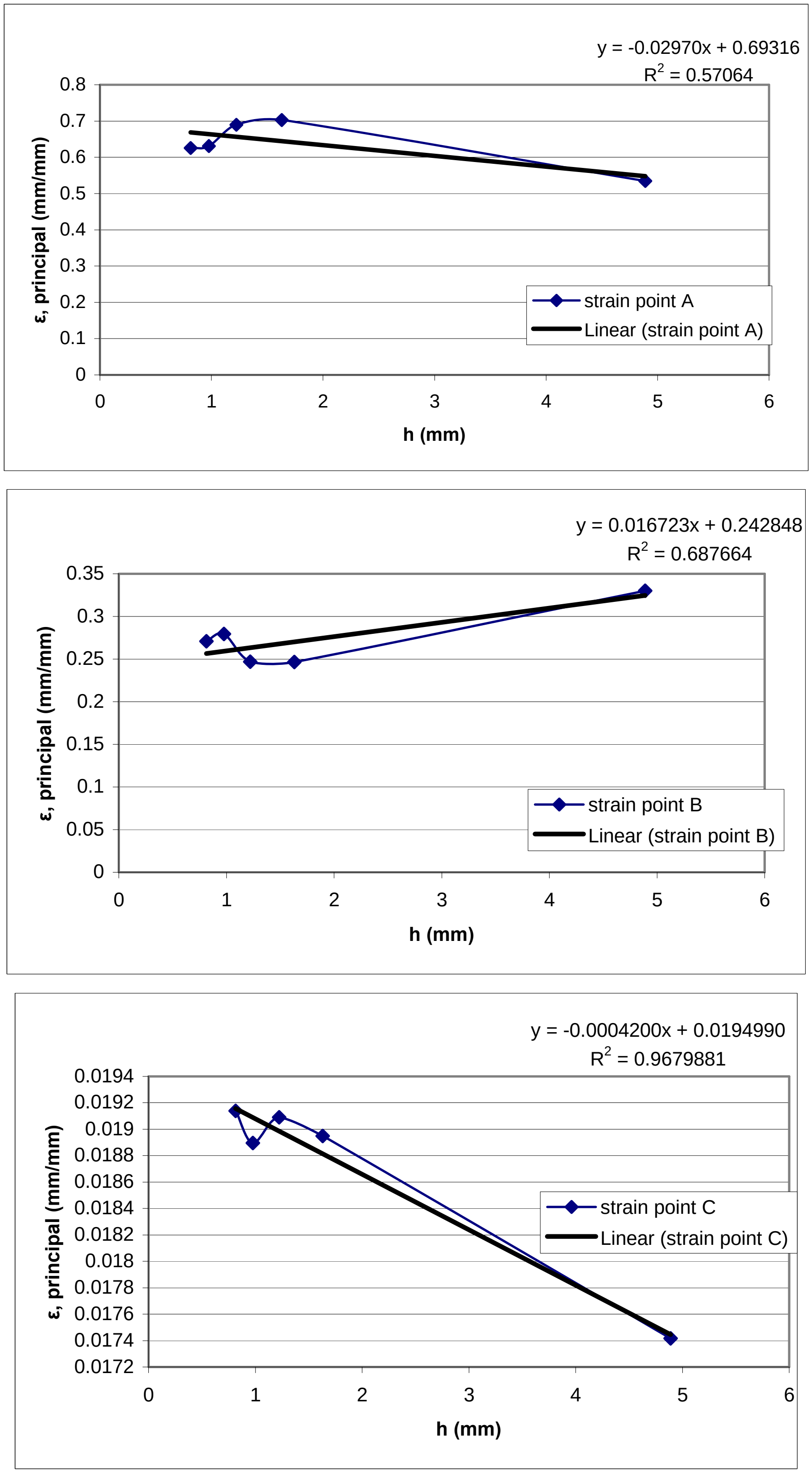

Figure 8 Strain convergence

Table 2 Error estimate

Error Estimate, $\%e = \dfrac{\phi_5 - \phi_\infty}{\phi_\infty} 100\%$		
	Displacement	Principal Strain
Point A	0.17	9.8
Point B	1.31	11.5
Point C	1.34	1.85

where ϕ_5 corresponds to the mesh with h = 0.8149 mm and ϕ_∞ to the estimated condition approaching h = 0.

Although singularities at the edge connections at the top of Figure 3b can cause greater error on field quantity predictions, there are no singularities at the center connections given that more accurate representation of the screws prevents large load reactions to appear at element nodes. Boundary conditions imposed on the screw head or washer can be the source of high linear reaction loads, which may yield unusually high values in derivatives of the field quantity. The error is attributable to the lowest degree term omitted in the interpolation function and depends on element size h, the degree of the highest complete polynomial in element field quantity p, and r^{th} derivative of the field quantity as suggested by Cook, Malkus, Plesha, and Witt (2002) in the form:

$$O(h^{p+1-r})$$

where O is a measure of the order of error.

For quadratic elements p = 2, r = 0 for displacements, and r = 1 for strains. Considering the element formulation in Section 3.3, in which the field quantity is represented by interpolation functions in equation 1, the highest complete polynomial is of order 2 since all the terms of order 2 are present, namely ξ^2, $\xi\eta$, and η^2. The error can then be traced to the omission of terms of order 3 in equation 1 given that a complete polynomial of order 3 cannot be defined. As a result a recursive equation can be defined in terms of the field quantity and the order of error.

$$\phi_n = \phi_\infty + e_n$$

$$\phi_{n+1} = \phi_\infty + e_n * \frac{O\phi_{n+1}}{O\phi_n} \qquad \text{(eq. 8)}$$

Using an order of error analysis, the order of error in each derivative of the field quantity is given for each mesh refinement in tables 3 and 4. The right column in tables 3 and 4 gives how many times the error is reduced upon each subsequent mesh refinement where *h* is plotted in figures 7 and 8 against the field quantity.

Table 3 Displacement order of error

Order of Error $O(h^{p+1-r})$; $p = 2$, $r = 0$.	
$O\phi_1 = 116.9$ $O\phi_2 = 4.33$ $O\phi_3 = 1.83$ $O\phi_4 = 0.935$ $O\phi_5 = 0.541$	$O\phi_1 / O\phi_2 = 27$ $O\phi_2 / O\phi_3 = 2.37$ $O\phi_3 / O\phi_4 = 1.95$ $O\phi_4 / O\phi_5 = 1.73$

Table 4 Strain order of error

Order of Error $O(h^{p+1-r})$; $p = 2$, $r = 1$.	
$O\phi_1 = 23.9$	$O\phi_1 / O\phi_2 = 9$
$O\phi_2 = 2.66$	$O\phi_2 / O\phi_3 = 1.78$
$O\phi_3 = 1.49$	$O\phi_3 / O\phi_4 = 1.56$
$O\phi_4 = 0.956$	$O\phi_4 / O\phi_5 = 1.44$
$O\phi_5 = 0.664$	

Since h is of degree 3 in displacements and 2 in strains in the order of error formulation, a linear relationship between error and element size h is not expected. Given this proof the method of error estimation in Table 5 should provide a more accurate error estimate than the method used on figures 7 and 8. The error in ϕ_1 in Table 5 is calculated by using n = 1 on equation 8 where ϕ_1 and ϕ_2 are displacements and strains from figures 7 and 8.

Table 5 Percent error

Error e_n, Percent Error *%e*	
Displacement Point A (mm)	Strain Point A (mm/mm)
ϕ_1 0.00293, 1.1%	ϕ_1 0.1895, 26.2%
ϕ_2 0.000109, 0.04%	ϕ_2 0.0211, 2.9%
ϕ_3 0.000046, 0.02%	ϕ_3 0.0118, 1.6%
	ϕ_4 0.0076, 1.0%

By substituting the order of error from tables 3 and 4 and solving for ϕ_∞ and e_1, e_n can then be taken as $e_{n-1} * \frac{O\phi_n}{O\phi_{n-1}}$. The largest reduction in error occurs by reducing element size from ϕ_1 to ϕ_2 as shown on figures 7 and 8 and tables 3 and 4. From Table 5 displacement converges in ϕ_1 with a 1% error while strain converges on ϕ_4. As a result an element size h = 1mm corresponding to ϕ_4 meets convergence requirements. Figure 6 is an example of ϕ_5.

Chapter 4: Results of Static Analysis

4.1 Introduction

A basic case has been initially solved in this Chapter. Three different models are considered in the finite element analysis to understand the effects of non-linearity in material and in geometry. In the first model the material is defined as elastic with no plastic zone defined and linear in geometry. In the second model, non-linear elasticity is considered. In the third model, plasticity as well as non-linearity in its geometry are considered.

4.2 Linear and Elastic Results

These results are calculated for configuration #3 defined in Table 1. For the linear case, the von Mises stresses and out-of-plane displacements are calculated. Figure 9 shows out of plane displacements and von Mises stresses on the envelope (maximum values) of the top and bottom surfaces measured by the distance from the edge of the center hole on the *x*-axis, as defined in Figure 4. It can be seen that the out of plane displacement is zero at 5mm on boundary 1, corresponding to a boundary condition imposed on the screw head. Figure 9 also shows the stress concentration near to the hole at the peak of the curve. The values are unusually high (values higher than 1500 Mpa at 5mm from the center hole) even for this dense finite element mesh; they will later be shown to be due to the assumption of elastic behavior made in the present model. Figure 10 shows the same results on an axis parallel to the previous one, with 1.75in (44.5mm) offset (boundary 3). In this figure the slopes are less pronounced given that less deformation and hence stresses exist at some distance away from the hole.

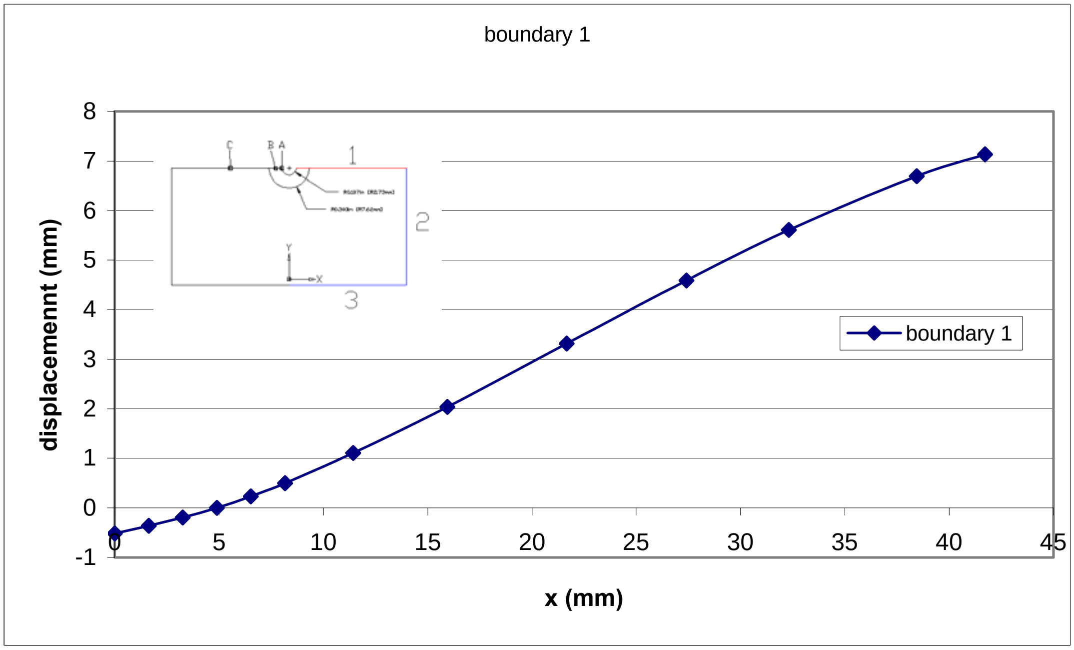

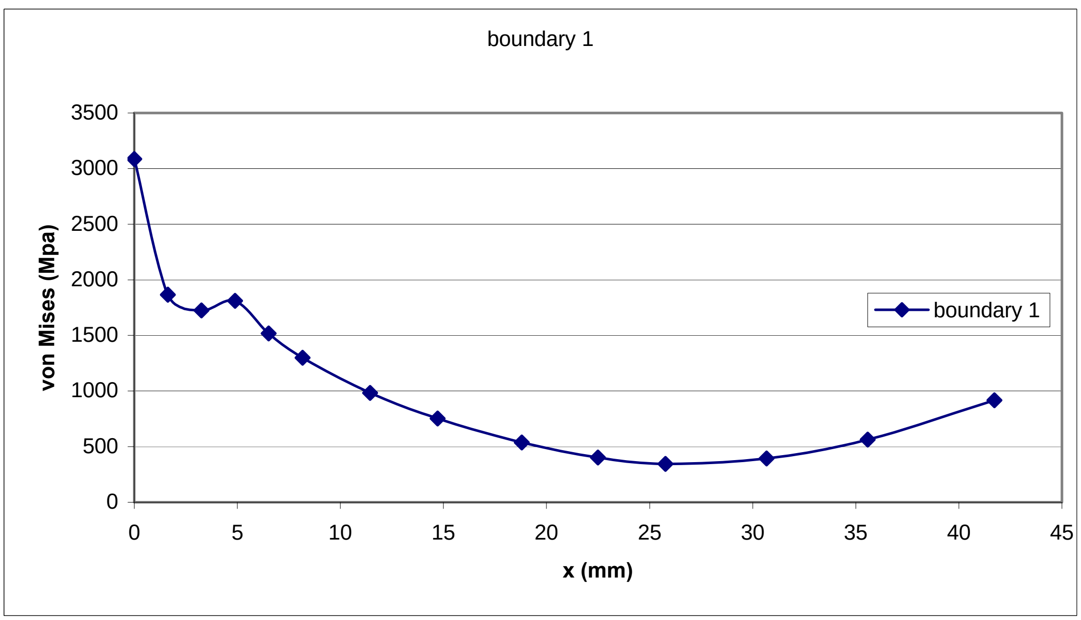

Figure 9 Linear results at boundary 1 in Figure 4

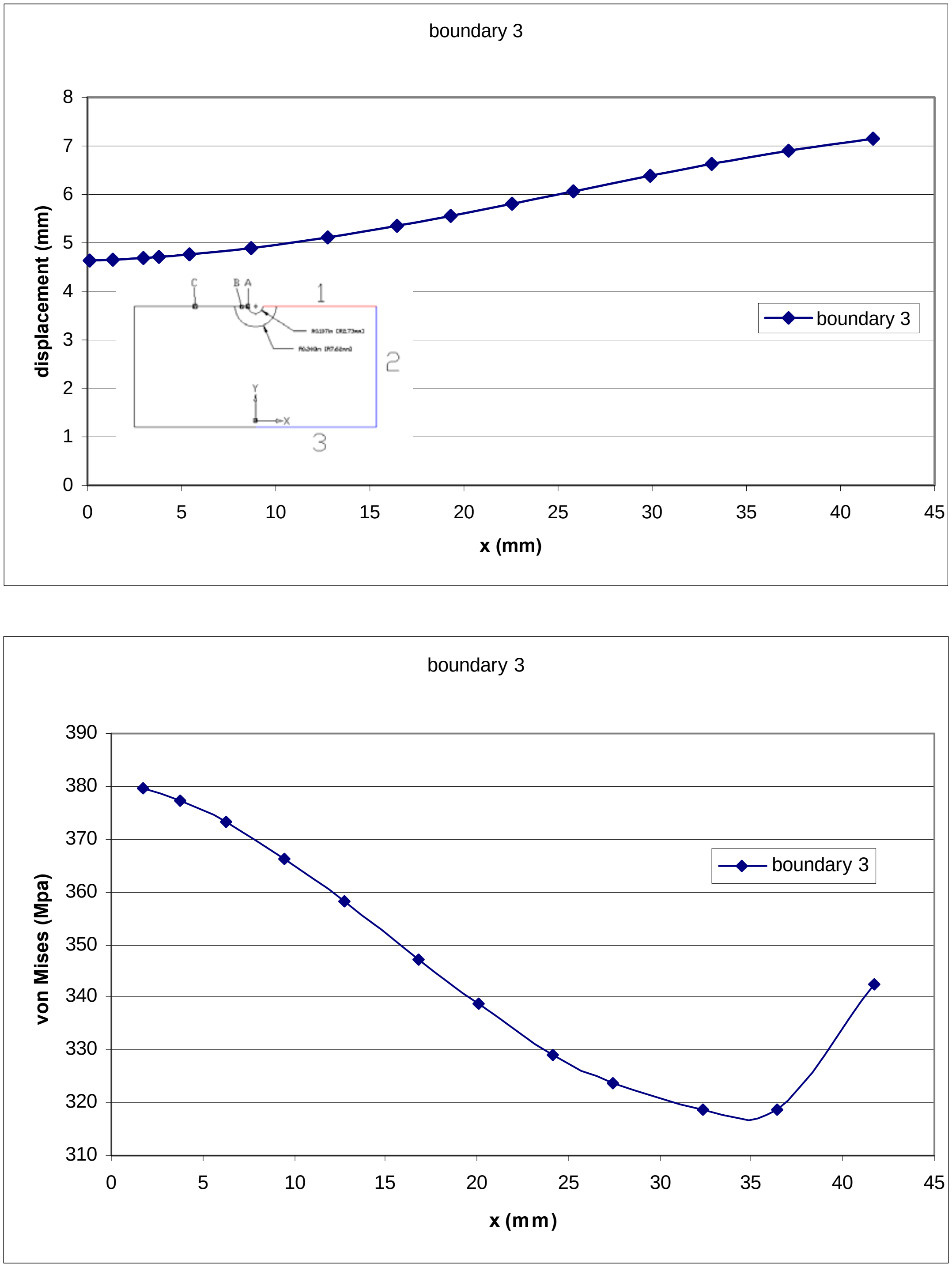

Figure 10 Linear results, boundary 3 in Figure 4

Figure 4b shows the direction of the bending moments and forces that are plotted in figures 11 and 12. Figure 11 shows membrane stresses acting perpendicular to the boundaries of Figure 4, where $x = 0$ represents the edge of the hole. Membrane stresses on boundaries one and three in Figure 11 are very similar except at a short distance from the hole, although boundary 1 is closer to the hole given that the reaction force of the screw is transmitted by bending and not by membrane stresses in a geometrically linear analysis not accounting for large defections. On the other hand, the stresses on boundary 2 are much lower because most of the bending action is taken in the longitudinal direction, as in the beam model where transverse deformation is zero. At the location of boundary 3 the membrane stress field is almost uniform, indicating that it is not affected by the connection. This value is well below the yield stress.

Figure 12 shows the bending moments on the axes of the boundaries. Figure 13 shows the shear stresses on the plane of the plate. The results may be interpreted as follows: the membrane stresses are larger on boundaries along the x-axis given that bending of the cladding in the longitudinal direction causes it to behave as a beam with tension and compression acting at the outermost fibers. The results of Figure 12 indicate that the moment along the boundary 1 grows fast as the distance from the hole is decreased because in a linear-elastic model not accounting for large displacements all of the load is transferred by bending action. Figure 13 shows zero shear on boundary 1 because of symmetry. The resultant force acting along the outer radius of a center connection in configuration #3 is 814-N acting perpendicular to the plate. This force represents the reaction force of the screw and displacements and forces in figures 11 to 13 are proportional to this force given a linear-elastic model. These results show large displacements and stresses well beyond the linear range.

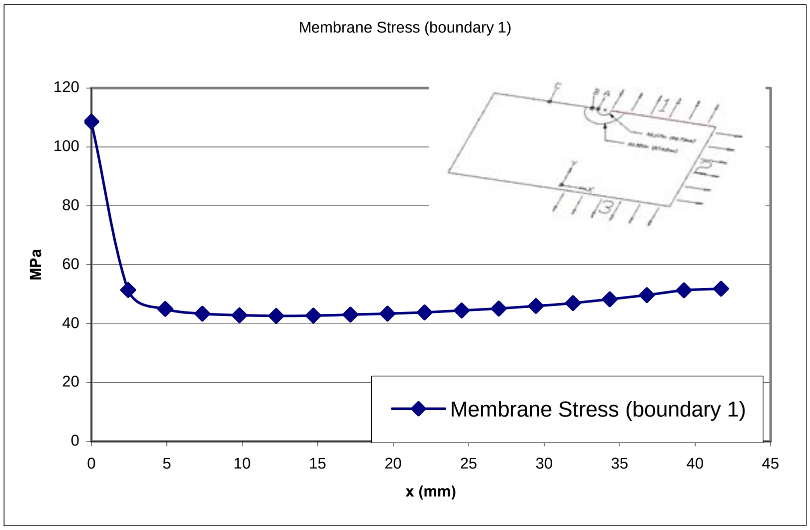

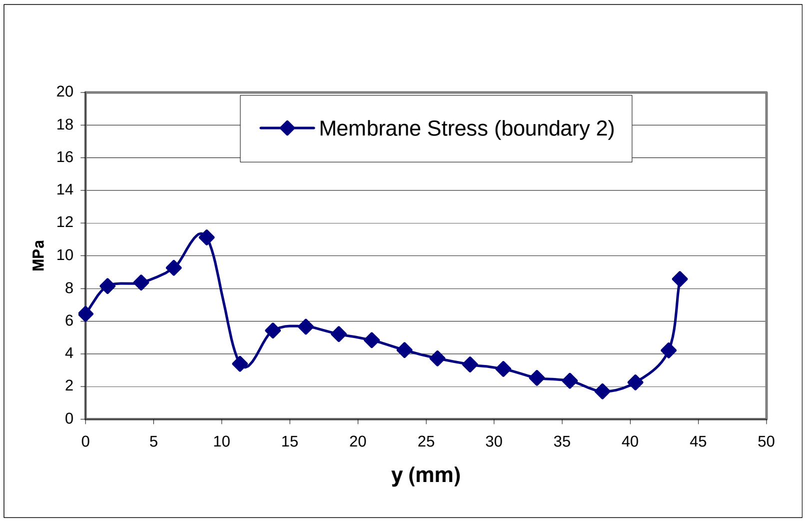

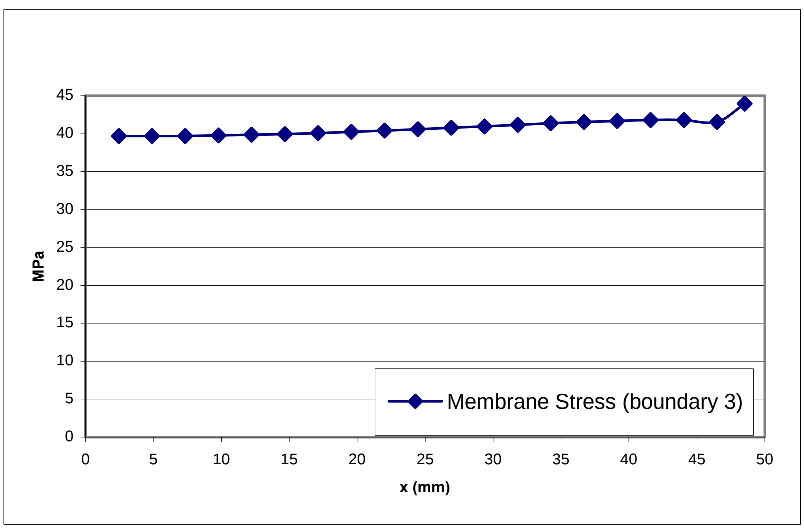

Figure 11 Linear results, membrane stress for load *P*

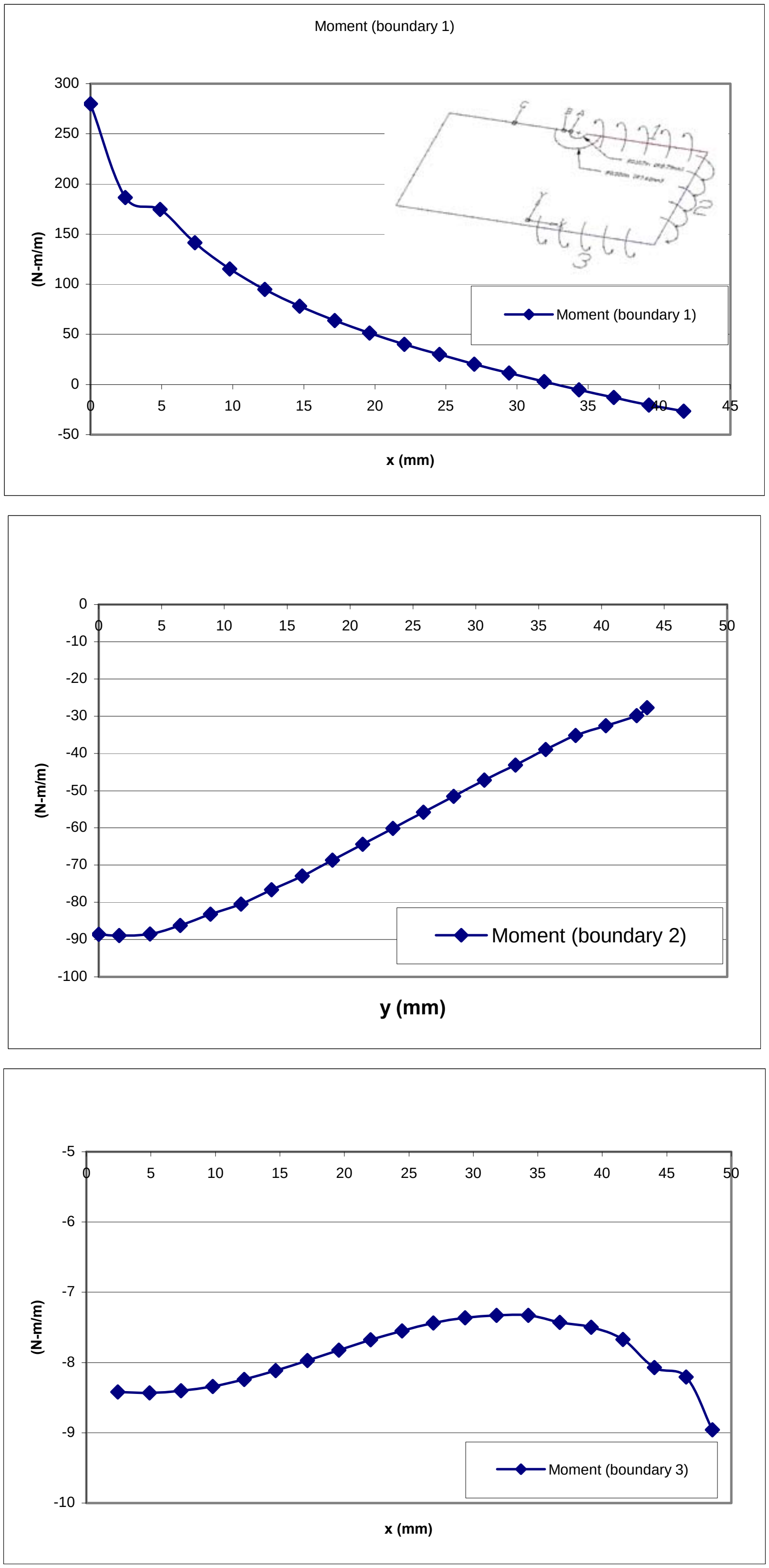

Figure 12 Linear results, moment for load *P*

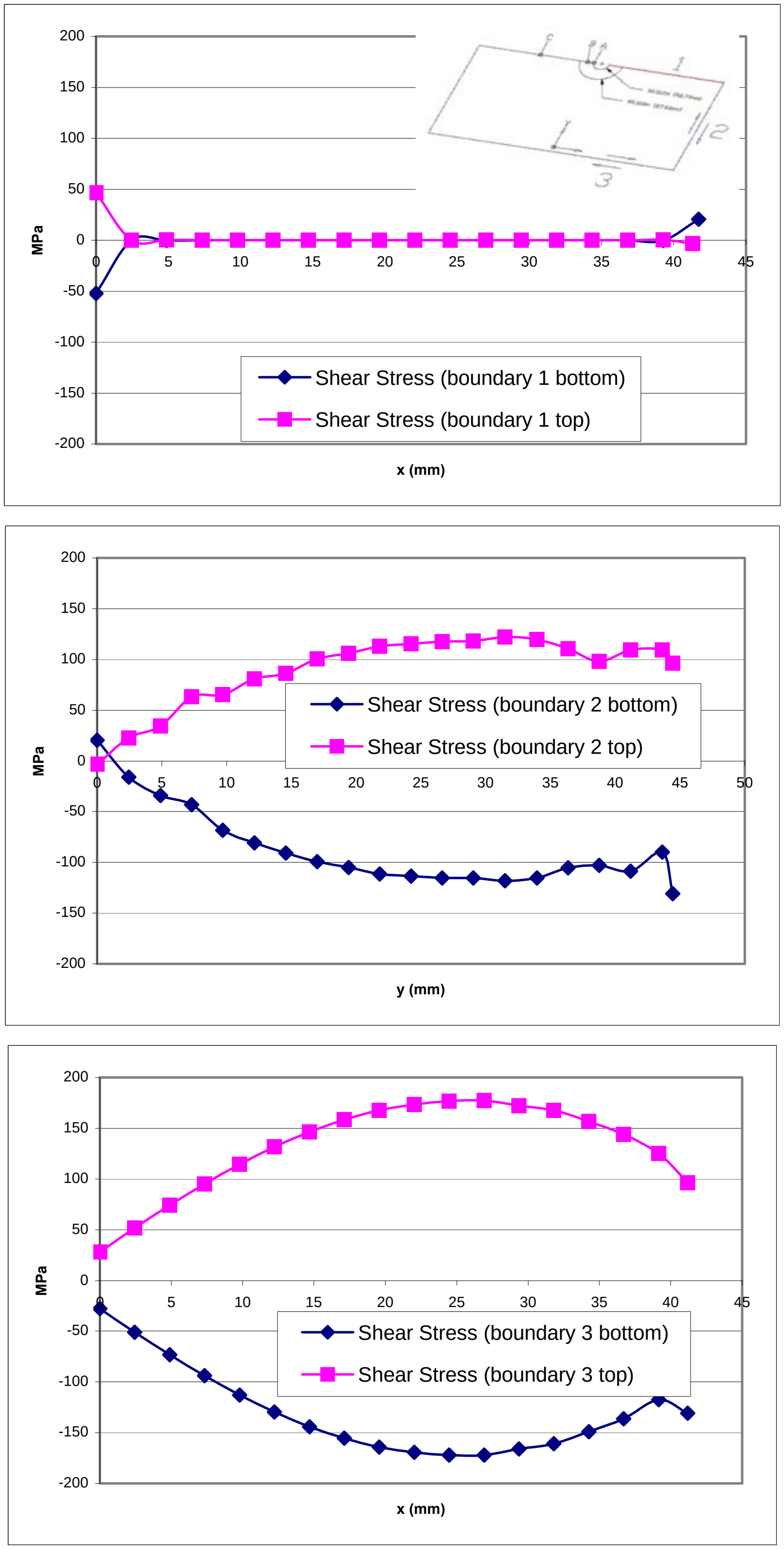

Figure 13 Linear results, shear stress for load *P*

According to thin plate theory, geometric linearity is fully justified provided displacements are smaller than the plate thickness. The material yield strength is 33ksi (228 Mpa) and the von Mises stresses are ten times larger, as shown in figures 9 and 10.

Because the results provide values that are in excess of linear theory, it is now justified to explore nonlinear behavior including geometric as well as material non-linearity.

4.3 Geometrically Non-linear and Elastic Analysis

In this section, the von Mises stresses are calculated on boundaries 1 and 3 as in figures 9 and 10 but now for the geometrically non-linear case as shown in figures 14 and 15. Geometric non-linearity is a kinematic non-linear dependence of strains on displacements; this causes that the structure stiffness matrix becomes dependent on displacements. For plates with large displacements, membrane action may dominate over bending and is a consequence of the dependence of the stiffness matrix on the geometry of the structure.

In order to solve a problem where the stiffness matrix is not known in advance, it is necessary to perform a series of linear increments, in which the initial stiffness matrix for the case of zero displacement is modified. At each increment, an initial estimate of the displacement is used to calculate the new stiffness matrix and then a new displacement can be calculated based on the increment size, which is the change in load required in order to reach equilibrium. In the execution of the ABAQUS model, the increment size is set to “automatic,” so that an algorithm determines an appropriate increment size based on the computed results.

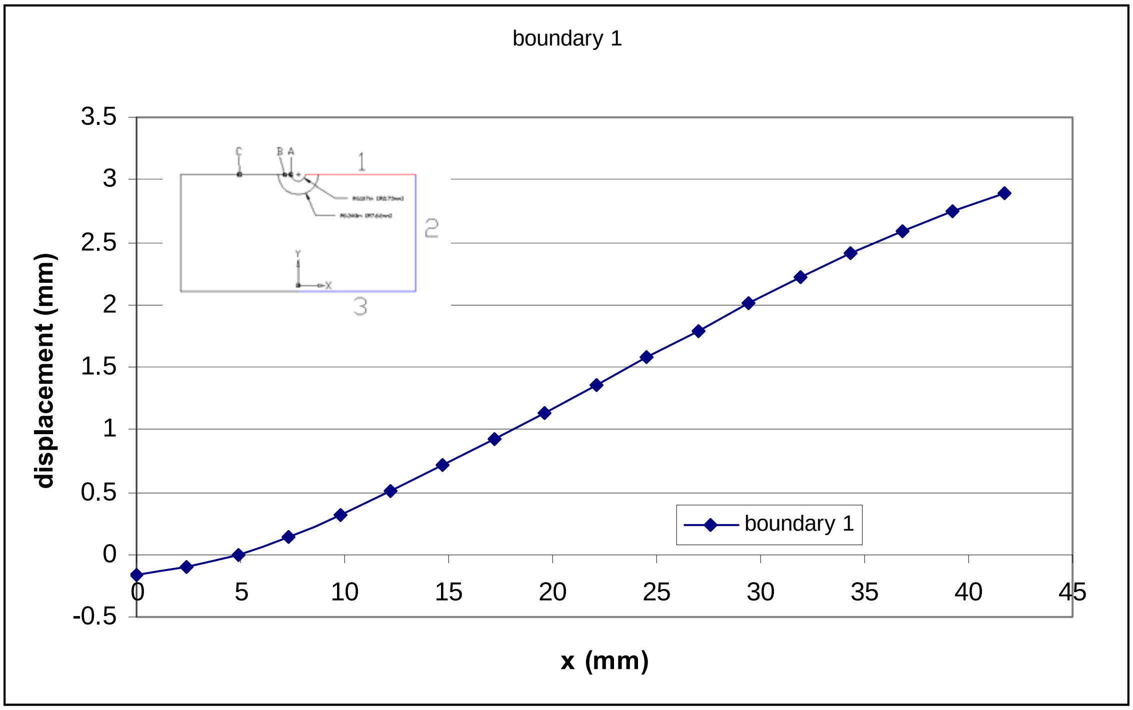

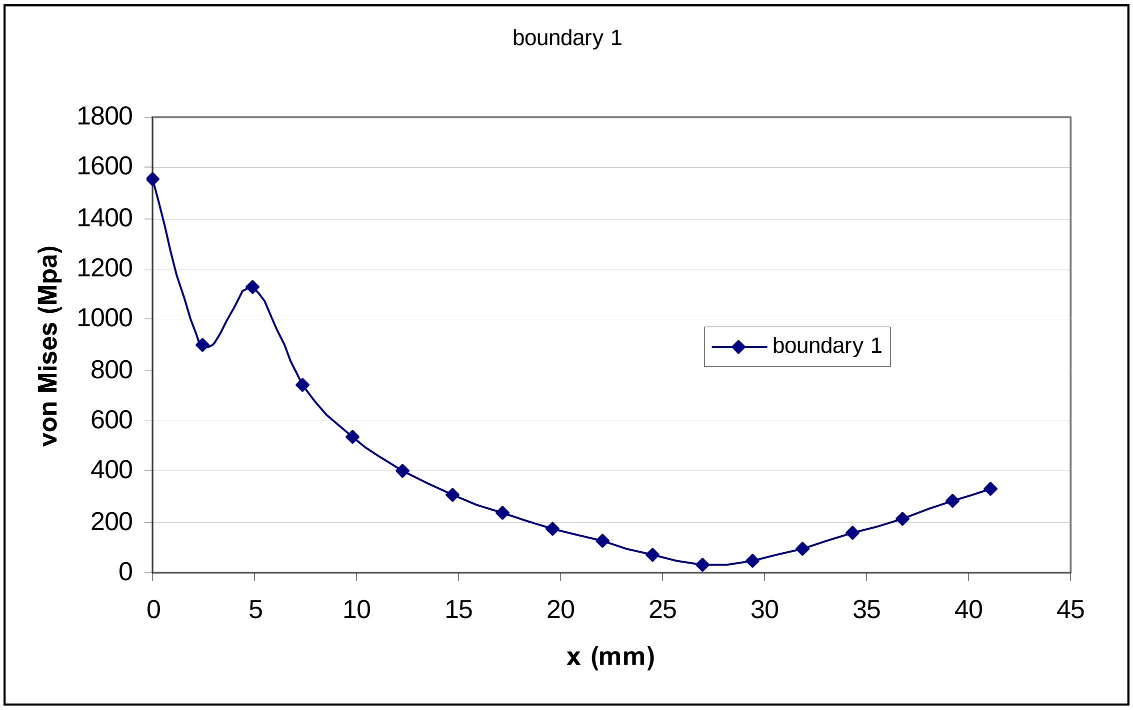

Figure 14 Geometrically non-linear and elastic results at boundary 1 in Figure 4

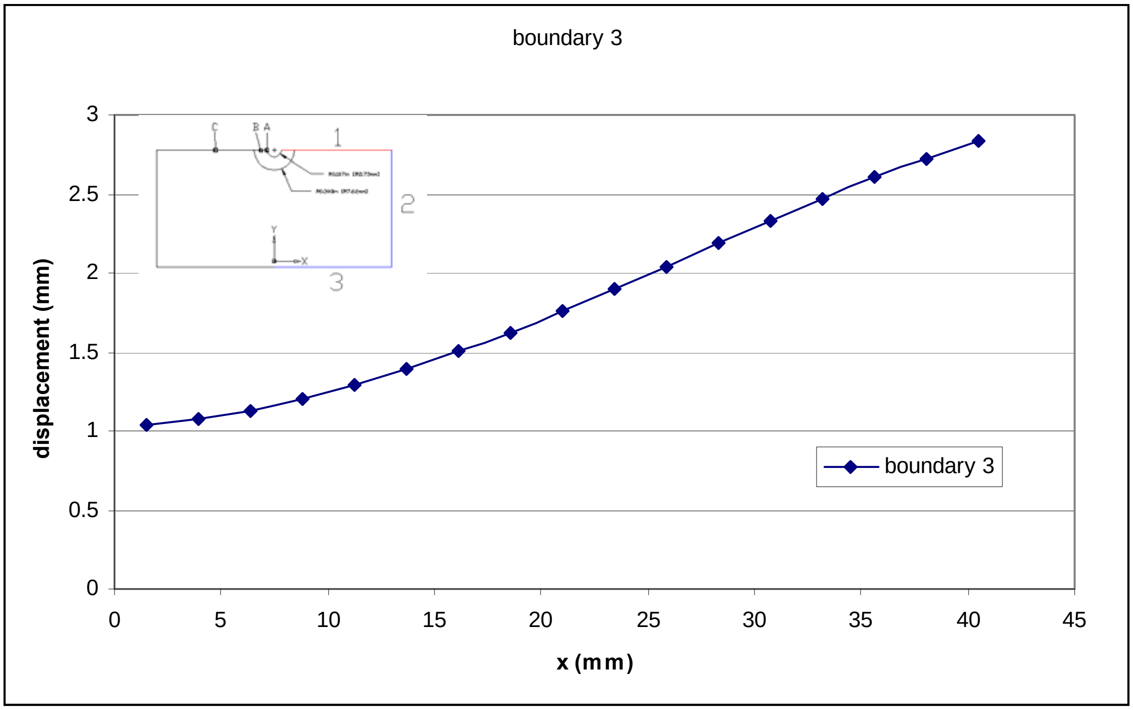

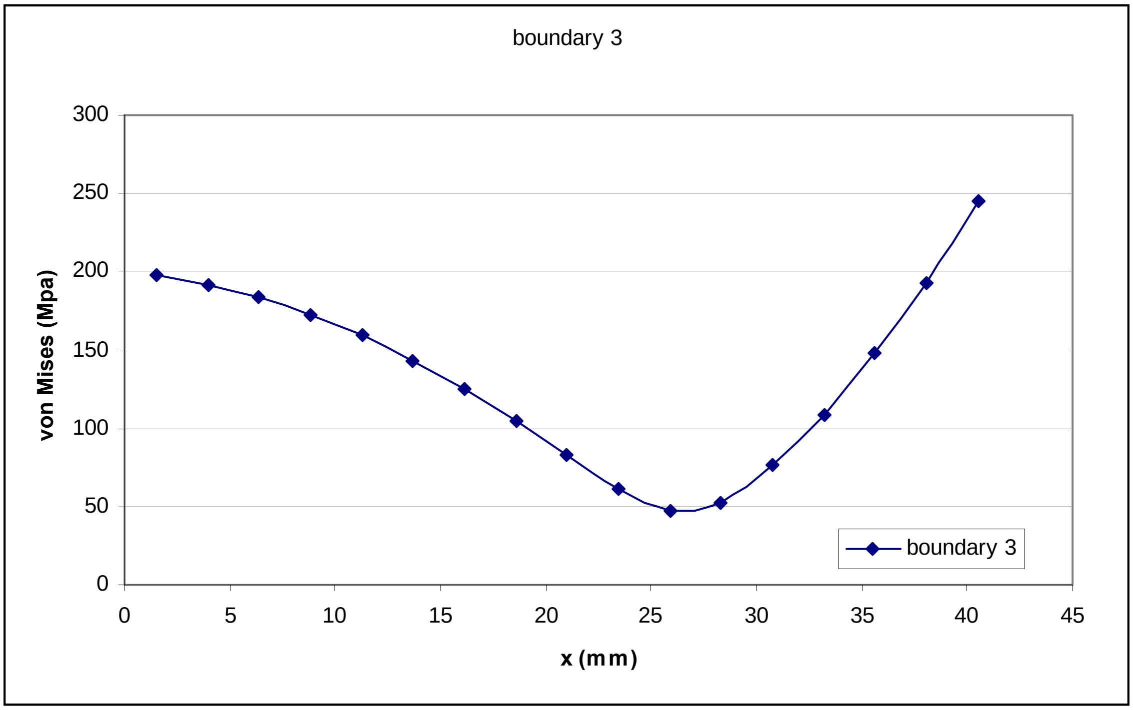

Figure 15 Geometrically non-linear and elastic results at boundary 3 in Figure 4

The procedure is continued until equilibrium is reached and the calculated displacement is a small fraction of the original displacement. The solution technique used by ABAQUS is the full Newton's method, in which the stiffness matrix used at each increment is modified by the current displacement estimate and an equivalent or tangent stiffness in the load versus displacement curve is used to calculate the new estimate. By comparing both analyses it is seen that displacements and stresses on the geometrically non-linear analysis are less than half of those computed in the linear analysis. This can be explained by the fact that membrane action provides additional stiffness not considered on the geometrically linear analysis. Because stresses are still well over the yield strength a non-linear analysis is justified.

4.4 Geometrically Non-linear and Elastic-Plastic Analysis

In this third analysis, two types of non-linearity are included simultaneously: namely material and geometric non-linearity. Material plasticity introduces additional complexity to the problem. When the yield strength is exceeded in an elastic-plastic material, the loading history plays an important part on the final state of the structure. For the present case the load is assumed to be statically applied and time independent.

In order to perform an elastic-plastic analysis, three aspects must be taken in consideration: the yield criterion, the flow rule, and the hardening rule. Normally the yield criterion determines when the material starts yielding and it is stated in terms of the von Mises or effective stress. Once this point is reached, the flow rule relates the state of stress to the state of strain in the material. For an elastic perfectly plastic material there is no hardening and increments in stress beyond the yield point are not possible. In order to determine the response of the structure, an incremental analysis is used in which the elastic modulus depends on the state of stress and elastic and plastic strains are treated independently.

4.5 Geometrically Nonlinear Results Including Ideal Plasticity

The finite element analysis of configuration #3 concluded with 23 increments, in which the occurrence of nonlinear behavior is evident as expected. Stress concentration occurred in the vicinity of the center holes with significant plasticity. Figures 16 and 17 show displacement and von Mises stresses computed at the same place as in the previous linear results but now for the nonlinear and elastic-plastic assumption. The displacements in Figure 16 are nearly half the displacements plotted in Figure 9 and many times more than the shell thickness, indicating that a nonlinear analysis is necessary in order to predict a more representative behavior of the structure. As compared to Figure 14, displacements in Figure 16 are a bit higher considering ideal plasticity. On the other hand, the values of von Mises stresses demonstrate that plasticity spreads in a zone extending about 15 mm from the hole on the x-axis and 65 mm on the y-axis as defined in Figure 4 and Figure 18 using orange color. The von Mises stresses in this case are computed as the envelope (maximum stresses) of the top and bottom surfaces in figures 16 and 17 and at the bottom surface in Figure 16.

Using the static strain criterion formulated by Mahaarachchi and Mahendran (2008), which states that failure occurs when the membrane tensile strain is 60% of the maximum surface tensile strength and the maximum surface tensile strain is the failure strain in a tensile coupon test, in conjunction with the finite element model, it is concluded that static failure has not occurred. The maximum tensile strain is the failure strain or elongation as given on the ASTM standard, which is 0.20, and the membrane tensile strain reached its peak at the edge of the hole as will be explained in the next section.

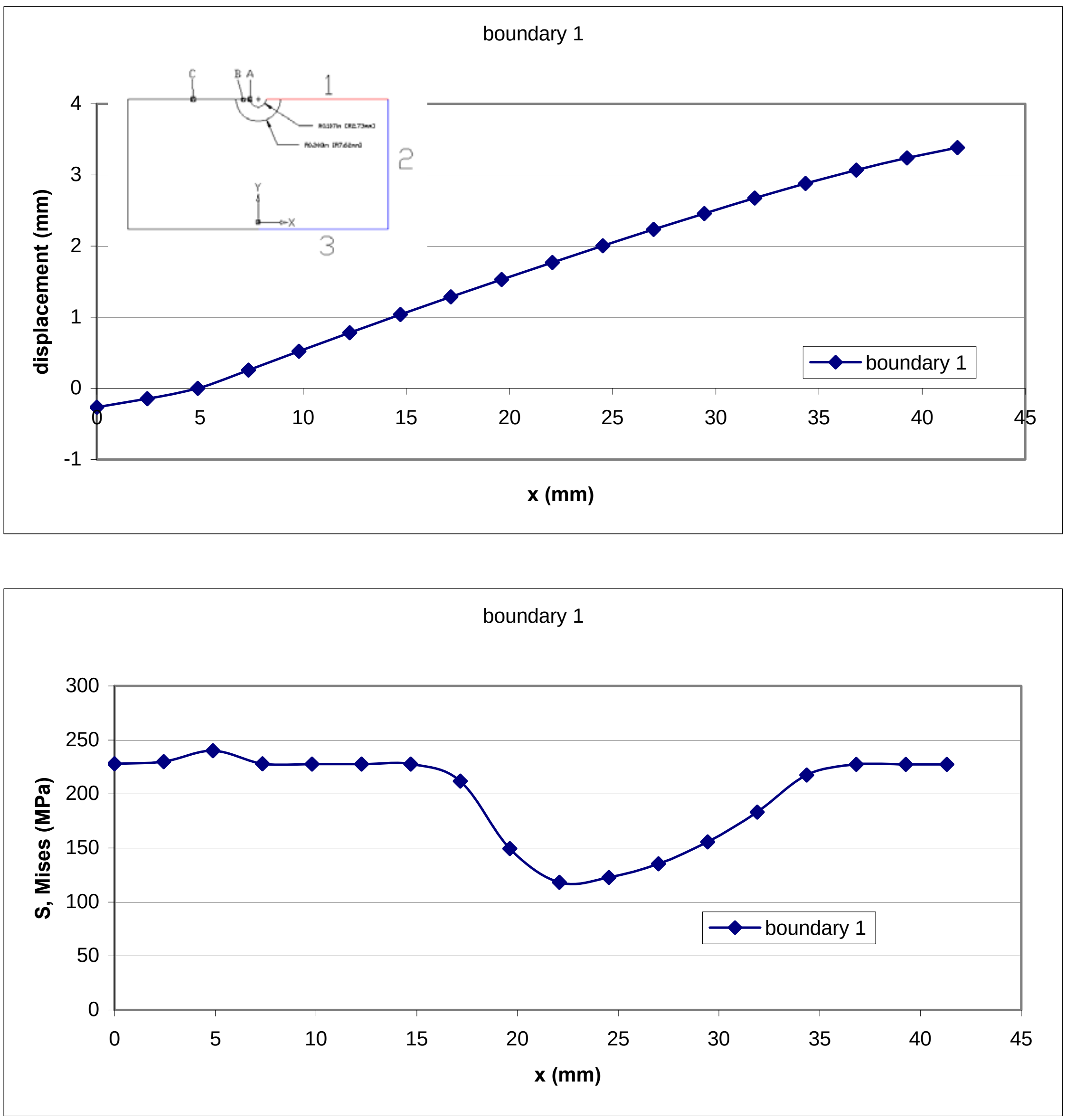

Figure 16 Non-linear results at boundary 1

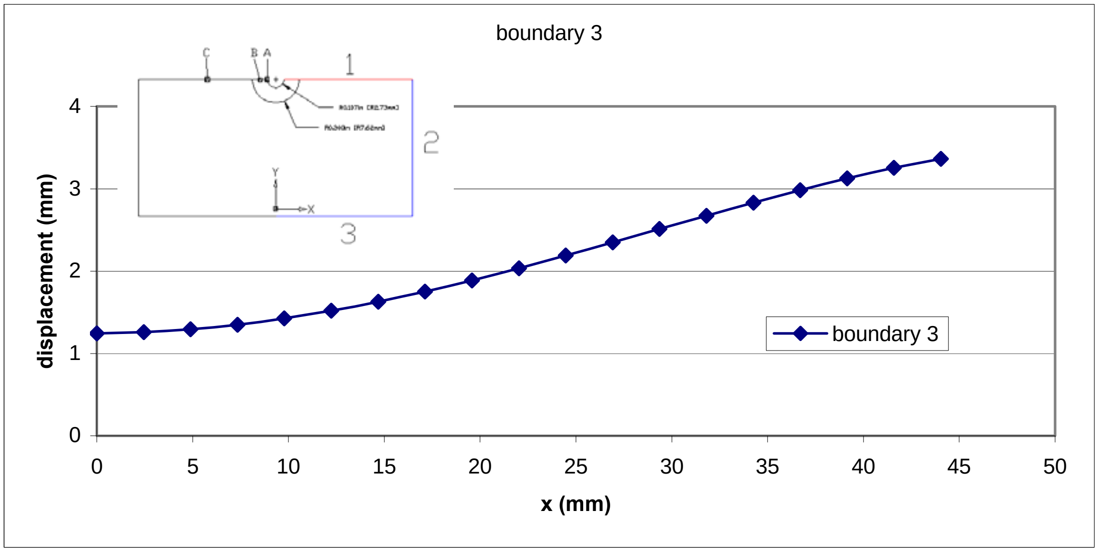

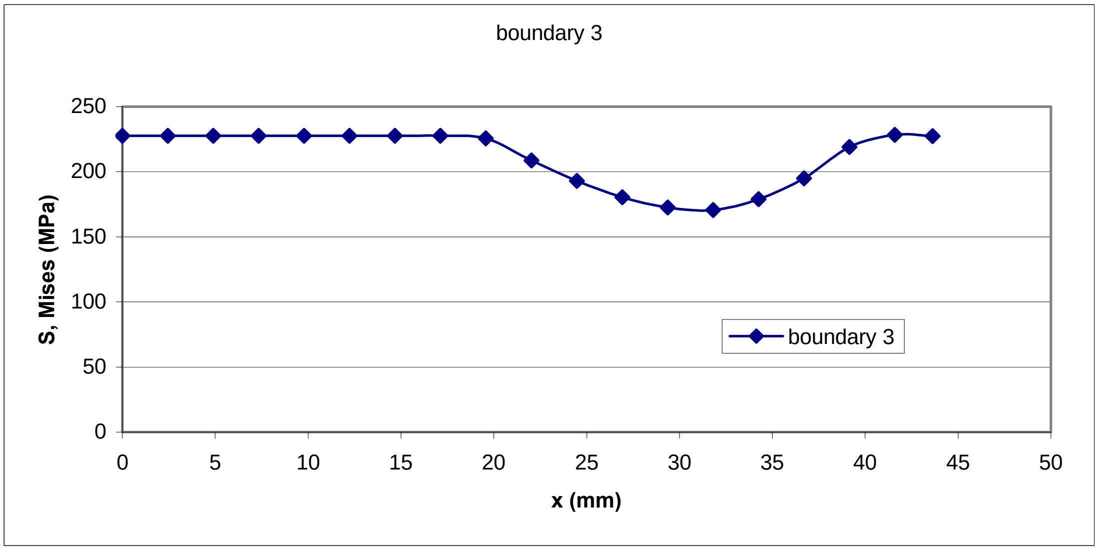

Figure 17 Non-linear results along boundary 3, computed as the envelope of the top and bottom surfaces

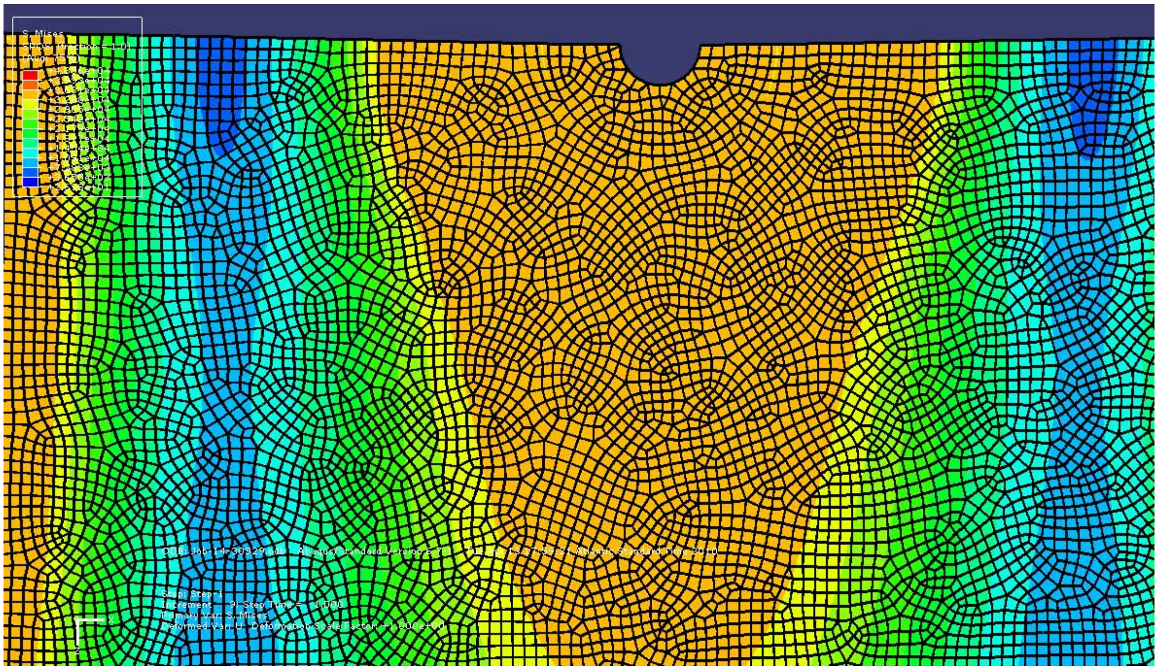

Figure 18 Plastic zone for load P = 5.81 kPa evaluated at the bottom surface

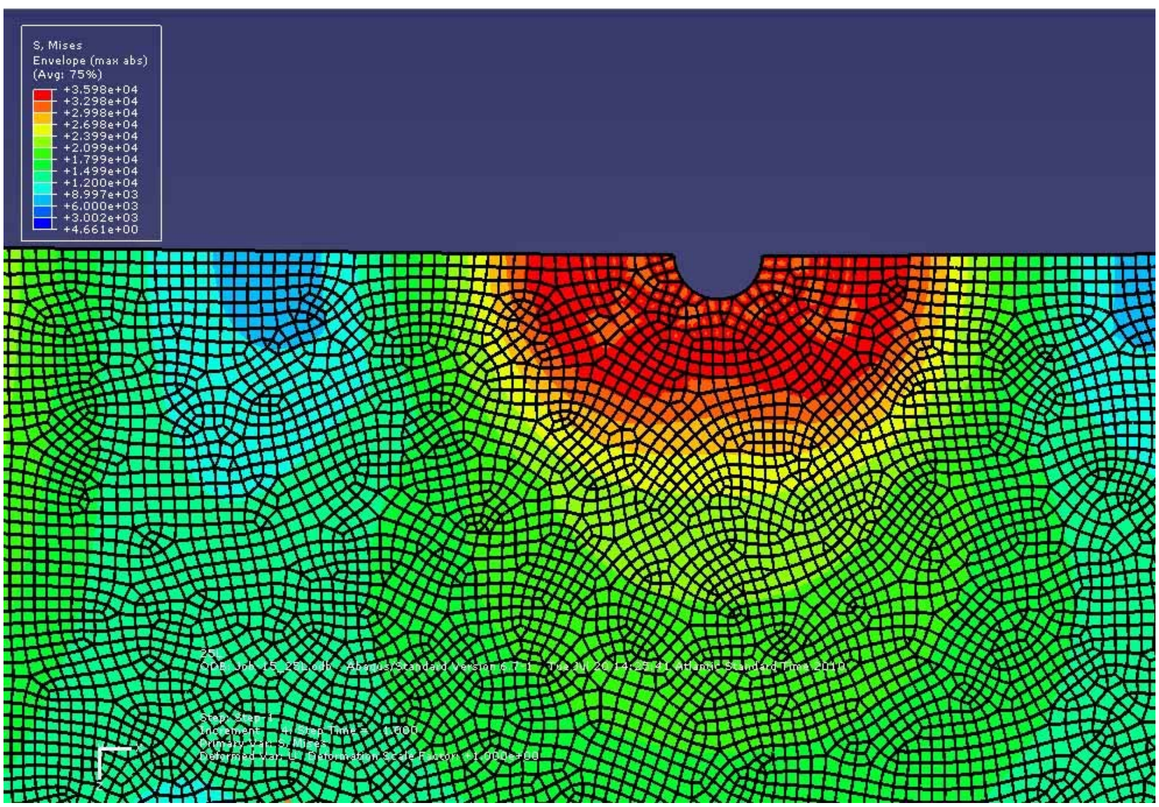

Figure 19 Plastic zone for load 0.25P at the bottom surface

4.6 Typical Center Connection

In a typical screwed connection, the direction of the major principal strain results are shown in Figure 20, where *x* is the distance from the edge of the hole in the *x*-axis defined in Figure 4. The major principal strain corresponds to the radial strain in the x-axis in every point, except for a small region around the circumference of the screw head, where the tangential strain corresponds to the major principal strain as can be seen in Figure 20 at a distance of about 5 mm from the hole. As a result, the maximum shear strain acts at 45 degrees from the principal direction in this configuration. The octahedral shear strain is defined in terms of the components of the strain tensor as:

$$\Delta\varepsilon_{eq} = \frac{1}{\sqrt{2}(1+\nu)}\sqrt{\left(\Delta\varepsilon_x - \Delta\varepsilon_y\right)^2 + \left(\Delta\varepsilon_y - \Delta\varepsilon_z\right)^2 + \left(\Delta\varepsilon_x - \Delta\varepsilon_z\right)^2 + \frac{3}{2}\left(\Delta\gamma_{xy}^2 + \Delta\gamma_{yz}^2 + \Delta\gamma_{xz}^2\right)}$$

The equivalent or octahedral shear strain is expressed in terms of the normal and shear strain components of the strain tensor at a point on the structure as shown in Figure 21.

The peak of the radial strain curve corresponds to a very steep slope or change of the radial strain in the top and bottom surfaces, which is equivalent to a change in radial moment. Consequently this change in moment can be expressed as a shear stress, according to plate theory, corresponding to the screw head reaction force acting at the position of the peak of the curve. The direction of the mayor principal strain corresponds to the *x*-axis in Figure 4 and its magnitude with the bottom surface where the wind pressure is applied. From this information the mechanism by which the steel cladding resists the reaction force of the screw is determined.

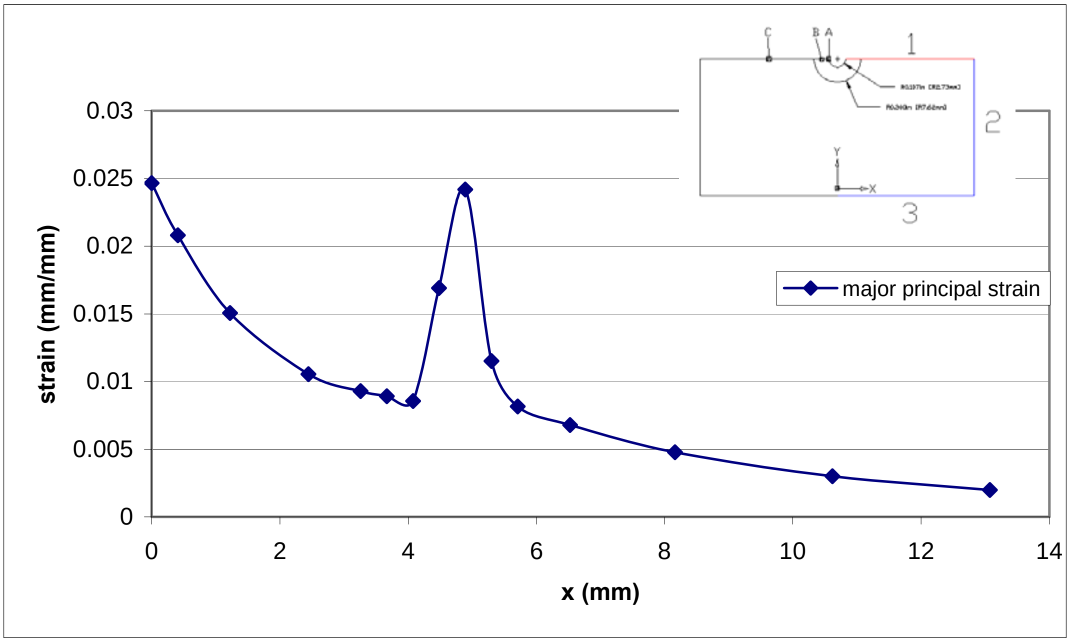

Figure 20a Strain concentration (major principal) at center connection, boundary 1

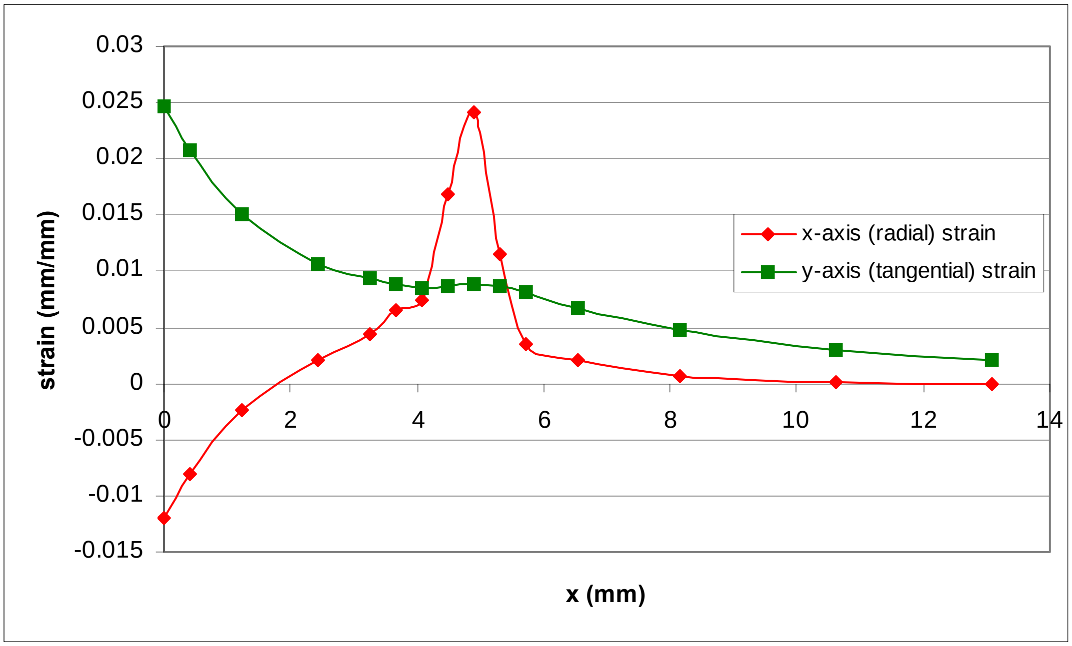

Figure 20b Strain concentration (components) at center connection, boundary 1

If the diameter of the screw head were to be increased, as by adding a washer, it would be equivalent to shifting the radial strain curve in Figure 20b to the right as discussed in Figure 20a where the peak of the curve is caused by the vertical reaction shear force of the screw head or washer. In other words, the washer has the effect of expanding the circumference where the vertical reaction force acts, thus lowering the vertical shear stress as it is distributed over a larger perimeter. Because shear can be expressed in terms of change in bending moment, the change in moment is also lowered. This would translate in a less pronounced peak on the radial strain curve.

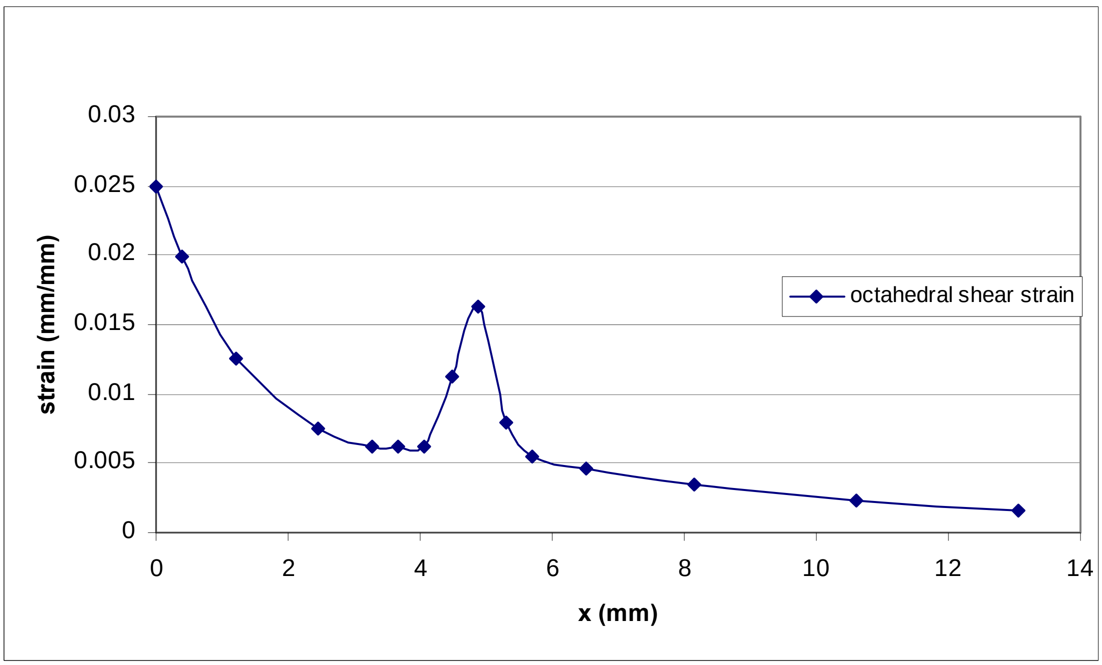

Figure 21 Octahedral shear strain at center connection, boundary 1

4.7 Discussion of Results

In the previous section on modeling of screwed connections, a model of the connection was defined where bending as well as membrane stresses were taken into account and appropriate boundary conditions defined. Now we can see the role that bending and membrane components play in resisting the reaction force from the screw and the effect of the screw hole on strains and stresses. Radial strains in the top and bottom surfaces, which are a measure of curvature, increase rapidly as they get closer to the circumference of the screw. Curvature in the radial direction (boundary 1) indicates that bending is responsible for high radial strains near the screw head. Strains on the mid-surface are above the yield strain under the screw head and are amplified by a factor of three by stress concentration around the screw hole. Comparing the linear analysis results with the nonlinear results may highlight the effect that the membrane stresses have. The nonlinear results show that displacements are almost half of the displacements in the linear analysis when considering non-linearity in geometry given that membrane action provides additional stiffness not considered in a linear analysis.

Chapter 5: Results of Fatigue Analysis

5.1 Fatigue Analysis Methodology

In order to predict fatigue life using total life approaches, several aspects need to be taken into consideration. First, it is necessary to determine if a stress-based or strain-based approach is appropriate. In order to use either approach, multiaxial stress effects, mean stresses, and variable amplitude loading have to be taken into account.

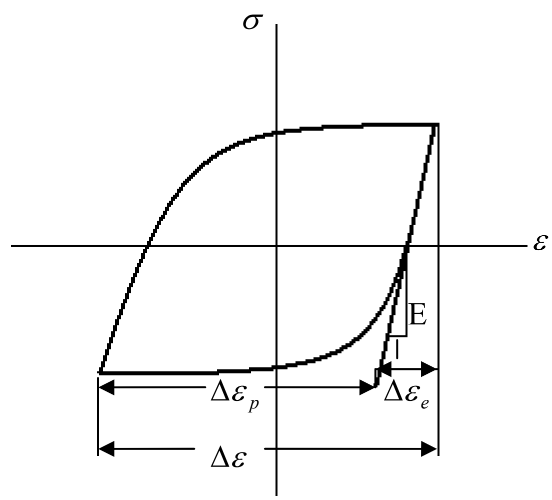

Figure 22 Completely reversed loading cycle (R = -1)

In general a loading cycle is composed of elastic and plastic deformation components as shown in Figure 22. For the present case it is assumed that loading is not completely reversed since the load P is defined to act always in the same direction and instead the stress ratio $R = 0$ is used for tension loading in the bottom of the plate. From the finite element model the maximum stresses and strains occur on the bottom surface because of stress concentration at the edge of the hole on the center connections as defined in Appendix B. When loading is removed the stresses return to zero and permanent plastic deformation remains, as shown in Figure 23. The fatigue process depends on several variables depending on the fatigue model to be used. These are maximum normal stress and strain amplitude, octahedral shear stress amplitude and mean stresses. It is noted that fatigue damage is independent of mean strains and hence, total plastic deformation. Since loading and unloading does not cause further plastic deformation on any given loading sublevel we are left with the elastic part of the cyclic hysteretic loop depicted by the dark colored line on the right of Figure 23. It is noted that some metals exhibit cyclic hardening while others exhibit cyclic softening when subjected to repetitive loading as shown on the light colored lines in Figure 23. The curved line to the right represents cyclic softening behavior characterized by having a yield strength lower than the nominal value and plastic deformation taking place as cycling continues. In comparison, the light colored line to the left represents cyclic hardening in which higher loads eventually increase the yield strength but without cyclic plasticity taking place on the same load level. This will have an effect on the monotonic behavior as compared to the cyclic stress-strain response for a given material.

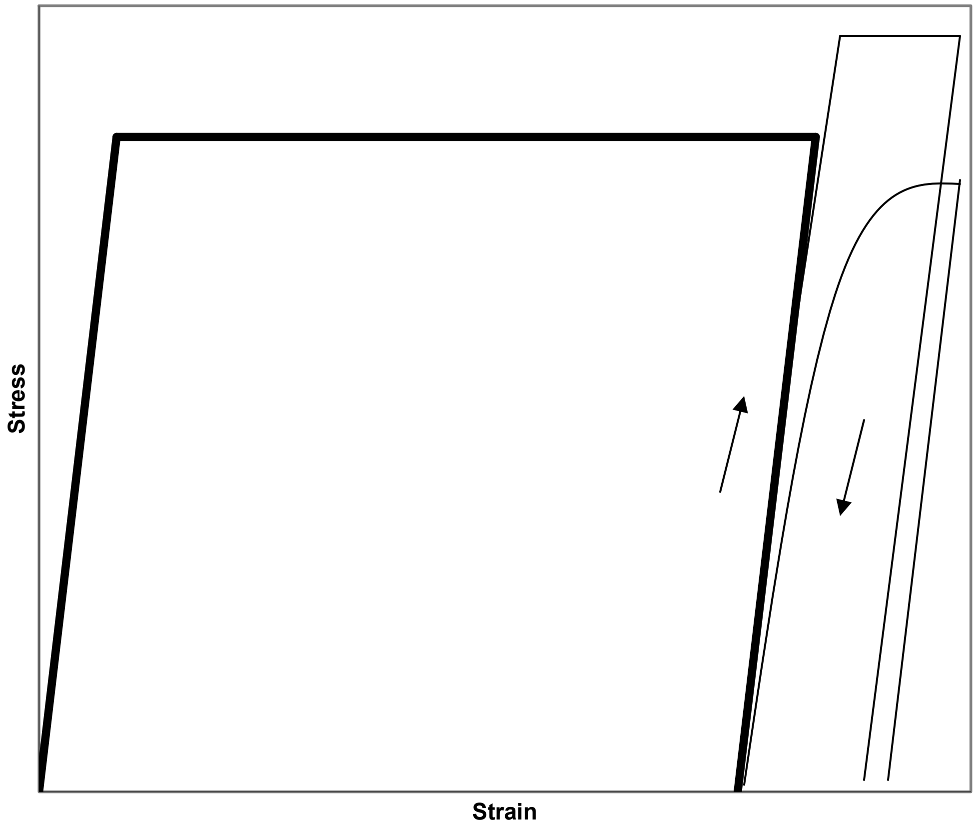

Figure 23 Plastic deformation and hysteretic loop for tension loading (R = 0) on one sublevel of the Sidgers protocol defined in Figure 24

If cyclic softening is considered one would expect to have a small increase on total plastic strain consisting of the sum of each individual plastic strain component taking place at each cycle until a stable behavior is achieved at a considerable portion of the fatigue life or by structural constraint along stress gradients or redundant equilibrium of forces on the structure. These plastic strain components are considered to be a small portion of the total strain amplitude and may be neglected on the fatigue damage predicted by equation 9. On the other hand if cyclic hardening is considered, the elastic strain amplitude may increase by a small amount at some fraction of the fatigue life until reaching a stable behavior without having cyclic plastic strain. For metals with an ultimate strength to yield strength ratio between 1.2 and 1.4, which is the case here, a metal is said to be generally stable but may harden or soften (Mitchell 1992). A stable behavior in which there is no cyclic hardening or softening is considered for the present case based on the ultimate to yield strength ratio.

In the strain-life curve also called the Coffin-Manson relationship, the strain amplitude ε_a is assumed as the sum of elastic and plastic components in the form:

$$\varepsilon_a = \frac{\sigma'_f}{E}\left(2N_f\right)^b + \varepsilon'_f\left(2N_f\right)^c \qquad \text{(eq. 9)}$$

where b is the slope of the elastic part and c is the slope of the plastic part of the strain-life curve on a logarithmic plot (Coffin 1971). If we eliminate the plastic component on the right side and multiply both sides by E, we are left with the classical stress-life equation as:

$$\sigma_a = \sigma'_f\left(2N_f\right)^b \qquad \text{(eq. 10)}$$

where σ_a is the alternating stress and σ'_f is the true fracture stress. In order to take into account mean stress effects, Morrow (1965) proposed to modify the number of cycles to failure as follows:

$$N_f = N_M\left(1 - \frac{\sigma_m}{\sigma'_f}\right)^{1/b} \qquad \text{(eq. 11)}$$

Substituting for N_f in equation 9 gives:

$$\varepsilon_a = \frac{\sigma'_f}{E}\left(1 - \frac{\sigma_m}{\sigma'_f}\right)\left(2N_M\right)^b + \varepsilon'_f\left(1 - \frac{\sigma_m}{\sigma'_f}\right)^{c/b}\left(2N_M\right)^c \qquad \text{(eq. 12)}$$

where σ_m is the mean alternating stress. Upon eliminating the plastic component, we are left with the stress-life relationship that includes the mean stress effect.

$$\sigma_a = (\sigma'_f - \sigma_m)(2N_M)^b \qquad \text{(eq. 13)}$$

Here the stress amplitude and mean stress are calculated from the major principal stress. Goodman (1899) proposed the following relation for addressing mean stresses:

$$\frac{\sigma_a}{\sigma_{am}} + \frac{\sigma_m}{\sigma_u} = 1 \qquad \text{(eq. 14)}$$

where σ_{am} is the equivalent stress amplitude for completely reverse loading that addresses the mean stress effect and the stress amplitude and mean stress are calculated from the Von Mises stress. Using the classical stress-life equation in terms of σ_{am} and a modified number of cycles to failure N_G:

$$\sigma_{am} = \sigma'_f (2N_G)^b \qquad \text{(eq. 15)}$$

Substituting for σ_{am} from equation 14:

$$\sigma_a = \sigma'_f \left(1 - \frac{\sigma_m}{\sigma_u}\right)(2N_G)^b \qquad \text{(eq. 16)}$$

The Morrow equation is similar to that due to Goodman, except for using the true fracture stress instead of the ultimate strength.

Another approach to the mean stress effect is due to the Smith, Watson, and Topper parameter (1970), which was developed for materials that fail predominantly on maximum tensile stress or strain planes. According to SWT the life for any situation of mean stresses depends on the product of maximum stress times strain amplitude on the principal plane and the resulting equation is:

$$\sigma_{\max}\varepsilon_a = \frac{(\sigma'_f)^2}{E}(2N_{SWT})^{2b} + \sigma'_f\,\varepsilon'_f\,(2N_{SWT})^{b+c} \qquad \text{(eq. 17)}$$

where $\sigma_{\max}$ is the major principal stress and N_{SWT} is the corresponding number of cycles to failure. Upon eliminating the plastic component of strain the SWT equation results in:

$$\sigma_{\max}\varepsilon_a = \frac{(\sigma'_f)^2}{E}(2N_{SWT})^{2b} \qquad \text{(eq. 18)}$$

or

$$\sigma_a = \frac{(\sigma'_f)^2}{\sigma_{\max}}(2N_{SWT})^{2b} \qquad \text{(eq. 19)}$$

Fatigue data collected for different materials shows that the fatigue process may be divided into three regions: nucleation, shear, and tension. The extent of each region in the fatigue life depends on the material and type of loading. As a result the choice of the fatigue model will also depend on these factors. Evidence shows that at a high number of cycles fatigue is dominated by tension and at low numbers by shear (Hua and Socie 1985; Socie et al. 1989; Bannantine and Socie 1985). Also at high lives or number of cycles, fatigue is dominated by elastic deformation as compared to plastic deformation at low lives as predicted by equation 9. Upon this premise it can be concluded that tension damage is dominated by elastic deformation and shear damage by plastic deformation. This fact is also seen in brittle materials, which fail in tension with no plastic deformation, as opposed to more ductile materials, which fail predominantly in shear and exhibit large plastic deformation.

In our case, where there is a mean stress, there is an exception from the above discussion, which applies for completely reversed cycles with zero mean stress. In this case, considering only tension loading, fatigue will be dominated by elastic deformation at low lives. This is a direct consequence of the mean stress effect given that mean stresses increase the fatigue damage caused by elastic deformation at low lives. As a result damage will be accumulated in the low cycle range and failure will occur before reaching the high cycle range. Tension models such as SWT should work better in predicting the fatigue life. Other critical plane models, such as Brown and Miller, and Fatemi and Socie, which were developed predominantly for shear damage require tension and torsion fatigue test data, which is not readily available.

Finally the Palmgren-Miner rule is used in order to take into account variable amplitude loading.

$$\sum_i \frac{n_i}{(N_f)_i} = 1 \qquad \text{(eq. 20)}$$

where n is the number of cycles at the stress level i at which N_f cycles would cause failure. Palmgren-Miner's linear damage rule has some limitations because the order in which distinct amplitude cycles are applied is found to have an effect on fatigue damage. Mahendran and Mahaarachchi (2002) suggested that Miner's rule should be modified in order to take into account experimental evidence from multilevel cyclic tests performed on claddings. The modified Miner's rule is as follows:

$$\sum_i \frac{1}{K} \frac{n_i}{(N_f)_i} = F \qquad \text{(eq. 21)}$$

where K is a modification factor equal to 0.7 and F equals the fatigue damage being zero for no damage and 1 for 100% damage, meaning that the fatigue life or number of cycles to failure has been reached. Although a better model can be constructed in which damage can be divided depending on the nature of loading, such as shear or tension, the total life is computed with just one model because in this case we are not dealing with combined loading. In order to get the equivalent stress and strain amplitude, the load sequence shown in Figure 24 is used on the finite element model and the number of cycles in each sublevel is multiplied by 5. For any level greater than E, the same sequence as on level E is used but the maximum load is increased by 0.25 on each subsequent level (e.g. level F has the same number of cycles and the same sequence as level E but with a load P = 2.25). For each load increment the cyclic stress-strain diagram has a specific path in which the order of load increments as well as loading history are necessary to determine the fatigue damage, as depicted in Figure 25.

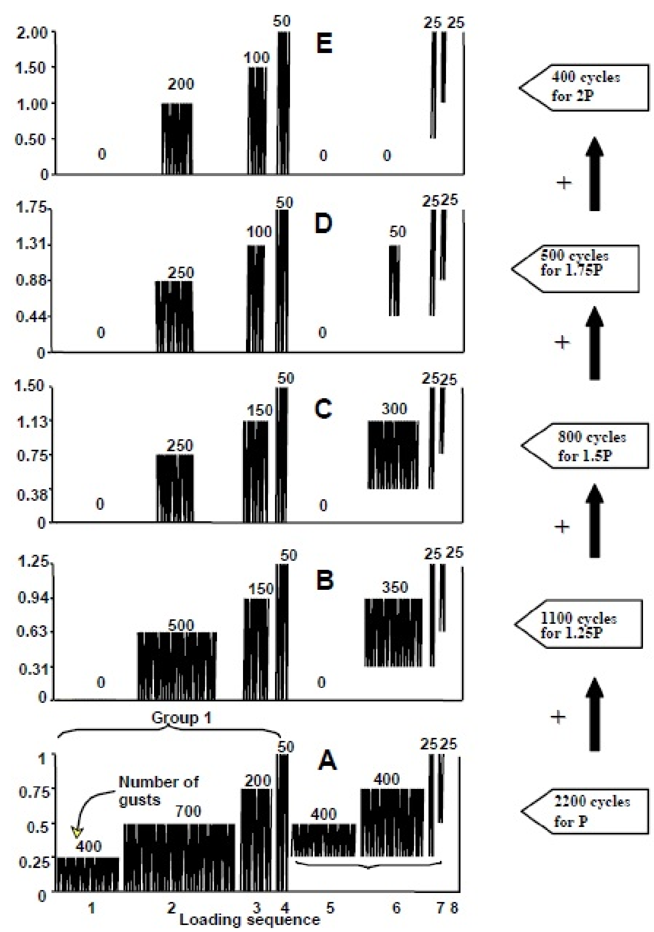

Figure 24 Load sequence used in Sidgers protocol (Baskaran et al. 2006)

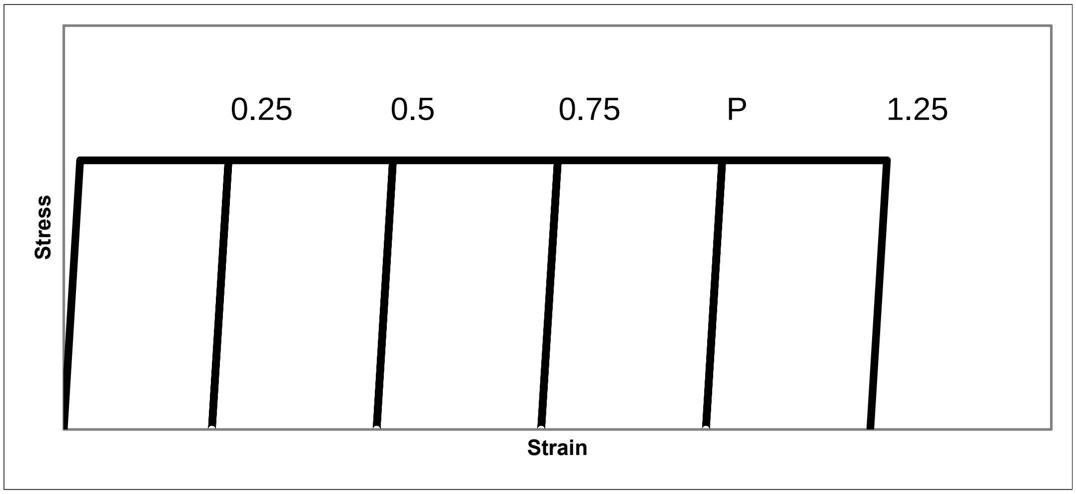

Figure 25 Cyclic stress-strain diagram

As the load increases in the first loading sequence, the equivalent strain passes the yield point until it reaches a plastic strain corresponding to a load of 0.25 *P*. When the load is removed in the first cycle the unloading path follows the second line until zero stress and permanent deformation remains. The loading and unloading cycle of the first load increment will remain on the second line as depicted in Figure 25 and considering a stable behavior as discussed in Figure 23. In the next load increment the process is repeated by shifting another half cycle to the right until the maximum increment corresponding to load *P* is reached on sublevel A4 of Figure 24. When the load is decreased on sublevel A5 from *P* to 0.25 *P* and then increased to 0.5 *P* the loading and unloading path remains as on sublevel A4, except that it will cover a smaller portion of stress and strain corresponding to 25 percent of the total trajectory. This is due to the strain hardening effect that the higher load had on the material and the stress and strain will be proportional to the load at any given unloading and reloading path for which the load does not exceeds the previously applied maximum load. The proportionality of the stress and strain in the unloading and reloading paths can be proven since on any specific path the maximum strain range will not exceed the elastic strain range for the elastic-plastic material definition on any given point in the structure. Because elastic strains are very small in comparison with plastic strains, the structure will not undergo large deformations beyond the previous permanent deformation in the elastic strain range. The element stiffness matrix will remain unchanged within any specific elastic strain range, and thus the proportionality assumption will remain valid. The remaining load increments on level A will remain on the same path but covering a greater portion depending on the amount the load is increased. For example consider load sublevel A6. Because the maximum load on sublevel A6 is $0.75P$ which is less than P from load sublevel A4, the loading and unloading path will remain as on sublevel A4 but the maximum stress will be 75% of the maximum stress on load sublevel A4 and the minimum stress would be 25% as proportional to the load. Sublevels B2 and B3 will also remain on the same path as no further plastic deformation is taking place. Upon reaching sublevel B4 corresponding to 1.25 P the loading path is continued until the total strain reaches the next cyclic step. The cyclic stress-strain diagram can be resumed by plastic and elastic strain components, where plastic strains correspond to horizontal lines and elastic strains to vertical lines in Figure 25. Because cyclic loading is not completely reversed and instead only tension loading acts at the bottom of the plate, where stress concentration occurs, only elastic strain plays an important role on fatigue. The other half cycles corresponding to transitions between load increments, where plastic deformation occurs, are ignored for determining the fatigue life, first because plastic fatigue parameters are unknown, and second because the fatigue damage done on these half cycles is not believed to be significant.

There are several methods for approximating fatigue parameters from monotonic tensile tests. The method of universal slopes (Manson 1965) is chosen in this thesis since it will be proven to yield good results later. From the method of universal slopes the fatigue strength coefficient and fatigue strength exponent are approximated from monotonic tensile tests parameters by the following equations.

$$\sigma'_f = 1.9018\sigma_u$$

$$b = -0.12$$

Another method, which only requires the ultimate strength, is the Uniform Material Law (Bäumel and Seeger 1990). From this method the fatigue parameters can be approximated by the following equations.

$$\sigma'_f = 1.5\sigma_u$$

$$b = -0.087$$

5.2 Fatigue Analysis Results

Using the total life approach, the strain-life method yields the same result as the stress-life method because of the load cycle occurring in the elastic regime. Results are compared for three different approaches of mean stress analysis and for two material definitions. Appendix C lists accumulated fatigue damage at each sublevel of the loading sequence for the elastic perfectly plastic material assumption and Appendix D is the same but with the strain hardening material assumption. These three approaches considered, namely Morrow, Goodman, and SWT, are based on the stress life equation 10, which accounts for the elastic strain range term of the strain-life equation.

Twelve cladding configurations were studied and compared with results obtained by García (2008). In these configurations thickness, location and type of screwed connections, and load P were varied as described in Section 3.4. From these, four are valley fixed, four are crest fixed and four are washer reinforced valley fixed connections. Appendix C and D list the fatigue damage calculated at each loading sublevel for the elastic-plastic and strain hardening material definitions respectively. From the finite element and fatigue models all configurations that yielded in the first loading sublevel yielded the same results for the von Mises stresses and the elastic-plastic material definition in contrast with the strain hardening material definition given that after first yield the calculated von Mises stress is equal to the yield stress for every configuration in the elastic-plastic material definition. For this reason the fatigue damage calculated with the Goodman approach, which is used with the von Mises stress, is expected to yield the same fatigue damage for every configuration on a given sublevel that yielded in the first loading sublevel.

For the comparison of fatigue models the reader is referred to Figure 26. The number of cycles to failure in this figure are N_M for Morrow, N_G for Goodman, and N_{SWT} for the Smith, Watson and Topper methods. The figure uses a mean stress of 113.8 Mpa, which is half of the yield strength, and the universal slopes method. The horizontal line crosses the curves at an alternating stress equal to the mean stress of 113.8 Mpa for tension loading. At this alternating stress SWT falls between Goodman and Morrow. The Goodman approach is the most conservative taking into account that Goodman gives good results for brittle materials and is more conservative for ductile materials. This should be the case given that the fatigue damage is being caused by elastic deformation and a brittle failure is expected.

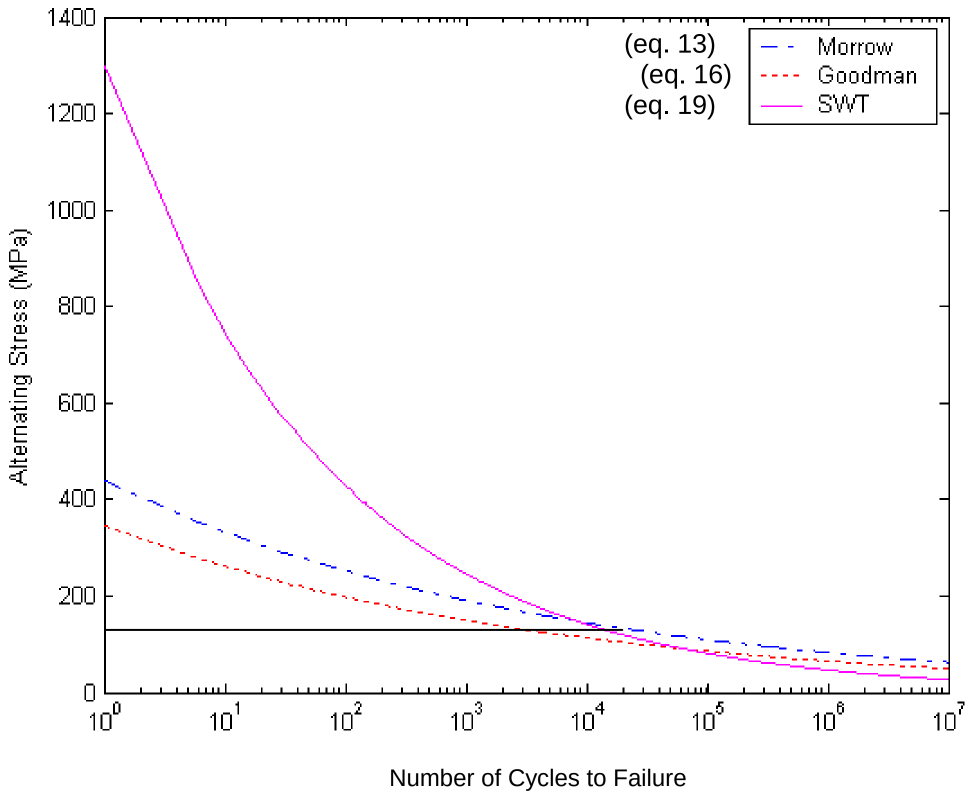

Figure 26 Comparison of Fatigue Models for the universal slopes method

5.3 Discussion of Results and Parametric Studies

Equation 10 is the basic stress-life equation that is used to calculate the fatigue life. In order to use this equation, the two parameters σ'_f and *b,* which are not provided in the ASTM standard, need to be calculated. The first one is the true fracture strength or fatigue strength coefficient and the second one is the slope of the log-log plot of the elastic component of the equation or the fatigue strength exponent. These two parameters are approximated by the universal slopes method and the uniform material law and correlated to monotonic tensile test parameters. These parameters are usually used to fit the strain-life equation to the fatigue tests data.

Figure 27 shows the fatigue damage for the 12 configurations defined in Table 1 calculated and plotted at the middle of the loading sublevel in which failure was observed in experiments performed by García (2008). Figure 28 shows the same results but with the strain hardening material definition instead. From these two figures it is concluded that the elastic-plastic material definition provides a better correlation for all three of the fatigue models than the strain hardening material definition since Figure 27 shows less scattering around the expected value of $F = 1$.

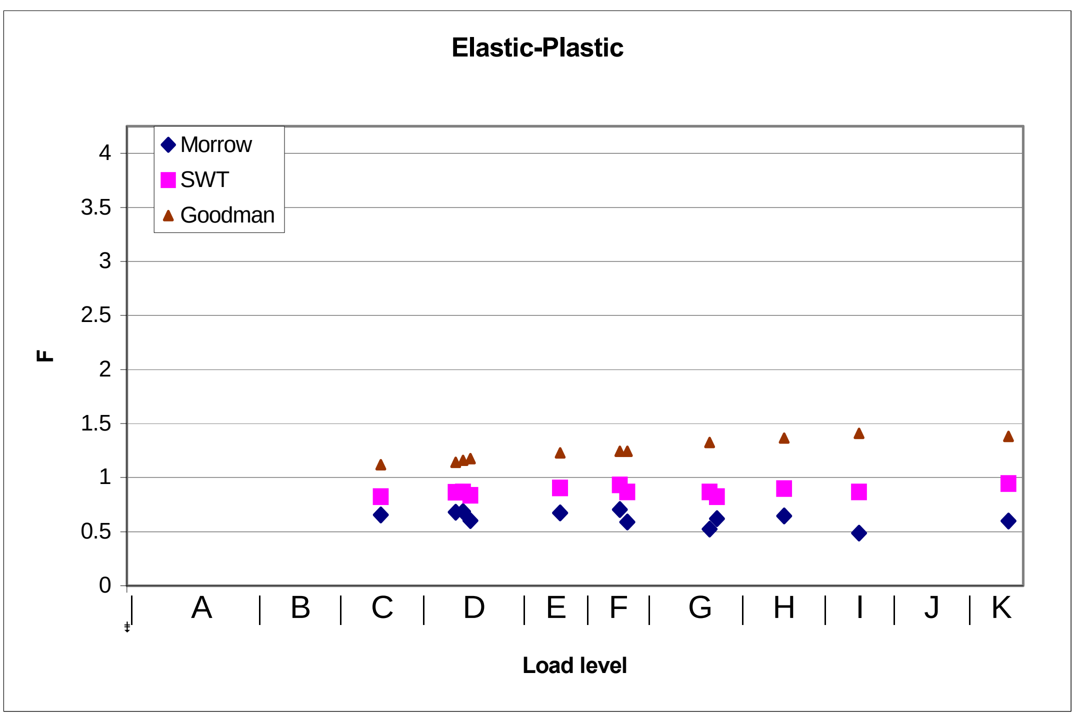

Figure 27 Comparison of fatigue models for the elastic-plastic material definition

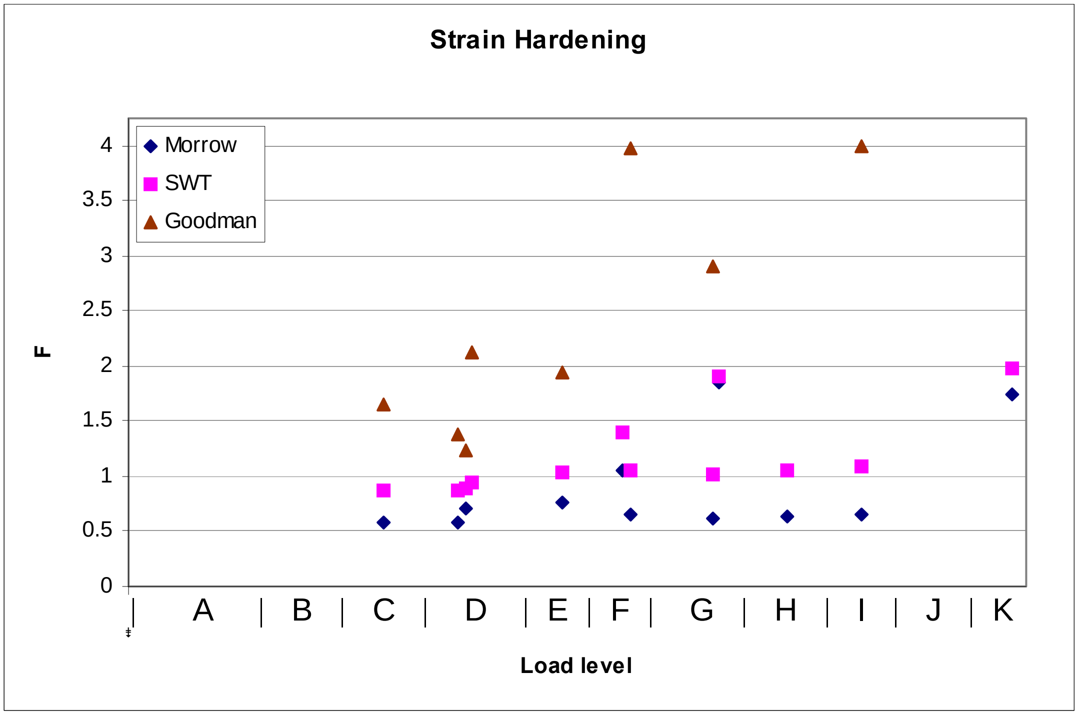

Figure 28 Comparison of fatigue models for the strain hardening material definition

Figure 29 is an expansion of Figure 27 and Table 6 lists the average and standard deviation of the fatigue life computed for each model. From the last row of Table 6 it is concluded that SWT provides the best correlation with a value of dispersion of nearly half of the other two fatigue models since SWT uses two parameters from the stress-strain tensor instead of one.

Figure 30 shows the SWT approach on Figure 29 for the different types of connections. From Figure 30 it is concluded that the fatigue damage calculated is independent of the type of connection, number of screws and configuration meaning that the SWT – elastic-plastic model works well with all 12 configurations predicting an average fatigue damage of 0.875. This value suggests that the fatigue model should be modified in order to fit the experimental data for which the expected fatigue damage is 1.

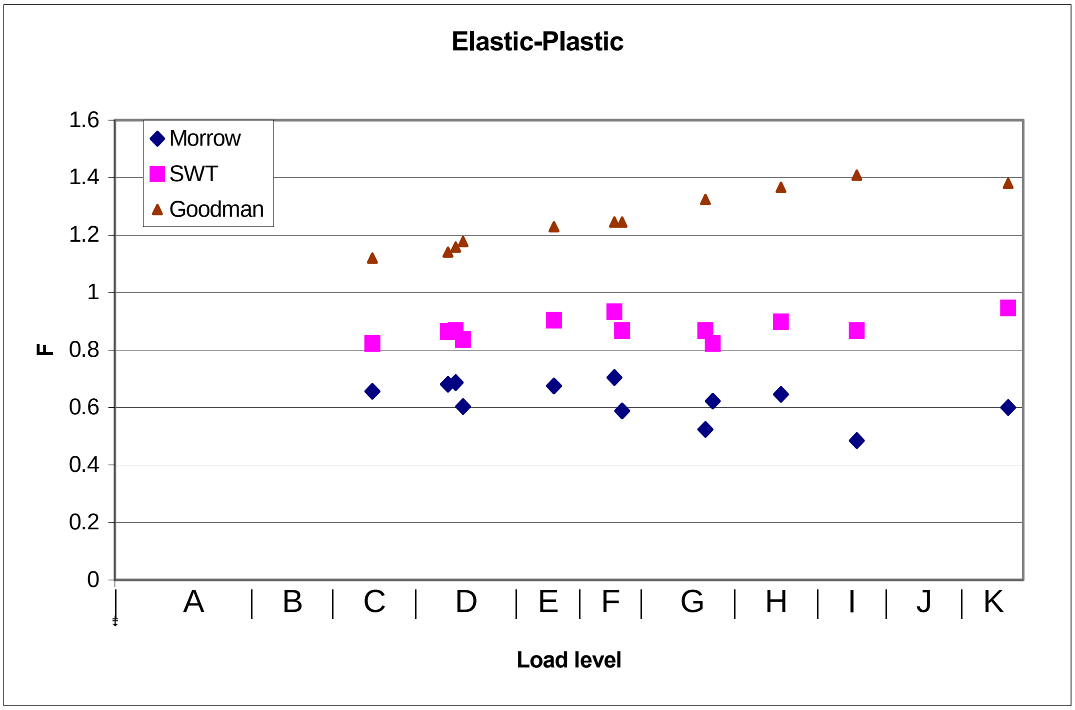

Figure 29 Comparison of fatigue models for the elastic-plastic material definition

Table 6 Fatigue damage average and standard deviation for the 12 configurations

	Goodman	Morrow	SWT
μ	1.269	0.623	0.875
s	0.1296	0.0671	0.0392
s/μ	0.1021	0.1078	0.0448

where μ is the sample mean, s is the sample standard deviation and s/μ is a measure of dispersion of the fatigue life F.

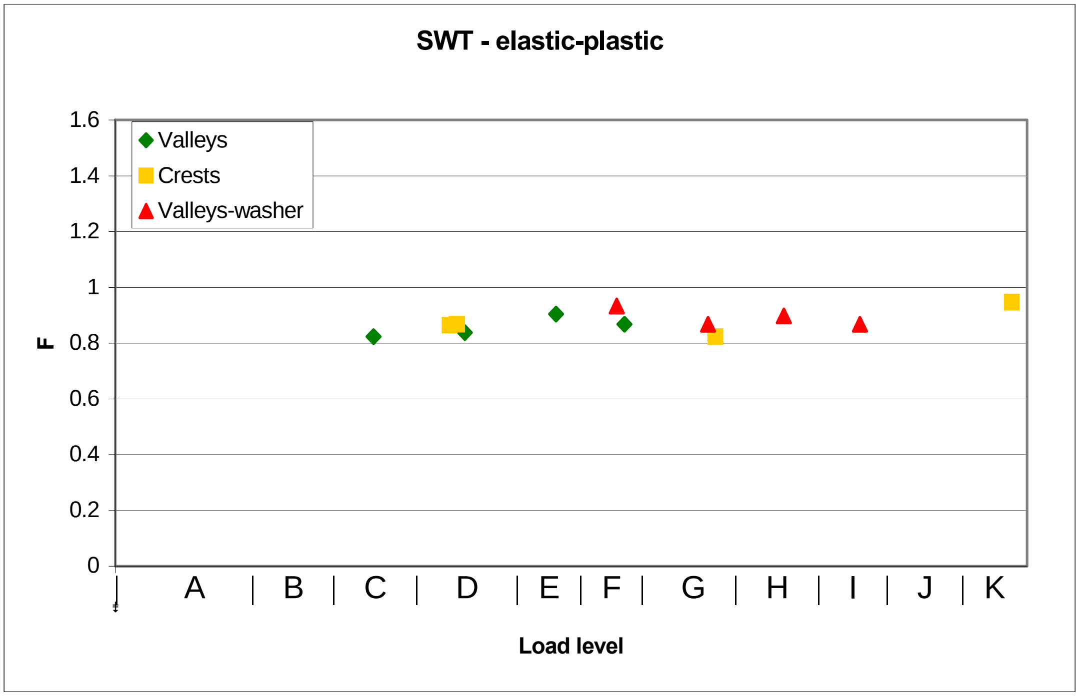

Figure 30 Comparison of connection types and fatigue damage

5.4 Development of a Suitable Parameter Estimation Method

In the previous section a fatigue model and material definition was found that correlated with the experimental data. The fatigue parameters used in the previous section were calculated using the universal slopes method proposed by Manson (1965). This method was developed mainly for completely reversed loading (R = -1), for a wide range in the number of cycles, and for the classic strain-life equation 9. In this section a new parameter estimation method is proposed for tension loading (R = 0), low cycle fatigue, and to be used with the SWT equation 19.

In the previous section the dispersion was defined as the ratio of sample standard deviation to the mean in the calculated fatigue life for the 12 configurations. This ratio is used in order to compare the dispersion of different models relative to the mean. In order to adjust the SWT – elastic-plastic model to more precisely fit the experimental data, the fatigue strength exponent b is changed using an iterative approach in order to minimize the dispersion. This parameter has to do with the shape of the curve in Figure 26. Once the dispersion is minimized, the true fracture stress σ'_f is changed using an iterative approach so that the mean of the calculated fatigue life of the 12 configurations reaches the expected value of 1. Changing the true fracture stress has the effect of stretching the curve in Figure 26 since it is a coefficient on equation 19 without affecting dispersion. Using this approach the fatigue parameters σ'_f and b were found.

$$\sigma'_f = 1.87\sigma_u$$

$$b = -0.12$$

Since the dispersion did not decreased by a significant amount by changing the fatigue strength exponent b then it is concluded that the value suggested by the universal slopes method of –0.12 is suitable to be used with the SWT fatigue model.

Figure 31 and Table 7 show the same results as Figure 30 and Table 6 but with the values of the fatigue parameters used to fit the experimental data proposed in this new method. Results are listed in Appendix E.

The fatigue damage calculated at the middle of the sublevel of the observed failure for the 12 configurations and for the proposed method varies between 0.948 and 1.089 damage with a mean of 1 and sample standard deviation of 0.0448. This is the difference in fatigue damage between the experimental result and the computed result. By using the normal distribution and the mean and sample standard deviation of the calculated fatigue damage, the range in fatigue damage for a 90% probability of failure is ± 0.074. For the proposed model to predict failure with a 90% confidence the calculated fatigue damage should fall between 0.926 and 1.074 or if an upper limit is not used 0.943 or higher.

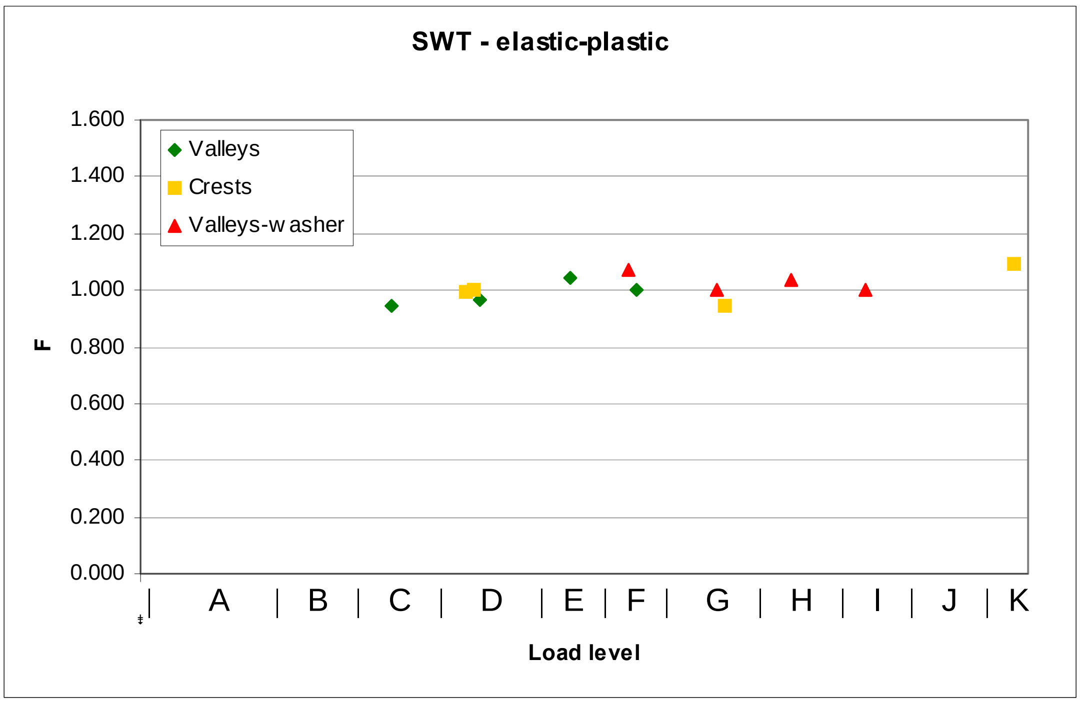

Figure 31 Comparison of connection types and fatigue damage for the proposed method

Table 7 Fatigue life average and standard deviation for the proposed method

	SWT
μ	1
S	0.0448
s/μ	0.0448

5.5 Fatigue failure

Figure 32 shows failures of two screwed connections in valleys due to fatigue. The left image shows the failure with a screw head diameter of 15.2 mm (0.6 in.) whereas the right image shows the same connection but reinforced with a washer with diameter of 38.1mm (1.5 in.). The failure in the right is dominated by vertical and horizontal cracks extending from the screw hole and the failure in the left is composed of smaller diagonal cracks. Once a crack forms, it will grow in mode I as predicted by previous studies (Socie and Marquis 2000). Under mode I loading a crack grows perpendicular to the major principal strain direction. The major principal strain, which corresponds to the tangential strain in Section 4.6, is always tangent to the screw hole. The difference between the two cases in Figure 32 is at the angle where the tangential strain is maximum. The finite element model shows that this angle is not the same for all 12 configurations meaning that the angle of crack propagation is dependent on the number of screwed connections, the thickness of the cladding, and the type of connection as shown in Figure B.1 in Appendix B.

Figure 32 Failure of Screwed connections by García, 2008, pp. 65.

Another finding is that loading sublevels that go after higher amplitude levels cause less damage because elastic deformation is less after permanent plastic deformation requiring a larger load in order to reach the yield strength than before. This can be seen in Appendix C, where most of the damage is on the first four loading sublevels. By comparing the fatigue damage between screwed connections in valleys and the same connections reinforced with washers on the same loading sublevel it is found that adding a washer increases the fatigue life of the connection by an average of 18%. This can be seen by comparing the fatigue damage of configuration 5 with 3, 17 with 15, and 18 with 13 on the same loading sublevel in Appendix C.

5.6 Proposed Method for the Fatigue Life Prediction of Steel Thin-Walled Folded Plates Using an Analytical and Computational Approach

In this section a straightforward method of fatigue life prediction is proposed based on parametric studies done for 12 different cladding configurations. A step by step procedure is stated in terms of finite element modeling considerations and fatigue theory developed throughout this research.

A. Construct a finite element model of the structure.

1. Use symmetric boundary conditions when appropriate in order to reduce computational time as shown in Figure 3.
2. Define the material as elastic perfectly plastic.

3. Identify critical connections carrying a higher load (center connections in this case).
4. Model critical connections by defining the radius of the screw hole and the radius of the largest of the screw head or washer (if reinforced with washer) as defined in Figure 4.
5. Impose displacement restrictions in the direction of the load at the perimeter of the screw head or washer. The other two directions are not restricted in order to model stress concentration around the hole.
6. Define the load (pressure) acting normal to a single plane perpendicular to an axis passing through the center of the screws. The load magnitude has to be defined for each sublevel of the loading protocol for which the maximum load exceeds the previously applied maximum load starting from the first loading sublevel. As an example consider loading level A in Figure 24. In this case only loading sublevels A1, A2, A3 and A4 have to be defined since A5, A6, A7 and A8 do not exceed the load in sublevel A4. The next sublevel would be B4 since it exceeds the load in A4. A separate analysis will have to be run for each load magnitude considered.
7. Choose an appropriate element type and size and construct a coarse mesh in a region surrounding the critical connections and less dense in the rest of the structure in order to reduce computational time. A quadratic shell element is recomended.
8. Use a nonlinear geometric analysis in order to account for large displacements.
9. Run a separate analysis for each load described in step 6 and determine the location of the highest maximum principal stress around the hole at the critical

connections. Normally this location is at the bottom surface where tension exists near the hole and the same location should be used for each load magnitude. If the location changes by changing the load magnitude then a location is chosen so that the calculated fatigue damage in step 14 is maximum. Ignore high stresses at the perimeter of the screw head or washer since in reality the reaction load is transmitted as a pressure and not as a line load and failure is documented to occur at the edge of the hole as explained in Section 5.4. Record the values of the maximum principal stress and maximum principal strain at this location. Reading the values at the element integration point is recommended.

B. Calculate the fatigue damage.

10. Determine the fatigue parameters σ'_f and b as a function of the ultimate tensile strength from the equations proposed in this research.

$$\sigma'_f = 1.87\sigma_u$$

$$b = -0.12$$

11. Determine the strain amplitude ε_a for each loading sublevel.

$$\varepsilon_a = \frac{\varepsilon_{\max}}{2}\left(1 - \frac{P_{\min}}{P_{sub\max}}\right) \quad ; \quad \varepsilon_{\max} \le \varepsilon_y$$

$$\varepsilon_a = \frac{\varepsilon_y}{2}\left(1 - \frac{P_{\min}}{P_{sub\max}}\right) \quad ; \quad \varepsilon_{\max} > \varepsilon_y,\ P_{sub\max} \ge P_{\max}$$

$$\varepsilon_a = \frac{\varepsilon_y}{2}\frac{P_{sub\max} - P_{\min}}{P_{\max}} \quad ; \quad \varepsilon_{\max} > \varepsilon_y,\ P_{sub\max} < P_{\max}$$

where $\varepsilon_{\max}$ is the maximum principal strain recorded in step 9, $P_{\max}$ is the previously applied maximum load starting from the first loading sublevel being zero at the first sublevel as explained in step 6, $P_{sub\max}$ is the maximum sublevel load, and $P_{\min}$ is the minimum sublevel load. It is noted that after first yield the strain amplitude is independent of the maximum principal strain and only depends on the loading sequence.

12. Determine the maximum stress $\sigma_{\max}$ for each loading sublevel.

$$\sigma_{\max} = \sigma_{\max p} \qquad ; \qquad P_{sub\max} \geq P_{\max}$$

$$\sigma_{\max} = \sigma_{\max prev} \frac{P_{sub\max}}{P_{\max}}; \qquad P_{sub\max} < P_{\max}$$

where $\sigma_{\max p}$ is the maximum principal stress recorded in step 9 and $\sigma_{\max prev}$ is the maximum previously applied maximum stress starting from the first loading sublevel.

13. Calculate the number of cycles to failure for each loading sublevel by solving for N_{SWT} in equation 19.

$$\sigma_{\max}\varepsilon_a = \frac{(\sigma'_f)^2}{E}(2N_{SWT})^{2b}$$

where ε_a and $\sigma_{\max}$ were found for each loading sublevel in steps 11 and 12 respectively and σ'_f and *b* were found in step 10.

14. Calculate the fatigue damage *F* by using equation 21.

$$\sum_i \frac{1}{K}\frac{n_i}{(N_f)_i} = F$$

where n is the number of cycles at loading sublevel i, $K = 0.7$ and $N_f = N_{SWT}$ for each loading sublevel. This summation is continued for each loading level until the fatigue damage F exceeds 1 indicating that failure has occurred. Cracks will start at the location determined in step nine and will propagate in mode I (perpendicular to the maximum principal strain direction on the sublevel where F =1), which in most cases is perpendicular to the screw hole.

15. Go to step 9 and check that the location chosen, which is the same for every loading sublevel, gives the highest fatigue damage F. The process may have to be repeated for several locations.

Chapter 6: Conclusions

6.1 Summary of Contributions

In this research the stresses and strains that are responsible for steel cladding failures at the connections have been investigated using finite element analysis. The variable amplitude load associated with wind fluctuations has been reported in Figure 24. Previous studies by García (2008) approached this problem based on full-scale testing under alternating loads. A recent loading protocol established by the Canadian Standards Association has been implemented for rating a specific structure according to the level of wind damage it can withstand.

Structural analysis was used to evaluate stresses under an assumed representation of the loads in the testing procedure. Different fatigue criteria were compared and one was validated in predicting the fatigue damage associated with wind fluctuations.

6.2. Main Conclusions Derived from this Research

From the results obtained in this thesis, several conclusions can be stated about the specific findings:

- The low-cycle fatigue damage of steel cladding configurations is found to be caused by elastic deformation and not by plastic deformation according to the Sidgers protocol as shown in Section 5.1. Because for roof claddings pressure is only applied on the outside where the wind suction forces act, the load always acts in the same direction and only tension loading exists ($R = 0$).

- The order in which high amplitude and low amplitude cycles are applied is found to have an effect on the final fatigue damage predicted after initial yielding occurs. The results supporting this conclusion were presented in Section 5.5 of the thesis. If during the low amplitude cycles initial yielding is reached, then applying the low amplitude cycles first and the high amplitude cycles later will result in a higher fatigue damage than if the high amplitude cycles are applied first.
- A fatigue parameter estimation method is developed which correlates the fatigue parameters with the monotonic tensile properties of the material. This method is developed for low cycle fatigue, tension loading (R = 0), and to be used with the Smith, Watson, and Topper fatigue model as shown in Section 5.4.
- A method for the fatigue life prediction of steel thin-walled folded plates is developed using an analytical and computational approach. This method, which only requires the monotonic tensile properties of the material, can be used to predict a fatigue failure mechanism for different types of connections, thickness, and configurations as shown in Section 5.6.

6.3. Original Contributions of this Thesis

The approach of using analytical methods provides a new insight on the factors that are responsible for fatigue damage and is applicable to a larger selection of configurations and materials that would result too expensive and time consuming to be done by experimental methods. One of the contributions made in this research is to be able to predict the fatigue life of steel claddings under fluctuating wind loads by directly applying fatigue theory using total life approaches. This minimizes the need to perform full-scale and small-scale testing. In order to perform this analysis a new methodology was developed, specifically the application of distinct fatigue and parameter estimation models.

6.4. Recommendations for Further Research

One of the limitations associated with fatigue analytical models is that one model is not applicable to all materials and kinds of loading since the methods presented here were developed specifically for low cycle fatigue and tension loading ($R = 0$). Future work should be aimed at exploring other materials and stress ratios (R). An improved finite element model of the connections can be investigated for a wider range of screws, washers and types of connections. Another important field of investigation associated with this research is the quantification of wind loading fluctuations associated with tropical storms and hurricanes, which are the main cause of steel cladding failure in Puerto Rico and the US. Other variables associated with uncertainties in the prediction of fatigue life such as manufacturing process and microstructure can be investigated.

References

ABAQUS v6.8. Simulia. Unified FEA. Dassault systemes. Warwick, Rhode Island. USA. 2008.

ASTM International. Standard Specification for Steel Sheet, Zinc-Coated (Galvanized) or Zinc-Iron Alloy-Coated (Galvannealed) by the Hot-Dip Process. ASTM-A653-09. American Society for Testing and Materials, West Conshohocken, PA, 2009.

Bannantine, J.A., and Socie, D.F., "Observations of Cracking Behavior in Tension and Torsion Low Cycle Fatigue," ASTM STP 942, American Society for Testing and Materials, West Conshohocken, PA, 1985, pp. 899-921.

Baskaran, A. Molleti, S. and Sexton, M. Wind performance evaluation of fully bonded roofing assemblies. *Construction and Building Materials*. Vol. 22, pp 1-21. 2006.

Bäumel, A., Seeger, T. Materials Data for Cyclic Loading, Supplement 1,Elsevier, Amsterdam, No. 61, 1990.

Boresi, A. P., Schmidt, R. J., Sidebottom, O. M. *Advanced Mechanics of Materials*. Fifth ed. John Wiley & Sons, 1993.

Coffin, L.F., Jr., ''A Note on Low Cycle Fatigue Laws,'' J. Mater., Vol. 6, No. 2, pp. 388–402, 1971.

Cook, R. D., Malkus, D. S., Plesha, M. E. and Witt, R. J. *Concepts and Applications of Finite Element Analysis*. John Wiley & Sons. Fifth ed. 2002.

CSA Number A123.21-04 2004. Standard test method for the dynamic wind uplift resistance of mechanically attached membrane-roofing systems, Canadian Standards Association, 2004.

Dowling, N. E. Estimating Fatigue Life. Fatigue and Fracture. In: ASM Handbook. Vol. 19, pp. 256-262, 1992.

Dowling, N. E. Parameters for Estimating Fatigue Life. Fatigue and Fracture. In: ASM Handbook. Vol. 19, pp. 963-968, 1992.

Dowling, N. E. *Mechanical Behavior of Materials: Engineering Methods for Deformation, Fracture, and Fatigue*, Prentice Hall, 1993.

García, A. J. *Estimación de daños producidos por viento en edificaciones industriales*. M. S. Thesis. Universidad de Puerto Rico Recinto Universitario de Mayagüez. 2008.

Goodman, J. *Mechanics Applied to Engineering*. Longman, Green & Company. London. 1899.

Hua, C.T., and Socie, D.F., "Fatigue Damage in 1045 Steel Under Variable Amplitude Loading," *Fatigue and Fracture Engineering Materials and Structures*, Vol. 8, No. 2, pp. 101-104, 1985.

Lee, K. H. and Rosowsky, D. V. Fragility assessment for roof sheathing failure in high wind regions. *Engineering Structures*. Vol. 27, pp 857-868, 2004.

Mahaarachchi, D. and Mahendran, M. A strain criterion for pull-through failures in crest-fixed steel claddings. *Engineering Structures*. Vol. 31, pp 498-506. 2008.

Mahaarachchi, D. and Mahendran, M. Wind uplift strength of trapezoidal steel cladding with closely spaced ribs. *Journal of Wind Engineering and Industrial Aerodynamics*. Vol. 97, pp 140-150, 2009.

Mahendran, M. Wind-resistant low-rise buildings in the tropics. *ASCE J. of Performance of Constructed Facilities,* Vol. 9, pp 330-346, 1995.

Mahendran, M. and Mahaarachchi, D. Splitting failures in trapezoidal steel roof cladding. *ASCE Journal of Performance of Constructed Facilities*. Vol. 18, pp 4-11, 2004.

Mahendran, M. and Tang, R. B. Pull-Out Strength of Steel Roof and Wall Cladding Systems. ASCE. J. Struct. Engrg. Volume 124, Issue 10, pp. 1192-1201. 1998.

Manson, S.S. "Fatigue: A Complex Subject – Some Simple Approximations," NASA-TM-X-52084, National Aeronautics and Space Administration, 1965.

Matcor. *Rolled Formed Metal Building Components*. Matcor, Inc. Guaynabo, PR. 2007.

Mitchell, M.R. Fundamentals of Modern Fatigue Analysis for Design. Fatigue and Fracture. In: ASM Handbook. Vol. 19, pp. 227-240, 1992.

Morrow, J. Cyclic Plastic Strain Energy and Fatigue of Metals. Internal Friction, Damping and Cyclic Plasticity. ASTM STP 378. American Society for Testing and Materials. West Conshohocken, PA, pp. 45-78, 1965.

Salmon, C. G., Johnson, J. E., Malhas, F. A. Steel Structures Design and Behavior. Fifth edition, Pearson Prentice Hall, New Jersey, 2009.

Smith, R.N., Watson, P., and Topper, T.H. A Stress-Strain Parameter for the Fatigue of Metals. *Journal of Materials*. Vol. 5, No. 4. pp. 767-778, 1970.

Socie, D.F., Kurath, P., and Koch, J.L., "A Multiaxial Fatigue Damage Parameter," European Group on Fracture, EGF Publication 3, Mechanical Engineering Publications, London, pp. 535-550, 1989.

Socie, D. F. and Marquis, G. B. *Multiaxial Fatigue*, Society of Automotive Engineers, Philadelphia, 2000.

Xu, Y. L. Determination of wind-induced fatigue damage loading on roof cladding, *Journal of Engineering Mechanics*, pp 956-963, 1995.

Appendix

A. Specifications for Steel Cladding Geometry and Configuration

Table A.1 Type B wide rib (WR) (Matcor, 2007) cladding specifications

Deck Gauge	Design Thickness (in.)	Fy (ksi)	Weight Galv. (psf)	I_e min. (in^4)	S_p Positive Bending (in^3)	S_n Negative Bending (in^3)
22	0.0299	33	1.47	0.1400	0.1853	0.1918
20	0.0359	33	2.04	0.1833	0.2287	0.2390
18	0.0478	33	2.70	0.2600	0.3083	0.3160

B. Finite Element Analysis Output Data for the Strain Hardening and Elastic-Plastic Material Definitions (Abaqus 2008)

Values read at element integration point at bottom surface

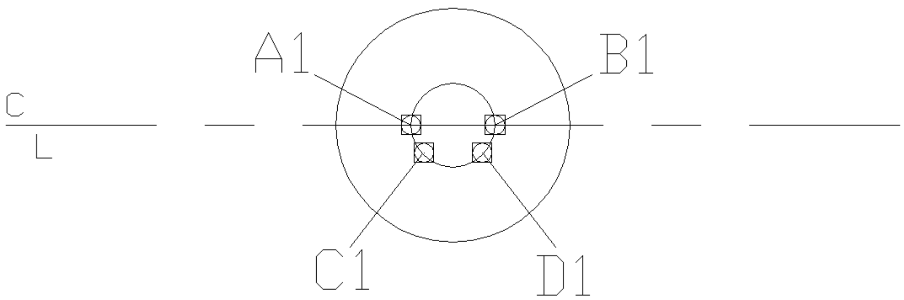

Figure B.1 Abaqus output points on center holes (Figs. 3c-d)

Table B.1 Config. #3 strain hardening

Location: Point A1 in Figure B.1 at column #5 in Figure 3c				
	Load (Mpa)	S, Mises (Mpa)	S, Max (Mpa)	E, Max
A1	0.001453	227.5	259.4	0.004049
A2	0.002905	227.5	258.8	0.010550
A3	0.004358	227.5	257.0	0.016600
A4	0.005810	231.9	256.2	0.022080
B4	0.007263	247.5	257.1	0.028160
C4	0.008715	264.9	273.3	0.035280
D4	0.010168	282.6	291.8	0.042580

Table B.2 Config. #3 elastic-plastic

Location: Point A1 in Figure B.1 at column #5 in Figure 3c				
	Load (Mpa)	S, Mises (Mpa)	S, Max (Mpa)	E, Max
A1	0.001453	227.5	259.4	0.004049
A2	0.002905	227.5	258.8	0.010550
A3	0.004358	227.5	258.8	0.016600
A4	0.005810	227.5	258.8	
B4	0.007263	227.5	258.8	
C4	0.008715	227.5	258.8	
D4	0.010168	227.5	258.8	

Table B.3 Config. #4 strain hardening

Location: Point C1 in Figure B1 at column #6 in Figure 3c				
	Load (Mpa)	S, Mises (Mpa)	S, Max (Mpa)	E, Max
A1	0.000726	227.5	254.6	0.002796
A2	0.001453	227.5	252.5	0.005641
A3	0.002179	227.5	252.5	0.009122
A4	0.002905	227.5	252.3	0.016290
B4	0.003631	238.5	255.1	0.024430
C4	0.004358	258.6	271.0	0.032660
D4	0.005084	274.8	283.2	0.039240
E4	0.005810	289.2	296.8	0.045020

Table B.4 Config. #4 elastic-plastic

Location: Point A1 in Figure B1 at column #6 in Figure 3c				
	Load (Mpa)	S, Mises (Mpa)	S, Max (Mpa)	E, Max
A1	0.000726	227.5	258.9	0.003924
A2	0.001453	227.5	257.6	0.008394
A3	0.002179	227.5	254.5	0.010350
A4	0.002905	227.5	255.4	0.011600
B4	0.003631	227.5	255.4	
C4	0.004358	227.5	255.4	
D4	0.005084	227.5	255.4	
E4	0.005810	227.5	255.4	

Table B.5 Config. #5 strain hardening

Location: Point A1 in Figure B1 at column #5 in Figure 3c				
	Load (Mpa)	S, Mises (Mpa)	S, Max (Mpa)	E, Max
A1	0.001453	227.6	240.6	0.001408
A2	0.002906	227.6	242.4	0.002347
A3	0.004359	227.6	244.1	0.003285
A4	0.005812	227.6	245.8	0.004224
B4	0.007266	227.6	247.5	0.005162
C4	0.008719	227.6	249.3	0.006101
D4	0.010172	227.6	249.5	0.019230
E4	0.011625	250.3	261.3	0.029250
F4	0.013078	275.8	280.1	0.039710
G4	0.014531	296.0	303.4	0.047980
H4	0.015984	315.3	327.0	0.055900

Table B.6 Config. #5 elastic-plastic

Location: Point B1 in Figure B1 at column #6 in Figure 3c			
	Load (Mpa)	S, Mises (Mpa)	S, Max (Mpa)
A1	0.001453		199.5
A2	0.002906	227.6	262.7
A3	0.004359	227.6	267.7
A4	0.005812	227.6	262.6
B4	0.007266	227.6	262.6
C4	0.008719	227.6	262.6
D4	0.010172	227.6	262.6
E4	0.011625	227.6	262.6
F4	0.013078	227.6	262.6
G4	0.014531	227.6	262.6
H4	0.015984	227.6	262.6

Table B.7 Config. #6 strain hardening

Location: Point A1 in Figure B1 at column #4 in Figure 3c				
	Load (Mpa)	S, Mises (Mpa)	S, Max (Mpa)	E, Max
A1	0.001089	227.5	254.0	0.001834
A2	0.002179	227.5	252.8	0.006096
A3	0.003268	227.5	251.6	0.010358
A4	0.004358	227.5	250.4	0.014620
B4	0.005447	250.4	258.8	0.029330
C4	0.006537	276.5	283.5	0.040030
D4	0.007626	296.6	309.7	0.048210
E4	0.008716	319.0	332.9	0.057410
F4	0.009805	341.6	355.6	0.066740

Table B.8 Config. #6 elastic-plastic

Location: Point B1 in Figure B1 at column #4 in Figure 3c				
	Load (Mpa)	S, Mises (Mpa)	S, Max (Mpa)	E, Max
A1	0.001089	227.5	262.1	0.001834
A2	0.002179	227.5	261.4	0.006096
A3	0.003268	227.5	260.8	0.010358
A4	0.004358	227.5	260.2	0.014620
B4	0.005447	227.5	260.2	
C4	0.006537	227.5	260.2	
D4	0.007626	227.5	260.2	
E4	0.008716	227.5	260.2	
F4	0.009805	227.5	260.2	

Table B.9 Config. #13 strain hardening

Location: Point B1 in Figure B.1 at column #4 in Figure 3c				
	Load (Mpa)	S, Mises (Mpa)	S, Max (Mpa)	E, Max
A1	0.001089	227.5	260.8	0.002283
A2	0.002179	227.5	261.2	0.007413
A3	0.003268	227.5	260.6	0.015480
A4	0.004358	231.6	260.0	0.021920
B4	0.005447	241.4	259.1	0.026810
C4	0.006537	250.3	265.8	0.031250
D4	0.007626	260.2	276.0	0.036170
E4	0.008715	270.5	291.3	0.041310

Table B.10 Config. #13 elastic-plastic

Location: Point B1 in Figure B.1 at column #4 in Figure 3c				
	Load (Mpa)	S, Mises (Mpa)	S, Max (Mpa)	E, Max
A1	0.001089	227.5	260.8	0.002283
A2	0.002179	227.5	261.2	0.007413
A3	0.003268	227.5	260.6	0.015480
A4	0.004358	227.5	260.0	
B4	0.005447	227.5	259.1	
C4	0.006537	227.5	259.1	
D4	0.007626	227.5	259.1	
E4	0.008715	227.5	259.1	

Table B.11 Config. #15 strain hardening

Location: Point C1 in Figure B.1 at column #6 in Figure 3c				
	Load (Mpa)	S, Mises (Mpa)	S, Max (Mpa)	E, Max
A1	0.001089	227.5	258.2	0.003757
A2	0.002179	227.5	257.4	0.007514
A3	0.003268	227.5	256.6	0.011271
A4	0.004358	235.0	255.8	0.023640
B4	0.005447	255.7	268.6	0.033980
C4	0.006537	273.7	285.0	0.042970

Table B.12 Config. #15 elastic-plastic

Location: Point B1 in Figure B.1 at column #4 in Figure 3c				
	Load (Mpa)	S, Mises (Mpa)	S, Max (Mpa)	E, Max
A1	0.001089	227.5	262.6	0.003267
A2	0.002179	227.5	262.6	0.018200
A3	0.003268	227.5	262.6	0.033133
A4	0.004358	227.5	262.6	0.048066
B4	0.005447	227.5	262.6	0.062999
C4	0.006537	227.5	262.6	0.018200

Table B.13 Config. #17 strain hardening

Location: Point B1 in Figure B.1 at column #4 in Figure 3c				
	Load (Mpa)	S, Mises (Mpa)	S, Max (Mpa)	E, Max
A1	0.001089	227.5	247.4	0.001428
A2	0.002179	227.5	248.0	0.003973
A3	0.003268	227.5	248.7	0.006519
A4	0.004358	227.5	249.3	0.009064
B4	0.005447	227.5	249.9	0.011609
C4	0.006537	227.5	250.5	0.014155
D4	0.007626	227.5	251.1	0.016700
E4	0.008716	241.8	252.9	0.025800
F4	0.009805	259.4	264.1	0.033010
G4	0.010894	274.5	280.6	0.039160
H4	0.011984	287.9	298.1	0.044660
I4	0.013073	300.6	313.0	0.04989

Table B.14 Config. #17 elastic-plastic

Location: Point B1 in Figure B.1 at column #4 in Figure 3c				
	Load (Mpa)	S, Mises (Mpa)	S, Max (Mpa)	E, Max
A1	0.001089	227.5	247.4	0.001428
A2	0.002179	227.5	248.0	0.003973
A3	0.003268	227.5	248.7	0.006519
A4	0.004358	227.5	249.3	0.009064
B4	0.005447	227.5	249.9	0.011609
C4	0.006537	227.5	250.5	0.014155
D4	0.007626	227.5	251.1	0.016700
E4	0.008716	227.5	251.1	
F4	0.009805	227.5	251.1	
G4	0.010894	227.5	251.1	
H4	0.011984	227.5	251.1	
I4	0.013073	227.5	251.1	

Table B.15 Config. #18 strain hardening

Location: Point B1 in Figure B.1 at column #4 in Figure 3c				
	Load (Mpa)	S, Mises (Mpa)	S, Max (Mpa)	E, Max
A1	0.001816	227.5	252.6	0.001540
A2	0.003631	227.5	252.6	0.003680
A3	0.005447	227.5	252.5	0.005820
A4	0.007263	227.5	252.5	0.007960
B4	0.009079	227.5	252.4	0.010100
C4	0.010894	227.5	253.0	0.015850
D4	0.012710	241.0	252.0	0.025480
E4	0.014526	261.2	263.7	0.033720
F4	0.016342	279.5	286.0	0.041240
G4	0.018157	295.6	306.2	0.047840

Table B.16 Config. #18 elastic-plastic

Location: Point B1 in Figure B.1 at column #4 in Figure 3c				
	Load (Mpa)	S, Mises (Mpa)	S, Max (Mpa)	E, Max
A1	0.001816	227.5	252.6	0.001540
A2	0.003631	227.5	252.6	0.003680
A3	0.005447	227.5	252.5	0.005820
A4	0.007263	227.5	252.5	0.007960
B4	0.009079	227.5	252.4	0.010100
C4	0.010894	227.5	252.4	0.015850
D4	0.012710	241.0	252.4	
E4	0.014526	261.2	252.4	
F4	0.016342	279.5	252.4	
G4	0.018157	295.6	252.4	

Table B.17 Config. #19 strain hardening

Location: Point B1 in Figure B.1 at column #5 in Figure 3d				
	Load (Mpa)	S, Mises (Mpa)	S, Max (Mpa)	E, Max
A1	0.000726	218.9	226.9	0.001110
A2	0.001453	227.5	259.3	0.002451
A3	0.002179	227.5	259.0	0.004311
A4	0.002905	227.5	259.2	0.008580
B4	0.003631	227.5	259.3	0.014070
C4	0.004358	234.3	257.4	0.022710
D4	0.005084	250.9	270.1	0.029500
E4	0.005810	267.5	282.8	0.036290
F4	0.006537	284.0	295.5	0.043080
G4	0.007263	300.6	308.1	0.049860
H4	0.007989	307.6	316.1	0.052710
I4	0.008716	314.5	324.1	0.055550
J4	0.009442	321.5	332.1	0.058390
K4	0.010168	328.3	340.1	0.061240

Table B.18 Config. #19 elastic-plastic

Location: Point B1 in Figure B.1 at column #5 in Figure 3d				
	Load (Mpa)	S, Mises (Mpa)	S, Max (Mpa)	E, Max
A1	0.000726	218.9	226.9	0.001110
A2	0.001453	227.5	259.3	0.002451
A3	0.002179	227.5	259.0	0.004311
A4	0.002905	227.5	259.2	0.008580
B4	0.003631	227.5	259.3	0.014070
C4	0.004358	227.5	257.2	
D4	0.005084	227.5	255.0	
E4	0.005810	227.5	252.9	
F4	0.006537	227.5	250.7	
G4	0.007263	227.5	250.1	
H4	0.007989	227.5	249.5	
I4	0.008716	227.5	248.9	
J4	0.009442	227.5	248.3	
K4	0.010168	227.5	247.7	

Table B19 Config. #20 strain hardening

Location: Point B1 in Figure B.1 at column #3 in Figure 3d				
	Load (Mpa)	S, Mises (Mpa)	S, Max (Mpa)	E, Max
A1	0.000872	227.5	257.8	0.001847
A2	0.001743	227.5	259.8	0.006436
A3	0.002615	227.5	257.8	0.014860
A4	0.003486	234.9	257.0	0.023600
B4	0.004358	243.8	258.6	0.028050
C4	0.005229	245.8	261.2	0.029060

Table B20 Config. #20 elastic-plastic

Location: Point B1 in Figure B.1 at column #3 in Figure 3d				
	Load (Mpa)	S, Mises (Mpa)	S, Max (Mpa)	E, Max
A1	0.000872	227.5	257.8	0.001847
A2	0.001743	227.5	259.8	0.006436
A3	0.002615	227.5	257.8	0.014860
A4	0.003486	227.5	257.0	
B4	0.004358	227.5	257.0	
C4	0.005229	227.5	257.0	

Table B.21 Config. #21 strain hardening

Location: Point D1 in Figure B.1 at column #5 in Figure 3d				
	Load (Mpa)	S, Mises (Mpa)	S, Max (Mpa)	E, Max
A1	0.000872	227.5	262.7	0.002666
A2	0.001743	227.5	262.7	0.007885
A3	0.002615	227.5	262.7	0.013300
A4	0.003486	230.0	262.9	0.019090
B4	0.004358	236.1	269.3	0.021410
C4	0.005229	235.9	269.2	0.021340

Table B.22 Config. #21 elastic-plastic

Location: Point D1 in Figure B.1 at column #5 in Figure 3d				
	Load (Mpa)	S, Mises (Mpa)	S, Max (Mpa)	E, Max
A1	0.000872	227.5	262.7	0.002666
A2	0.001743	227.5	262.7	0.007885
A3	0.002615	227.5	262.7	0.013300
A4	0.003486	227.5	262.7	0.019090
B4	0.004358	227.5	262.7	
C4	0.005229	227.5	262.7	

Table B.23 Config. #24 strain hardening

Location: Point B1 in Figure B.1 at column #5 in Figure 3d				
	Load (Mpa)	S, Mises (Mpa)	S, Max (Mpa)	E, Max
A1	0.000872	227.5	235.9	0.001230
A2	0.001743	227.5	258.3	0.003021
A3	0.002615	227.5	257.8	0.006977
A4	0.003486	227.5	257.9	0.014200
B4	0.004358	245.7	259.2	0.027390
C4	0.005229	278.0	288.6	0.040640
D4	0.006101	300.7	307.5	0.049930
E4	0.006972	317.1	326.7	0.056610
F4	0.007844	332.3	343.5	0.062910
G4	0.008716	346.7	358.9	0.068810

Table B.24 Config. #24 elastic-plastic

Location: Point B1 in Figure B.1 at column #5 in Figure 3d				
	Load (Mpa)	S, Mises (Mpa)	S, Max (Mpa)	E, Max
A1	0.000872		209.4	0.001230
A2	0.001743	227.5	262.6	0.003021
A3	0.002615	227.5	262.4	0.006977
A4	0.003486	227.5	262.3	0.013940
B4	0.004358	227.5	262.2	
C4	0.005229	227.5	262.2	
D4	0.006101	227.5	262.2	
E4	0.006972	227.5	262.1	
F4	0.007844	227.5	262.1	
G4	0.008716	227.5	262.1	

C. Fatigue Damage Results, Elastic-Plastic

Table C.1 Config. #3

	$\Delta\varepsilon_{\max}$ x 10^{-3}	σ_m	$\sigma_{\max}$	n	N_M	N_{SWT}	N_G	F_M	F_{SWT}	F_G
A1	1.138	129.7	259.4	2000	19182	14576	10065	0.149	0.196	0.284
A2	1.138	129.4	258.8	3500	19652	14715	10065	0.403	0.536	0.781
A3	1.138	129.4	258.8	1000	19652	14715	10065	0.476	0.633	0.923
A4	1.138	129.4	258.8	250	19652	14715	10065	0.494	0.657	0.958
A5	0.285	97.1	129.4	2000	3599611629	85235994	#	0.494	0.657	0.958
A6	0.569	129.4	194.1	2000	6338445	876229	3246250	0.495	0.660	0.959
A7	0.854	161.8	258.8	125	117751	48789	30063	0.496	0.664	0.965
A8	0.569	194.1	258.8	125	1795078	264265	188072	0.496	0.665	0.966
B2	0.717	80.9	161.8	2500	2274833	715038	2599950	0.498	0.670	0.967
B3	1.070	121.3	242.6	750	38902	24917	23176	0.525	0.713	1.013
B4	1.138	129.4	258.8	250	19652	14715	10065	0.544	0.737	1.049
B6	0.569	129.4	194.1	1750	6338445	876229	3246250	0.544	0.740	1.050
B7	0.854	161.8	258.8	125	117751	48789	30063	0.546	0.744	1.056
B8	0.569	194.1	258.8	125	1795078	264265	188072	0.546	0.744	1.057
C2	0.683	77.6	155.3	1250	3369887	1038694	4031757	0.546	0.746	1.057
C3	1.029	116.5	232.9	750	59566	34756	38710	0.564	0.777	1.085
C4	1.138	129.4	258.8	250	19652	14715	10065	0.582	0.801	1.120
C6	0.569	129.4	194.1	1500	6338445	876229	3246250	0.583	0.804	1.121
C7	0.854	161.8	258.8	125	117751	48789	30063	0.584	0.807	1.127
C8	0.569	194.1	258.8	125	1795078	264265	188072	0.584	0.808	1.128
D2	0.668	75.5	151.0	1250	4415806	1283022	5444514	0.585	0.809	1.128
D3	0.994	113.2	226.5	500	79725	45130	54824	0.594	0.825	1.141
D4	1.138	129.4	258.8	250	19652	14715	10065	0.612	0.849	1.177

D4 - first failure observed (García 2008)

Tables C.1 through C.12 were calculated using the procedure in Section 5.6 where Column one is the strain range as defined in Section 5.6, columns two and three are the mean and maximum stresses as defined in Section 5.6, Column four is the number of cycles on each loading sublevel, columns five, six, and seven are calculated from equations 13, 16 and 19, and columns eight, nine and ten are calculated from equation 21.

Table C.2 Config. #4										
	$\Delta\varepsilon_{\max}$ x 10^{-3}	σ_m	$\sigma_{\max}$	n	N_M	N_{SWT}	N_G	F_M	F_{SWT}	F_G
A1	1.138	129.5	258.9	2000	19571	14691	10066	0.146	0.194	0.284
A2	1.138	128.8	257.6	3500	20651	15002	10066	0.388	0.528	0.781
A3	1.138	127.3	254.5	1000	23491	15779	10066	0.449	0.618	0.923
A4	1.138	127.3	254.5	250	23491	15779	10066	0.464	0.641	0.958
A5	0.285	95.4	127.3	2000	4253180041	91399058	#	0.464	0.641	0.958
A6	0.569	127.3	190.9	2000	7576637	939586	3246626	0.465	0.644	0.959
A7	0.854	159.1	254.5	125	142642	52317	30067	0.466	0.647	0.965
A8	0.569	190.9	254.5	125	2208448	283373	188103	0.466	0.648	0.966
B2	0.717	79.5	159.1	2500	2673792	766739	2600197	0.467	0.653	0.967
B3	1.070	119.3	238.6	750	46360	26719	23178	0.490	0.693	1.013
B4	1.138	127.3	254.5	250	23491	15779	10066	0.505	0.715	1.049
B6	0.569	127.3	190.9	1750	7576637	939586	3246626	0.506	0.718	1.050
B7	0.854	159.1	254.5	125	142642	52317	30067	0.507	0.722	1.056
B8	0.569	190.9	254.5	125	2208448	283373	188103	0.507	0.722	1.056
C2	0.683	76.4	152.7	1250	3956894	1113798	4032136	0.508	0.724	1.057
C3	1.029	114.5	229.1	750	70859	37270	38715	0.523	0.753	1.085
C4	1.138	127.3	254.5	250	23491	15779	10066	0.538	0.775	1.120
C6	0.569	127.3	190.9	1500	7576637	939586	3246626	0.538	0.777	1.121
C7	0.854	159.1	254.5	125	142642	52317	30067	0.539	0.781	1.127
C8	0.569	190.9	254.5	125	2208448	283373	188103	0.540	0.781	1.128
D2	0.668	74.2	148.4	1250	5181542	1375792	5445022	0.540	0.783	1.128
D3	0.994	111.3	222.7	500	94730	48393	54830	0.547	0.798	1.141
D4	1.138	127.3	254.5	250	23491	15779	10066	0.563	0.820	1.176
D6	0.569	127.3	190.9	250	7576637	939586	3246626	0.563	0.821	1.177
D7	0.854	159.1	254.5	125	142642	52317	30067	0.564	0.824	1.183
D8	0.569	190.9	254.5	125	2208448	283373	188103	0.564	0.825	1.183
E2	0.650	72.7	145.4	1000	6304752	1672917	6770673	0.564	0.825	1.184
E3	0.975	109.1	218.1	500	117078	57023	70572	0.570	0.838	1.194
E4	1.138	127.3	254.5	250	23491	15779	10066	0.586	0.861	1.229
E7	0.854	159.1	254.5	125	142642	52317	30067	0.587	0.864	1.235
E8	0.569	190.9	254.5	125	2208448	283373	188103	0.587	0.865	1.236

Cont. Table C.2										
	$\Delta\varepsilon_{\max}$ x 10^{-3}	σ_m	$\sigma_{\max}$	n	N_M	N_{SWT}	N_G	F_M	F_{SWT}	F_G
F2	0.643	61.6	123.2	1000	29872449	3494340	37401242	0.587	0.865	1.236
*F3	0.962	92.2	184.3	500	635401	122076	508814	0.588	0.871	1.238

* first failure observed (García 2008)

Table C.3 Config. #5										
	$\Delta\varepsilon_{\max}$ x 10^{-3}	σ_m	$\sigma_{\max}$	n	N_M	N_{SWT}	N_G	F_M	F_{SWT}	F_G
A1	1.138	99.8	199.5	2000	289104	43518	10066	0.010	0.066	0.284
A2	1.138	131.4	262.7	3500	16746	13826	10066	0.308	0.427	0.781
A3	1.138	131.4	262.7	1000	16746	13826	10066	0.394	0.531	0.923
A4	1.138	131.3	262.6	250	16814	13847	10066	0.415	0.556	0.958
A5	0.285	98.5	131.3	2000	3111884196	80213258	#	0.415	0.556	0.958
A6	0.569	131.3	197.0	2000	5423343	824595	3246626	0.416	0.560	0.959
A7	0.854	164.1	262.6	125	99559	45914	30067	0.417	0.564	0.965
A8	0.569	197.0	262.6	125	1496849	248693	188103	0.417	0.565	0.966
B2	0.717	82.1	164.1	2500	1975803	672903	2600197	0.419	0.570	0.967
B3	1.070	123.1	246.2	750	33376	23449	23178	0.451	0.616	1.013
B4	1.138	131.3	262.6	250	16814	13847	10066	0.473	0.641	1.049
B6	0.569	131.3	197.0	1750	5423343	824595	3246626	0.473	0.644	1.050
B7	0.854	164.1	262.6	125	99559	45914	30067	0.475	0.648	1.056
B8	0.569	197.0	262.6	125	1496849	248693	188103	0.475	0.649	1.056
C2	0.683	78.8	157.6	1250	2929538	977487	4032136	0.476	0.651	1.057
C3	1.029	118.2	236.3	750	51186	32708	38715	0.497	0.684	1.085
C4	1.138	131.3	262.6	250	16814	13847	10066	0.518	0.709	1.120
C6	0.569	131.3	197.0	1500	5423343	824595	3246626	0.518	0.712	1.121
C7	0.854	164.1	262.6	125	99559	45914	30067	0.520	0.716	1.127
C8	0.569	197.0	262.6	125	1496849	248693	188103	0.520	0.717	1.128
D2	0.668	76.6	153.2	1250	3841063	1207416	5445022	0.521	0.718	1.128
D3	0.994	114.9	229.8	500	68580	42471	54830	0.531	0.735	1.141
D4	1.138	131.3	262.6	250	16814	13847	10066	0.552	0.761	1.176
D6	0.569	131.3	197.0	250	5423343	824595	3246626	0.552	0.761	1.177
D7	0.854	164.1	262.6	125	99559	45914	30067	0.554	0.765	1.183
D8	0.569	197.0	262.6	125	1496849	248693	188103	0.554	0.766	1.183
E2	0.650	75.0	150.0	1000	4677868	1468178	6770673	0.554	0.767	1.184
E3	0.975	112.5	225.1	500	84891	50044	70572	0.563	0.781	1.194
E4	1.138	131.3	262.6	250	16814	13847	10066	0.584	0.807	1.229
E7	0.854	164.1	262.6	125	99559	45914	30067	0.586	0.811	1.235
E8	0.569	197.0	262.6	125	1496849	248693	188103	0.586	0.811	1.236

Cont. Table C.3										
	$\Delta\varepsilon_{\max}$ x 10^{-3}	σ_m	$\sigma_{\max}$	n	N_M	N_{SWT}	N_G	F_M	F_{SWT}	F_G
F2	0.643	63.6	127.2	1000	22305887	3066688	37401242	0.586	0.812	1.236
F3	0.962	95.1	190.2	500	465873	107136	508814	0.588	0.818	1.238
F4	1.138	131.3	262.6	250	16814	13847	10066	0.609	0.844	1.273
F7	0.854	164.1	262.6	125	99559	45914	30067	0.611	0.848	1.279
F8	0.569	197.0	262.6	125	1496849	248693	188103	0.611	0.849	1.280
G2	0.632	52.8	105.7	1000	123637216	7119365	#	0.611	0.849	1.280
G3	0.951	79.5	158.9	500	2698186	237343	3679806	0.611	0.852	1.280
G4	1.138	131.3	262.6	250	16814	13847	10066	0.632	0.878	1.316
G7	0.854	163.8	262.1	125	101773	46280	30067	0.634	0.882	1.322
G8	0.569	196.6	262.1	125	1532948	250675	188103	0.634	0.882	1.323
H2	0.628	43.9	87.7	1000	669166868	15877453	#	0.634	0.883	1.323
H3	0.938	65.5	130.9	500	16962434	563482	27776585	0.634	0.884	1.323
H4	1.138	131.3	262.6	250	16814	13847	10066	0.655	0.910	1.358
H7	0.854	163.8	262.1	125	101773	46280	30067	0.657	0.913	1.364
H8	0.569	196.6	262.1	125	1532948	250675	188103	0.657	0.914	1.365

H - first failure observed (García 2008)

Table C.4 Config. #6										
	$\Delta\varepsilon_{\max}$ x 10^{-3}	σ_m	$\sigma_{\max}$	n	N_M	N_{SWT}	N_G	F_M	F_{SWT}	F_G
A1	1.138	131.1	262.1	2000	17161	13958	10066	0.166	0.205	0.284
A2	1.138	130.7	261.4	3500	17660	14114	10066	0.450	0.559	0.781
A3	1.138	130.4	260.8	1000	18100	14250	10066	0.529	0.659	0.923
A4	1.138	130.1	260.2	250	18551	14388	10066	0.548	0.684	0.958
A5	0.285	97.6	130.1	2000	3410935578	83341334	#	0.548	0.684	0.958
A6	0.569	130.1	195.2	2000	5983461	856752	3246626	0.548	0.687	0.959
A7	0.854	162.6	260.2	125	110672	47705	30067	0.550	0.691	0.965
A8	0.569	195.2	260.2	125	1678593	258391	188103	0.550	0.692	0.966
B2	0.717	81.3	162.6	2500	2159299	699144	2600197	0.552	0.697	0.967
B3	1.070	122.0	243.9	750	36760	24363	23178	0.581	0.741	1.013
B4	1.138	130.1	260.2	250	18551	14388	10066	0.600	0.766	1.049
B6	0.569	130.1	195.2	1750	5983461	856752	3246626	0.600	0.769	1.050
B7	0.854	162.6	260.2	125	110672	47705	30067	0.602	0.772	1.056
B8	0.569	195.2	260.2	125	1678593	258391	188103	0.602	0.773	1.056
C2	0.683	78.1	156.1	1250	3199793	1015606	4032136	0.603	0.775	1.057
C3	1.029	117.1	234.2	750	56319	33984	38715	0.622	0.806	1.085
C4	1.138	130.1	260.2	250	18551	14388	10066	0.641	0.831	1.120
C6	0.569	130.1	195.2	1500	5983461	856752	3246626	0.641	0.834	1.121
C7	0.854	162.6	260.2	125	110672	47705	30067	0.643	0.837	1.127
C8	0.569	195.2	260.2	125	1678593	258391	188103	0.643	0.838	1.128
D2	0.668	75.9	151.8	1250	4193835	1254502	5445022	0.644	0.840	1.128
D3	0.994	113.8	227.7	500	75408	44127	54830	0.653	0.856	1.141
D4	1.138	130.1	260.2	250	18551	14388	10066	0.672	0.881	1.176
D6	0.569	130.1	195.2	250	5983461	856752	3246626	0.672	0.881	1.177
D7	0.854	162.6	260.2	125	110672	47705	30067	0.674	0.885	1.183
D8	0.569	195.2	260.2	125	1678593	258391	188103	0.674	0.885	1.183
E2	0.650	74.3	148.7	1000	5106139	1525433	6770673	0.674	0.886	1.184
E3	0.975	111.5	223.0	500	93300	51996	70572	0.682	0.900	1.194
E4	1.138	130.1	260.2	250	18551	14388	10066	0.701	0.925	1.229
E7	0.854	162.6	260.2	125	110672	47705	30067	0.703	0.929	1.235
E8	0.569	195.2	260.2	125	1678593	258391	188103	0.703	0.929	1.236

Cont. Table C.4										
	$\Delta\varepsilon_{\max}$ x 10^{-3}	σ_m	$\sigma_{\max}$	n	N_M	N_{SWT}	N_G	F_M	F_{SWT}	F_G
F2	0.643	63.0	126.0	1000	24301972	3186280	37401242	0.703	0.930	1.236
*F3	0.962	94.2	188.4	500	510325	111314	508814	0.704	0.936	1.236

* first failure observed (García 2008)

Table C.5 Config. #13

	$\Delta\varepsilon_{\max}$ x 10^{-3}	σ_m	$\sigma_{\max}$	n	N_M	N_{SWT}	N_G	F_M	F_{SWT}	F_G
A1	1.138	130.4	260.8	2000	18130	14260	10066	0.158	0.200	0.284
A2	1.138	130.6	261.2	3500	17770	14149	10066	0.439	0.554	0.781
A3	1.138	130.3	260.6	1000	18249	14296	10066	0.517	0.654	0.923
A4	1.138	130.0	260.0	250	18704	14434	10066	0.536	0.678	0.958
A5	0.285	97.5	130.0	2000	3437222388	83608779	3230672125	0.536	0.678	0.958
A6	0.569	130.0	195.0	2000	6032847	859502	3246626	0.537	0.682	0.959
A7	0.854	162.5	260.0	125	111655	47858	30067	0.538	0.686	0.965
A8	0.569	195.0	260.0	125	1694740	259220	188103	0.539	0.686	0.966
B2	0.717	81.3	162.5	2500	2175406	701387	2600197	0.540	0.691	0.967
B3	1.070	121.9	243.8	750	37058	24442	23178	0.569	0.735	1.013
B4	1.138	129.6	259.1	250	19410	14644	10066	0.587	0.760	1.049
B6	0.569	129.6	194.3	1750	6260528	872010	3246626	0.588	0.762	1.050
B7	0.854	161.9	259.1	125	116195	48555	30067	0.589	0.766	1.056
B8	0.569	194.3	259.1	125	1769427	262992	188103	0.590	0.767	1.056
C2	0.683	77.7	155.5	1250	3332626	1033692	4032136	0.590	0.768	1.057
C3	1.029	116.6	233.2	750	58854	34589	38715	0.608	0.799	1.085
C4	1.138	129.6	259.1	250	19410	14644	10066	0.627	0.824	1.120
C6	0.569	129.6	194.3	1500	6260528	872010	3246626	0.627	0.826	1.121
C7	0.854	161.9	259.1	125	116195	48555	30067	0.629	0.830	1.127
C8	0.569	194.3	259.1	125	1769427	262992	188103	0.629	0.831	1.128
D2	0.668	75.6	151.1	1250	4367185	1276843	5445022	0.629	0.832	1.128
D3	0.994	113.4	226.7	500	78778	44913	54830	0.638	0.848	1.141
D4	1.138	129.6	259.1	250	19410	14644	10066	0.657	0.872	1.176
D6	0.569	129.6	194.3	250	6260528	872010	3246626	0.657	0.873	1.177
D7	0.854	161.9	259.1	125	116195	48555	30067	0.658	0.876	1.183
D8	0.569	194.3	259.1	125	1769427	262992	188103	0.658	0.877	1.183
E2	0.650	74.0	148.0	1000	5316554	1552599	6770673	0.658	0.878	1.184
E3	0.975	111.0	222.1	500	97449	52921	70572	0.666	0.892	1.194
*E4	1.138	129.6	259.1	250	19410	14644	10066	0.684	0.916	1.229

* first failure observed (García 2008)

Table C.6 Config. #15										
	$\Delta\varepsilon_{\max}$ x 10^{-3}	σ_m	$\sigma_{\max}$	n	N_M	N_{SWT}	N_G	F_M	F_{SWT}	F_G
A1	1.138	131.3	262.6	2000	16814	13847	10066	0.170	0.206	0.284
A2	1.138	131.3	262.6	3500	16814	13847	10066	0.467	0.567	0.781
A3	1.138	131.3	262.6	1000	16814	13847	10066	0.552	0.671	0.923
A4	1.138	131.3	262.6	250	16814	13847	10066	0.573	0.696	0.958
A5	0.285	98.5	131.3	2000	3111884196	80213258	#	0.573	0.696	0.958
A6	0.569	131.3	197.0	2000	5423343	824595	3246626	0.574	0.700	0.959
A7	0.854	164.1	262.6	125	99559	45914	30067	0.576	0.704	0.965
A8	0.569	197.0	262.6	125	1496849	248693	188103	0.576	0.704	0.966
B2	0.717	82.1	164.1	2500	1975803	672903	2600197	0.578	0.710	0.967
B3	1.070	123.1	246.2	750	33376	23449	23178	0.610	0.755	1.013
B4	1.138	131.3	262.6	250	16814	13847	10066	0.631	0.781	1.049
B6	0.569	131.3	197.0	1750	5423343	824595	3246626	0.632	0.784	1.050
B7	0.854	164.1	262.6	125	99559	45914	30067	0.633	0.788	1.056
B8	0.569	197.0	262.6	125	1496849	248693	188103	0.633	0.789	1.056
C2	0.683	78.8	157.6	1250	2929538	977487	4032136	0.634	0.791	1.057
C3	1.029	118.2	236.3	750	51186	32708	38715	0.655	0.823	1.085
C4	1.138	131.3	262.6	250	16814	13847	10066	0.676	0.849	1.120
C7	0.569	131.3	197.0	125	5423343	824595	3246626	0.677	0.852	1.121
C8	0.854	164.1	262.6	125	99559	45914	30067	0.678	0.856	1.127

C - first failure observed (García 2008)

Table C.7 Config. #17										
	$\Delta\varepsilon_{\max}$ x 10^{-3}	σ_m	$\sigma_{\max}$	n	N_M	N_{SWT}	N_G	F_M	F_{SWT}	F_G
A1	1.138	123.7	247.4	2000	31692	17753	10066	0.090	0.161	0.284
A2	1.138	124.3	248.5	3500	30243	17428	10066	0.255	0.448	0.781
A3	1.138	124.8	249.5	1000	28987	17138	10066	0.305	0.531	0.923
A4	1.138	125.3	250.5	250	27787	16855	10066	0.318	0.552	0.958
A5	0.285	93.9	125.3	2000	4977474649	97635695	#	0.318	0.552	0.958
A6	0.569	125.3	187.9	2000	8962320	1003699	3246626	0.318	0.555	0.959
A7	0.854	156.6	250.5	125	170812	55887	30067	0.319	0.558	0.965
A8	0.569	187.9	250.5	125	2682417	302709	188103	0.319	0.559	0.966
B2	0.717	78.3	156.6	2500	3113966	819058	2600197	0.320	0.563	0.967
B3	1.070	117.4	234.8	750	54685	28542	23178	0.340	0.601	1.013
B4	1.138	125.8	251.5	250	26639	16578	10066	0.353	0.622	1.049
B6	0.569	125.8	188.6	1750	8592220	987175	3246626	0.353	0.625	1.050
B7	0.854	157.2	251.5	125	163258	54967	30067	0.355	0.628	1.056
B8	0.569	188.6	251.5	125	2554760	297725	188103	0.355	0.629	1.056
C2	0.683	75.5	150.9	1250	4432063	1170210	4032136	0.355	0.630	1.057
C3	1.029	113.2	226.4	750	80089	39157	38715	0.368	0.658	1.085
C4	1.138	126.3	252.5	250	25542	16306	10066	0.382	0.680	1.120
C6	0.569	126.3	189.4	1500	8238409	970986	3246626	0.383	0.682	1.121
C7	0.854	157.8	252.5	125	156057	54066	30067	0.384	0.685	1.127
C8	0.569	189.4	252.5	125	2433428	292843	188103	0.384	0.686	1.128
D2	0.668	73.6	147.3	1250	5586033	1421770	5445022	0.384	0.687	1.128
D3	0.994	110.5	220.9	500	102719	50010	54830	0.391	0.701	1.141
D4	1.138	126.4	252.8	250	25223	16225	10066	0.405	0.723	1.176
D6	0.569	126.4	189.6	250	8135327	966194	3246626	0.405	0.724	1.177
D7	0.854	158.0	252.8	125	153963	53799	30067	0.407	0.727	1.183
D8	0.569	189.6	252.8	125	2398213	291398	188103	0.407	0.728	1.183
E2	0.650	72.2	144.4	1000	6719250	1720293	6770673	0.407	0.728	1.184
E3	0.975	108.3	216.7	500	125375	58637	70572	0.413	0.741	1.194
E4	1.138	126.6	253.2	250	24803	16119	10066	0.427	0.763	1.229
E7	0.854	158.3	253.2	125	151216	53446	281401	0.428	0.766	1.230
E8	0.569	189.9	253.2	125	2352084	289485	2601114	0.428	0.767	1.230

Cont. Table C.7										
	$\Delta\varepsilon_{\max}$ x 10^{-3}	σ_m	$\sigma_{\max}$	n	N_M	N_{SWT}	N_G	F_M	F_{SWT}	F_G
F2	0.643	61.2	122.4	1000	31794020	3593297	37401242	0.428	0.767	1.230
F3	0.962	91.5	183.1	500	678855	125533	508814	0.429	0.773	1.231
F4	1.138	126.8	253.5	250	24493	16040	10066	0.444	0.795	1.267
F7	0.854	158.4	253.5	125	149190	53183	2539689	0.445	0.798	1.267
F8	0.569	190.1	253.5	125	2318094	288060	31141824	0.445	0.799	1.267
G2	0.632	50.9	101.7	1000	175007528	8341896	#	0.445	0.799	1.267
G3	0.951	76.5	153.0	500	3887592	278099	3679806	0.445	0.802	1.267
G4	1.138	126.9	253.8	250	24188	15961	10066	0.460	0.824	1.303
G7	0.854	158.6	253.8	125	147193	52921	21841432	0.461	0.828	1.303
G8	0.569	190.4	253.8	125	2284617	286644	#	0.461	0.828	1.303
H2	0.628	42.2	84.4	1000	941918293	18603917	#	0.461	0.828	1.303
H3	0.938	63.0	126.1	500	24207877	660242	27776585	0.461	0.829	1.303
H4	1.138	127.1	254.1	250	23886	15882	10066	0.476	0.852	1.338
H7	0.854	158.8	254.1	125	145224	52661	#	0.478	0.855	1.338
H8	0.569	190.6	254.1	125	2251643	285236	#	0.478	0.856	1.338
I2	0.621	34.4	68.8	1000	5878308923	46033988	#	0.478	0.856	1.338
I3	0.931	51.6	103.1	500	154197241	1569103	#	0.478	0.856	1.338
*I4	1.138	127.2	254.4	250	23589	15804	10066	0.493	0.879	1.374

* first failure observed (García 2008)

Table C.8 Config. #18

	$\Delta\varepsilon_{\max}$ x 10^{-3}	σ_m	$\sigma_{\max}$	n	N_M	N_{SWT}	N_G	F_M	F_{SWT}	F_G
A1	1.138	126.3	252.6	2000	25435	16279	10066	0.112	0.176	0.284
A2	1.138	126.3	252.6	3500	25435	16279	10066	0.309	0.483	0.781
A3	1.138	126.3	252.5	1000	25542	16306	10066	0.365	0.570	0.923
A4	1.138	126.2	252.4	250	25650	16333	10066	0.379	0.592	0.958
A5	0.285	94.7	126.2	2000	4618060881	94609599	##	0.379	0.592	0.958
A6	0.569	126.2	189.3	2000	8273079	972590	3246626	0.379	0.595	0.959
A7	0.854	157.8	252.4	125	156762	54155	30067	0.380	0.598	0.965
A8	0.569	189.3	252.4	125	2445287	293327	188103	0.380	0.599	0.966
B2	0.717	78.9	157.8	2500	2895775	793672	2600197	0.382	0.604	0.967
B3	1.070	118.3	236.6	750	50547	27658	23178	0.403	0.642	1.013
B4	1.138	126.2	252.4	250	25650	16333	10066	0.417	0.664	1.049
B6	0.569	126.2	189.3	1750	8273079	972590	3246626	0.417	0.667	1.050
B7	0.854	157.8	252.4	125	156762	54155	30067	0.418	0.670	1.056
B8	0.569	189.3	252.4	125	2445287	293327	188103	0.418	0.671	1.056
C2	0.683	75.7	151.4	1250	4283296	1152922	4032136	0.419	0.672	1.057
C3	1.029	113.6	227.2	750	77191	38579	38715	0.432	0.700	1.085
C4	1.138	126.2	252.4	250	25650	16333	10066	0.446	0.722	1.120
C6	0.569	126.2	189.3	1500	8273079	972590	3246626	0.447	0.724	1.121
C7	0.854	157.8	252.4	125	156762	54155	30067	0.448	0.727	1.127
C8	0.569	189.3	252.4	125	2445287	293327	188103	0.448	0.728	1.128
D2	0.668	73.6	147.2	1250	5607141	1424119	5445022	0.448	0.729	1.128
D3	0.994	110.4	220.9	500	103137	50093	54830	0.455	0.743	1.141
D4	1.138	126.2	252.4	250	25650	16333	10066	0.469	0.765	1.176
D6	0.569	126.2	189.3	250	8273079	972590	3246626	0.469	0.766	1.177
D7	0.854	157.8	252.4	125	156762	54155	30067	0.470	0.769	1.183
D8	0.569	189.3	252.4	125	2445287	293327	188103	0.470	0.770	1.183
E2	0.650	72.1	144.2	1000	6821040	1731681	6770673	0.471	0.770	1.184
E3	0.975	108.2	216.3	500	127417	59026	70572	0.476	0.782	1.194
E4	1.138	126.2	252.4	250	25650	16333	10066	0.490	0.804	1.229
E7	0.854	157.8	252.4	125	156762	54155	281401	0.491	0.808	1.230
E8	0.569	189.3	252.4	125	2445287	293327	2601114	0.491	0.808	1.230

Cont. Table C.8

	$\Delta\varepsilon_{\max}$ x 10^{-3}	σ_m	$\sigma_{\max}$	n	N_M	N_{SWT}	N_G	F_M	F_{SWT}	F_G
F2	0.643	61.1	122.2	1000	32265568	3617084	37401242	0.491	0.809	1.230
F3	0.962	91.4	182.8	500	689540	126364	508814	0.492	0.814	1.231
F4	1.138	126.2	252.4	250	25650	16333	10066	0.506	0.836	1.267
F7	0.854	157.8	252.4	125	156762	54155	2539689	0.507	0.839	1.267
F8	0.569	189.3	252.4	125	2445287	293327	31141824	0.507	0.840	1.267
G2	0.632	50.8	101.6	1000	177552966	8397118	#	0.507	0.840	1.267
G3	0.951	76.4	152.7	500	3946977	279940	3679806	0.508	0.843	1.267
G4	1.138	126.0	252.0	250	26085	16441	10066	0.521	0.865	1.303
G7	0.854	157.5	252.0	125	159615	54514	21841432	0.522	0.868	1.303
G8	0.569	189.0	252.0	125	2493325	295272	#	0.523	0.868	1.303

E4 - visible cracking (García 2008)

Table C.9 Config. #19										
	$\Delta\varepsilon_{\max}$ x 10^{-3}	σ_m	$\sigma_{\max}$	n	N_M	N_{SWT}	N_G	F_M	F_{SWT}	F_G
A1	113.5	113.5	226.9	2000	78109	28240	16622	0.037	0.101	0.172
A2	129.7	129.7	259.3	3500	19251	14597	10066	0.296	0.444	0.669
A3	129.5	129.5	259.0	1000	19490	14667	10066	0.370	0.541	0.811
A4	129.6	129.6	259.2	250	19330	14620	10066	0.388	0.566	0.846
A5	97.2	97.2	129.6	2000	3544579326	84689261	#	0.388	0.566	0.846
A6	129.6	129.6	194.4	2000	6234783	870609	3246626	0.389	0.569	0.847
A7	162.0	162.0	259.2	125	115681	48477	30067	0.390	0.573	0.853
A8	194.4	194.4	259.2	125	1760962	262570	188103	0.390	0.573	0.854
B2	81.0	81.0	162.0	2500	2241152	710451	2600197	0.392	0.578	0.855
B3	121.5	121.5	243.0	750	38277	24758	23178	0.420	0.622	0.901
B4	129.7	129.7	259.3	250	19251	14597	10066	0.438	0.646	0.937
B6	129.7	129.7	194.5	1750	6209151	869211	3246626	0.439	0.649	0.938
B7	162.1	162.1	259.3	125	115169	48399	30067	0.440	0.653	0.944
B8	194.5	194.5	259.3	125	1752539	262148	188103	0.440	0.653	0.945
C2	77.8	77.8	155.6	1250	3308035	1030374	4032136	0.441	0.655	0.945
C3	116.7	116.7	233.4	750	58384	34478	38715	0.459	0.686	0.973
C4	128.6	128.6	257.2	250	20995	15100	10066	0.476	0.710	1.008
C6	128.6	128.6	192.9	1500	6771865	899166	3246626	0.477	0.712	1.009
C7	160.8	160.8	257.2	125	126430	50067	30067	0.478	0.716	1.015
C8	192.9	192.9	257.2	125	1938574	271183	188103	0.478	0.716	1.016
D2	75.0	75.0	150.0	1250	4685279	1316607	5445022	0.478	0.718	1.016
D3	112.5	112.5	225.1	500	84986	46311	54830	0.487	0.733	1.029
D4	127.5	127.5	255.0	250	23006	15650	10066	0.502	0.756	1.065
D6	127.5	127.5	191.3	250	7420227	931933	3246626	0.502	0.756	1.065
D7	159.4	159.4	255.0	125	139482	51891	30067	0.504	0.760	1.071
D8	191.3	191.3	255.0	125	2155666	281065	188103	0.504	0.760	1.072
E2	72.9	72.9	145.7	1000	6188210	1659291	6770673	0.504	0.761	1.072
E3	109.3	109.3	218.6	500	114751	56558	70572	0.510	0.774	1.082
E4	126.5	126.5	252.9	250	25117	16199	10066	0.524	0.796	1.117
E7	158.1	158.1	252.9	125	153271	53710	30067	0.526	0.799	1.123
E8	189.7	189.7	252.9	125	2386593	290918	188103	0.526	0.800	1.124

Cont. Table C.9										
	$\Delta\varepsilon_{\max}$ x 10^{-3}	σ_m	$\sigma_{\max}$	n	N_M	N_{SWT}	N_G	F_M	F_{SWT}	F_G
F2	0.643	61.5	122.9	1000	30567429	3530516	39119332	0.526	0.800	1.124
F3	0.962	92.2	184.4	500	632012	121801	517083	0.527	0.806	1.126
F4	1.138	125.4	250.7	250	27553	16799	10066	0.540	0.827	1.161
F7	0.854	156.7	250.7	125	169272	55702	30067	0.541	0.831	1.167
F8	0.569	188.0	250.7	125	2656364	301704	188103	0.541	0.831	1.168
G2	0.632	51.2	102.5	1000	163696927	8091183	#	0.541	0.831	1.168
G3	0.951	76.8	153.7	500	3722142	272887	3845889	0.541	0.834	1.168
G4	1.138	125.1	250.1	250	28260	16968	10066	0.554	0.855	1.204
G7	0.854	156.3	250.1	125	173936	56260	30067	0.555	0.858	1.210
G8	0.569	187.6	250.1	125	2735328	304731	188103	0.555	0.859	1.211
H2	0.628	42.3	84.5	1000	934248552	18533443	#	0.555	0.859	1.211
H3	0.938	63.4	126.8	500	22942212	644602	28613377	0.555	0.860	1.211
H4	1.138	124.8	249.5	250	28987	17138	10066	0.567	0.881	1.246
H7	0.854	155.9	249.5	125	178735	56826	30067	0.568	0.884	1.252
H8	0.569	187.1	249.5	125	2816745	307796	188103	0.568	0.885	1.253
I2	0.621	34.6	69.2	1000	5582348775	44927942	#	0.568	0.885	1.253
I3	0.931	51.9	103.7	500	146273281	1531793	#	0.568	0.885	1.253
I4	1.138	124.5	248.9	250	29734	17311	10066	0.580	0.906	1.288
I7	0.854	155.6	248.9	125	183675	57399	30067	0.581	0.909	1.294
I8	0.569	186.7	248.9	125	2900696	310900	188103	0.581	0.909	1.295
J2	0.618	28.1	56.2	1000	34697325916	108468242	#	0.581	0.909	1.295
J3	0.926	42.1	84.3	500	958220241	3729848	#	0.581	0.910	1.295
J4	1.138	124.2	248.3	250	30501	17486	10066	0.593	0.930	1.331
J7	0.854	155.2	248.3	125	188759	57979	30067	0.594	0.933	1.337
J8	0.569	186.2	248.3	125	2987262	314042	188103	0.594	0.934	1.338
K2	0.613	22.7	45.4	1000	222765457835	274194362	#	0.594	0.934	1.338
K3	0.921	34.0	68.1	500	6419921317	9274700	#	0.594	0.934	1.338
K4	1.138	123.9	247.7	250	31290	17663	10066	0.606	0.954	1.373
K7	0.854	154.8	247.7	125	193992	58567	30067	0.606	0.957	1.379
K8	0.569	185.8	247.7	125	30567429	3530516	188103	0.607	0.958	1.380

K - first failure observed (García 2008)

Table C.10 Config. #20										
	$\Delta\varepsilon_{\max}$ x 10^{-3}	σ_m	$\sigma_{\max}$	n	N_M	N_{SWT}	N_G	F_M	F_{SWT}	F_G
A1	1.138	131.4	262.7	2000	16746	13826	10066	0.171	0.207	0.284
A2	1.138	131.3	262.5	3500	16883	13869	10066	0.467	0.567	0.781
A3	1.138	131.2	262.4	1000	16952	13892	10066	0.551	0.670	0.923
A4	1.138	131.2	262.3	250	17022	13914	10066	0.572	0.696	0.958
A5	0.285	98.4	131.2	2000	3147666449	80596210	#	0.572	0.696	0.958
A6	0.569	131.2	196.7	2000	5490191	828532	3246626	0.573	0.699	0.959
A7	0.854	163.9	262.3	125	100881	46134	30067	0.574	0.703	0.965
A8	0.569	196.7	262.3	125	1518401	249880	188103	0.574	0.704	0.966
B2	0.717	82.0	163.9	2500	1997784	676115	2600197	0.576	0.709	0.967
B3	1.070	123.0	245.9	750	33781	23561	23178	0.608	0.754	1.013
B4	1.138	131.1	262.1	250	17161	13958	10066	0.629	0.780	1.049
B6	0.569	131.1	196.6	1750	5535244	831170	3246626	0.629	0.783	1.050
B7	0.854	163.8	262.1	125	101773	46280	30067	0.631	0.787	1.056
B8	0.569	196.6	262.1	125	1532948	250675	188103	0.631	0.788	1.056
C2	0.683	78.6	157.3	1250	2983723	985280	4032136	0.632	0.789	1.057
C3	1.029	117.9	235.9	750	52212	32969	38715	0.652	0.822	1.085
C4	1.138	131.0	262.0	250	17232	13980	10066	0.673	0.848	1.120
C6	0.569	131.0	196.5	1500	5557918	832492	3246626	0.673	0.850	1.121
C7	0.854	163.8	262.0	125	102222	46354	30067	0.675	0.854	1.127
C8	0.569	196.5	262.0	125	1540275	251074	188103	0.675	0.855	1.128
D2	0.668	76.4	152.8	1250	3926119	1218979	5445022	0.676	0.856	1.128
*D3	0.994	114.6	229.3	500	70222	42877	54830	0.686	0.873	1.141

* first failure observed (García 2008)

Table C.11 Config. #21										
	$\Delta\varepsilon_{\max}$ x 10^{-3}	σ_m	$\sigma_{\max}$	n	N_M	N_{SWT}	N_G	F_M	F_{SWT}	F_G
A1	1.138	131.4	262.7	2000	16746	13826	10066	0.171	0.207	0.284
A2	1.138	131.4	262.7	3500	16746	13826	10066	0.469	0.568	0.781
A3	1.138	131.4	262.7	1000	16746	13826	10066	0.555	0.672	0.923
A4	1.138	131.4	262.7	250	16746	13826	10066	0.576	0.697	0.958
A5	0.285	98.5	131.4	2000	3100054596	80086109	#########	0.576	0.698	0.958
A6	0.569	131.4	197.0	2000	5401253	823288	3246626	0.576	0.701	0.959
A7	0.854	164.2	262.7	125	99122	45842	30067	0.578	0.705	0.965
A8	0.569	197.0	262.7	125	1489736	248298	188103	0.578	0.706	0.966
B2	0.717	82.1	164.2	2500	1968534	671836	2600197	0.580	0.711	0.967
B3	1.070	123.1	246.3	750	33243	23412	23178	0.612	0.757	1.013
B4	1.138	131.4	262.7	250	16746	13826	10066	0.634	0.782	1.049
B6	0.569	131.4	197.0	1750	5401253	823288	3246626	0.634	0.786	1.050
B7	0.854	164.2	262.7	125	99122	45842	30067	0.636	0.789	1.056
B8	0.569	197.0	262.7	125	1489736	248298	188103	0.636	0.790	1.056
C2	0.683	78.8	157.6	1250	2918830	975937	4032136	0.637	0.792	1.057
C3	1.029	118.2	236.4	750	50983	32657	38715	0.658	0.825	1.085
C4	1.138	131.4	262.7	250	16746	13826	10066	0.679	0.851	1.120
C6	0.569	131.4	197.0	1500	5401253	823288	3246626	0.679	0.853	1.121
C7	0.854	164.2	262.7	125	99122	45842	30067	0.681	0.857	1.127
C8	0.569	197.0	262.7	125	1489736	248298	188103	0.681	0.858	1.128
D2	0.668	76.6	153.2	1250	3827083	1205503	5445022	0.682	0.859	1.128
*D3	0.994	114.9	229.9	500	68310	42403	54830	0.692	0.876	1.141

* first failure observed (García 2008)

Table C.12 Config. #24								
	$\Delta\varepsilon_{\max}$ x 10^{-3}	σ_m	$\sigma_{\max}$	n	N_M	N_{SWT}	F_M	F_{SWT}
A1	0.874	104.7	209.4	2000	177435	106618	0.016	0.027
A2	1.138	131.3	262.6	3500	16814	13847	0.313	0.388
A3	1.138	131.2	262.4	1000	16952	13892	0.398	0.491
A4	1.138	131.2	262.3	250	17022	13914	0.419	0.516
A5	0.285	98.4	131.2	2000	3147666449	80596210	0.419	0.516
A6	0.569	131.2	196.7	2000	5490191	828532	0.419	0.520
A7	0.854	163.9	262.3	125	100881	46134	0.421	0.524
A8	0.569	196.7	262.3	125	1518401	249880	0.421	0.524
B2	0.717	82.0	163.9	2500	1997784	676115	0.423	0.530
B3	1.070	123.0	245.9	750	33781	23561	0.455	0.575
B4	1.138	131.1	262.2	250	17091	13936	0.476	0.601
B6	0.569	131.1	196.7	1750	5512668	829850	0.476	0.604
B7	0.854	163.9	262.2	125	101326	46207	0.478	0.608
B8	0.569	196.7	262.2	125	1525656	250277	0.478	0.608
C2	0.683	78.7	157.3	1250	2972799	983715	0.478	0.610
C3	1.029	118.0	236.0	750	52005	32917	0.499	0.643
C4	1.138	131.1	262.2	250	17091	13936	0.520	0.668
C6	0.569	131.1	196.7	1500	5512668	829850	0.520	0.671
C7	0.854	163.9	262.2	125	101326	46207	0.522	0.675
C8	0.569	196.7	262.2	125	1525656	250277	0.522	0.676
D2	0.668	76.5	152.9	1250	3897541	1215110	0.523	0.677
D3	0.994	114.7	229.4	500	69670	42741	0.533	0.694
D4	1.138	131.1	262.2	250	17091	13936	0.554	0.719
D6	0.569	131.1	196.7	250	5512668	829850	0.554	0.720
D7	0.854	163.9	262.2	125	101326	46207	0.556	0.724
D8	0.569	196.7	262.2	125	1525656	250277	0.556	0.724
E2	0.650	74.9	149.8	1000	4746440	1477533	0.556	0.725
E3	0.975	112.4	224.7	500	86234	50363	0.564	0.740
E4	1.138	131.1	262.1	250	17161	13958	0.585	0.765
E7	0.854	163.8	262.1	125	101773	46280	0.587	0.769
E8	0.569	196.6	262.1	125	1532948	250675	0.587	0.770

Cont. Table C.12								
	$\Delta\varepsilon_{\max}$ x 10^{-3}	σ_m	$\sigma_{\max}$	n	N_M	N_{SWT}	F_M	F_{SWT}
F2	0.643	63.2	126.4	1000	23582091	3143784	0.587	0.770
F3	0.962	94.8	189.6	500	479704	108459	0.589	0.777
F4	1.138	131.1	262.1	250	17161	13958	0.609	0.802
F7	0.854	163.8	262.1	125	101773	46280	0.611	0.806
F8	0.569	196.6	262.1	125	1532948	250675	0.611	0.807
G2	0.632	52.7	105.4	1000	126922418	7204877	0.611	0.807
G3	0.951	79.0	158.0	500	2848962	242995	0.612	0.810
*G4	1.138	131.1	262.1	250	17161	13958	0.632	0.836

* first failure observed (García 2008)

D. Fatigue Damage Results, Strain Hardening

Table D.1 Config. #3

	$\Delta\varepsilon_{\max}$ x 10^{-3}	σ_m	$\sigma_{\max}$	n	N_M	N_{SWT}	N_G	F_M	F_{SWT}	F_G
A1	1.138	129.7	259.4	2000	19182	14576	10065	0.149	0.196	0.284
A2	1.138	129.4	258.8	3500	19685	14724	10065	0.403	0.536	0.781
A3	1.138	128.5	257.0	1000	21170	15149	10065	0.470	0.630	0.923
A4	1.159	128.1	256.2	250	21885	14221	7812	0.487	0.655	0.968
A5	0.290	96.1	128.1	2000	3980618657	82377053	#	0.487	0.655	0.968
A6	0.580	128.1	192.2	2000	7058741	846839	2519629	0.487	0.658	0.969
A7	0.869	160.1	256.2	125	132195	47153	22337	0.489	0.662	0.977
A8	0.580	192.2	256.2	125	2034282	255401	131359	0.489	0.663	0.979
B2	0.730	80.1	160.1	2500	2507634	691054	2112509	0.490	0.668	0.981
B3	1.089	120.1	240.2	750	43243	24082	18150	0.515	0.713	1.040
B4	1.220	128.6	257.1	250	21083	11318	3227	0.532	0.744	1.150
B6	0.610	128.6	192.8	1750	6799984	673965	1040887	0.532	0.748	1.153
B7	0.915	160.7	257.1	125	126995	37527	7822	0.534	0.753	1.175
B8	0.610	192.8	257.1	125	1947930	203263	36139	0.534	0.753	1.180
C2	0.732	77.1	154.3	1250	3589782	798927	1620714	0.534	0.756	1.181
C3	1.103	115.7	231.4	750	63781	26733	13265	0.551	0.796	1.262
C4	1.292	136.7	273.3	250	10931	6909	1230	0.584	0.847	1.553
C6	0.646	136.7	205.0	1500	3525827	411436	396802	0.584	0.853	1.558
C7	0.969	170.8	273.3	125	62553	22909	2427	0.587	0.860	1.632
C8	0.646	205.0	273.3	125	903583	124087	8158	0.587	0.862	1.653
D2	0.758	79.7	159.4	1250	2617235	602447	1046023	0.588	0.865	1.655
D3	1.128	119.6	239.1	500	45271	21191	7863	0.604	0.899	1.746
D4	1.365	145.9	291.8	250	5334	4183	469	0.671	0.984	2.508

D4 - first failure observed (García 2008)

Tables D.1 through D.12 were calculated using the procedure in Section 5.6 where Column one is the strain range as defined in Section 5.6, columns two and three are the mean and maximum stresses as defined in Section 5.6, Column four is the number of cycles on each loading sublevel, columns five, six, and seven are calculated from equations 13, 16 and 19, and columns eight, nine and ten are calculated from equation 21.

Table D.2 Config. #4										
	$\Delta\varepsilon_{\max}$ x 10^{-3}	σ_m	$\sigma_{\max}$	n	N_M	N_{SWT}	N_G	F_M	F_{SWT}	F_G
A1	1.138	127.3	254.6	2000	23393	15753	10065	0.122	0.181	0.284
A2	1.138	126.3	252.5	3500	25542	16306	10065	0.318	0.488	0.781
A3	1.138	126.3	252.5	1000	25542	16306	10065	0.374	0.576	0.923
A4	1.138	126.2	252.3	250	25758	16360	10065	0.388	0.597	0.958
A5	0.285	94.6	126.2	2000	4636260469	94765942	#	0.388	0.597	0.958
A6	0.569	126.2	189.2	2000	8307906	974198	3246250	0.388	0.600	0.959
A7	0.854	157.7	252.3	125	157470	54244	30063	0.389	0.604	0.965
A8	0.569	189.2	252.3	125	2457205	293812	188072	0.389	0.604	0.966
B2	0.717	78.8	157.7	2500	2906834	794984	2599950	0.390	0.609	0.967
B3	1.070	118.3	236.5	750	50756	27703	23176	0.412	0.647	1.013
B4	1.183	127.6	255.1	250	22910	13293	5360	0.427	0.674	1.080
B6	0.592	127.6	191.3	1750	7389361	791586	1728904	0.428	0.678	1.082
B7	0.887	159.4	255.1	125	138859	44076	14321	0.429	0.682	1.094
B8	0.592	191.3	255.1	125	2145268	238737	76384	0.429	0.682	1.096
C2	0.710	76.5	153.1	1250	3868686	938357	2426286	0.429	0.684	1.097
C3	1.069	114.8	229.6	750	69154	31399	21367	0.445	0.718	1.147
C4	1.265	135.5	271.0	250	11979	7815	1741	0.475	0.764	1.352
C6	0.633	135.5	203.3	1500	3863824	465385	561385	0.475	0.769	1.356
C7	0.949	169.4	271.0	125	69060	25913	3710	0.478	0.776	1.404
C8	0.633	203.3	271.0	125	1006317	140357	14089	0.478	0.777	1.417
D2	0.742	79.0	158.1	1250	2839121	681442	1364860	0.479	0.779	1.418
D3	1.105	118.6	237.1	500	49447	23970	10806	0.493	0.809	1.484
D4	1.332	141.6	283.2	250	7416	5246	716	0.541	0.877	1.983
D6	0.666	141.6	212.4	250	2391894	312420	230977	0.541	0.878	1.985
D7	0.999	177.0	283.2	125	41081	17396	1242	0.546	0.889	2.129
D8	0.666	212.4	283.2	125	571087	94224	3384	0.546	0.891	2.181
E2	0.761	80.9	161.8	1000	2265283	556259	874663	0.547	0.893	2.183
E3	1.142	121.4	242.7	500	38725	18960	6347	0.565	0.931	2.295
E4	1.390	148.4	296.8	250	4417	3613	328	0.646	1.030	3.384
E7	1.043	185.5	296.8	125	23368	11980	463	0.654	1.045	3.769
E8	0.695	222.6	296.8	125	307484	64887	888	0.654	1.047	3.970

Cont. Table D.2										
	$\Delta\varepsilon_{\max}$ x 10^{-3}	σ_m	$\sigma_{\max}$	n	N_M	N_{SWT}	N_G	F_M	F_{SWT}	F_G
F2	0.785	68.6	137.1	1000	10980928	972837	5284778	0.654	1.049	3.971
*F3	1.175	102.6	205.1	500	218763	33986	54961	0.658	1.070	3.984

* first failure observed (García 2008)

Table D.3 Config. #5										
	$\Delta\varepsilon_{\max}$ x 10^{-3}	σ_m	$\sigma_{\max}$	n	N_M	N_{SWT}	N_G	F_M	F_{SWT}	F_G
A1	1.138	120.3	240.5	2000	42587	19960	10065	0.067	0.143	0.284
A2	1.138	121.1	242.3	3500	39518	19375	10065	0.194	0.401	0.781
A3	1.138	122.0	244.0	1000	36673	18809	10065	0.233	0.477	0.923
A4	1.138	122.9	245.7	250	34080	18270	10065	0.243	0.497	0.958
A5	0.285	92.1	122.9	2000	6027547108	105832570	#	0.243	0.497	0.958
A6	0.569	122.9	184.3	2000	10992226	1087963	3246250	0.243	0.499	0.959
A7	0.854	153.6	245.7	125	212572	60579	30063	0.244	0.502	0.965
A8	0.569	184.3	245.7	125	3394755	328123	188072	0.244	0.503	0.966
B2	0.717	76.8	153.6	2500	3749124	887821	2599950	0.245	0.507	0.967
B3	1.070	115.2	230.3	750	66847	30938	23176	0.261	0.542	1.013
B4	1.138	123.7	247.4	250	31630	17739	10065	0.272	0.562	1.049
B6	0.569	123.7	185.6	1750	10201909	1056326	3246250	0.273	0.564	1.050
B7	0.854	154.7	247.4	125	196250	58817	30063	0.274	0.567	1.056
B8	0.569	185.6	247.4	125	3115102	318581	188072	0.274	0.568	1.057
C2	0.683	74.2	148.5	1250	5175571	1252183	4031757	0.274	0.569	1.057
C3	1.029	111.4	222.7	750	94668	41900	38710	0.285	0.595	1.085
C4	1.138	124.6	249.2	250	29396	17233	10065	0.297	0.615	1.120
C6	0.569	124.6	186.9	1500	9481245	1026214	3246250	0.298	0.617	1.121
C7	0.854	155.7	249.2	125	181436	57141	30063	0.299	0.621	1.127
C8	0.569	186.9	249.2	125	2862621	309499	188072	0.299	0.621	1.128
D2	0.668	72.7	145.3	1250	6338032	1502637	5444514	0.299	0.622	1.128
D3	0.994	109.0	218.0	500	117674	52855	54824	0.305	0.636	1.141
D4	1.138	124.7	249.4	250	29088	17162	10065	0.317	0.657	1.177
D6	0.569	124.7	187.1	250	9382037	1021966	3246250	0.317	0.657	1.177
D7	0.854	155.9	249.4	125	179402	56904	30063	0.318	0.660	1.183
D8	0.569	187.1	249.4	125	2828064	308218	188072	0.318	0.661	1.184
E2	0.650	71.3	142.5	1000	7635063	1819592	6770046	0.319	0.661	1.184
E3	0.975	106.9	213.8	500	143823	62022	70564	0.324	0.673	1.194
E4	1.231	130.6	261.2	250	17795	10205	2774	0.344	0.708	1.323
E7	0.923	133.6	213.8	125	984071	77989	6523	0.345	0.713	1.350
E8	0.616	160.3	213.8	125	17460773	422420	28791	0.346	0.714	1.356

Cont. Table D.3										
	$\Delta\varepsilon_{\max}$ x 10^{-3}	σ_m	$\sigma_{\max}$	n	N_M	N_{SWT}	N_G	F_M	F_{SWT}	F_G
F2	0.696	60.4	120.8	1000	36032127	2739781	37397911	0.346	0.715	1.356
F3	1.040	90.3	180.6	500	775181	95715	508763	0.346	0.722	1.358
F4	1.336	140.0	280.0	250	8400	5433	683	0.389	0.788	1.881
F7	1.002	175.0	280.0	125	47031	18015	6523	0.393	0.798	1.908
F8	0.668	210.0	280.0	125	662071	97576	28791	0.393	0.800	1.914
G2	0.742	50.2	100.4	1000	197863294	4522401	#	0.393	0.800	1.914
G3	1.116	75.5	150.9	500	4422114	150766	3679460	0.393	0.805	1.915
G4	1.420	151.7	303.3	250	3463	3019	229	0.496	0.923	3.473
G7	1.065	189.6	303.3	125	17913	10010	6523	0.506	0.941	3.500
G8	0.710	227.5	303.3	125	229352	54218	28791	0.507	0.944	3.507
H2	0.784	41.7	83.3	1000	1062887580	7822895	#	0.507	0.944	3.507
H3	1.170	62.2	124.4	500	27446518	277630	27774095	0.507	0.947	3.507
*H4	1.500	163.4	326.9	250	1479	1759	81	0.749	1.150	7.906

* first failure observed (García 2008)

Table D.4 Config. #6											
	$\Delta\varepsilon_{\max}$ x 10^{-3}	σ_m	$\sigma_{\max}$	n	N_M	N_{SWT}	N_G	F_M	F_{SWT}	F_G
A1	1.138	127.0	254.0	2000	23986	15908	10065	0.119	0.180	0.284
A2	1.138	126.4	252.8	3500	25223	16225	10065	0.317	0.488	0.781
A3	1.138	125.8	251.6	1000	26527	16550	10065	0.371	0.574	0.923
A4	1.138	125.2	250.4	250	27904	16883	10065	0.384	0.595	0.958
A5	0.285	93.9	125.2	2000	4997211332	97798264	#	0.384	0.595	0.958
A6	0.569	125.2	187.8	2000	9000257	1005370	3246250	0.384	0.598	0.959
A7	0.854	156.5	250.4	125	171587	55980	30063	0.385	0.601	0.965
A8	0.569	187.8	250.4	125	2695544	303213	188072	0.385	0.602	0.966
B2	0.717	78.3	156.5	2500	3125935	820422	2599950	0.387	0.606	0.967
B3	1.070	117.4	234.8	750	54913	28590	23176	0.406	0.644	1.013
B4	1.232	129.4	258.8	250	19652	10571	2737	0.424	0.677	1.144
B6	0.616	129.4	194.1	1750	6338445	629505	882861	0.425	0.681	1.147
B7	0.924	161.8	258.8	125	117751	35052	6418	0.426	0.687	1.175
B8	0.616	194.1	258.8	125	1795078	189855	28211	0.426	0.687	1.181
C2	0.739	77.6	155.3	1250	3369887	746224	1423362	0.427	0.690	1.182
C3	1.114	116.5	232.9	750	59566	24970	11368	0.445	0.733	1.276
C4	1.340	141.8	283.5	250	7330	5095	651	0.494	0.803	1.825
C6	0.670	141.8	212.6	1500	2364281	303380	210048	0.494	0.810	1.835
C7	1.005	177.2	283.5	125	40566	16893	1103	0.499	0.821	1.997
C8	0.670	212.6	283.5	125	563265	91497	2889	0.499	0.822	2.059
D2	0.786	82.7	165.4	1250	1836827	444225	646653	0.500	0.827	2.062
D3	1.170	124.0	248.1	500	30811	15625	4402	0.523	0.872	2.224
D4	1.422	154.9	309.7	250	2741	2752	221	0.654	1.002	3.843
D6	0.711	154.9	232.3	250	883973	163892	71139	0.654	1.004	3.848
D7	1.067	193.6	309.7	125	13860	9126	278	0.667	1.024	4.491
D8	0.711	232.3	309.7	125	172682	49429	432	0.668	1.027	4.904
E2	0.813	88.5	177.0	1000	948759	291807	369307	0.669	1.032	4.908
E3	1.219	132.7	265.4	500	14978	9946	2222	0.717	1.104	5.229
E4	1.515	166.5	332.9	250	1198	1564	66	1.015	1.332	10.629
E7	1.136	208.1	332.9	125	5565	5187	56	1.047	1.367	13.808
E8	0.758	249.7	332.9	125	62419	28095	40	1.050	1.373	18.260

Cont. Table D.4										
	$\Delta\varepsilon_{\max}$ x 10^{-3}	σ_m	$\sigma_{\max}$	n	N_M	N_{SWT}	N_G	F_M	F_{SWT}	F_G
F2	0.856	75.0	150.0	1000	4699906	468112	2332955	1.050	1.376	18.261
*F3	1.280	112.2	224.3	500	87957	16354	21186	1.058	1.420	18.295

* first failure observed (García 2008)

Table D.5 Config. #13										
	$\Delta\varepsilon_{\max}$ x 10^{-3}	σ_m	$\sigma_{\max}$	n	N_M	N_{SWT}	N_G	F_M	F_{SWT}	F_G
A1	1.138	130.4	260.8	2000	18130	14260	10065	0.158	0.200	0.284
A2	1.138	130.6	261.2	3500	17770	14149	10065	0.439	0.554	0.781
A3	1.138	130.3	260.6	1000	18249	14296	10065	0.517	0.654	0.923
A4	1.157	130.0	260.0	250	18704	13471	7936	0.536	0.680	0.968
A5	0.289	97.5	130.0	2000	3437222388	78034918	2625958138	0.536	0.680	0.968
A6	0.579	130.0	195.0	2000	6032847	802202	2559828	0.537	0.684	0.969
A7	0.868	162.5	260.0	125	111655	44668	22756	0.538	0.688	0.977
A8	0.579	195.0	260.0	125	1694740	241939	134355	0.539	0.689	0.978
B2	0.729	81.3	162.5	2500	2175406	654629	2140013	0.540	0.694	0.980
B3	1.088	121.9	243.8	750	37058	22812	18430	0.569	0.741	1.038
B4	1.207	129.6	259.1	250	19410	11459	4538	0.587	0.772	1.116
B6	0.604	129.6	194.3	1750	6260528	682340	1463594	0.588	0.776	1.118
B7	0.905	161.9	259.1	125	116195	37993	11751	0.589	0.780	1.133
B8	0.604	194.3	259.1	125	1769427	205789	59885	0.590	0.781	1.136
C2	0.724	77.7	155.5	1250	3332626	808854	2124070	0.590	0.784	1.137
C3	1.091	116.6	233.2	750	58854	27066	18268	0.608	0.823	1.196
C4	1.251	132.9	265.8	250	14761	8874	2753	0.632	0.863	1.326
C6	0.626	132.9	199.4	1500	4760964	528416	887971	0.633	0.867	1.328
C7	0.938	166.1	265.8	125	86519	29423	6463	0.635	0.874	1.356
C8	0.626	199.4	265.8	125	1285489	159367	28458	0.635	0.875	1.362
D2	0.734	77.5	155.0	1250	3419408	773735	1947534	0.636	0.877	1.363
D3	1.093	116.3	232.6	500	60478	27216	16477	0.647	0.903	1.406
D4	1.301	138.0	276.0	250	9808	6439	1593	0.684	0.959	1.630
D6	0.651	138.0	207.0	250	3163425	383418	513915	0.684	0.960	1.631
D7	0.976	172.5	276.0	125	55626	21349	3331	0.687	0.968	1.685
D8	0.651	207.0	276.0	125	795133	115636	12274	0.687	0.970	1.699
E2	0.743	78.9	157.7	1000	2899172	682669	1599529	0.688	0.972	1.700
E3	1.115	118.3	236.6	500	50611	23269	13059	0.702	1.002	1.755
*E4	1.353	145.6	291.3	250	5443	4373	906	0.768	1.084	2.149

* first failure observed (García 2008)

Table D.6 Config. #15											
	$\Delta\varepsilon_{\max}$ x 10^{-3}	σ_m	$\sigma_{\max}$	n	N_M	N_{SWT}	N_G	F_M	F_{SWT}	F_G
A1	1.138	129.1	258.2	2000	20178	14867	10065	0.142	0.192	0.284
A2	1.138	128.7	257.4	3500	20821	15051	10065	0.382	0.524	0.781
A3	1.138	128.3	256.6	1000	21486	15237	10065	0.448	0.618	0.923
A4	1.175	127.9	255.8	250	22269	13523	6542	0.464	0.645	0.977
A5	0.294	95.9	127.9	2000	4045967212	78335143	#	0.464	0.645	0.977
A6	0.588	127.9	191.8	2000	7182719	805288	2110048	0.465	0.648	0.979
A7	0.881	159.9	255.8	125	134692	44839	18125	0.466	0.652	0.988
A8	0.588	191.8	255.8	125	2075816	242870	101891	0.466	0.653	0.990
B2	0.740	79.9	159.9	2500	2547500	657147	1827970	0.467	0.658	0.992
B3	1.105	119.9	239.8	750	43990	22900	15298	0.492	0.705	1.062
B4	1.279	134.3	268.6	250	13164	7741	2044	0.519	0.751	1.237
B6	0.640	134.3	201.5	1750	4245841	460985	659127	0.520	0.757	1.241
B7	0.959	167.9	268.6	125	76463	25668	4509	0.522	0.764	1.280
B8	0.640	201.5	268.6	125	1124108	139030	18063	0.522	0.765	1.290
C2	0.767	80.6	161.2	1250	2352682	546458	1131913	0.523	0.768	1.292
C3	1.156	120.9	241.8	750	40350	18285	8649	0.549	0.827	1.416
C4	1.369	142.5	285.0	250	6907	4556	760	0.601	0.905	1.885

C4 - first failure observed (García 2008)

Table D.7 Config. #17										
	$\Delta\varepsilon_{\max}$ x 10^{-3}	σ_m	$\sigma_{\max}$	n	N_M	N_{SWT}	N_G	F_M	F_{SWT}	F_G
A1	1.138	123.7	247.4	2000	31692	17753	10065	0.090	0.161	0.284
A2	1.138	124.0	248.0	3500	30893	17575	10065	0.252	0.445	0.781
A3	1.138	124.4	248.7	1000	29987	17369	10065	0.300	0.528	0.923
A4	1.138	124.7	249.3	250	29234	17196	10065	0.312	0.548	0.958
A5	0.285	93.5	124.7	2000	5219991587	99608867	#	0.312	0.548	0.958
A6	0.569	124.7	187.0	2000	9429077	1023983	3246250	0.312	0.551	0.959
A7	0.854	155.8	249.3	125	180366	57017	30063	0.313	0.554	0.965
A8	0.569	187.0	249.3	125	2844443	308827	188072	0.313	0.555	0.966
B2	0.717	77.9	155.8	2500	3260950	835611	2599950	0.314	0.559	0.967
B3	1.070	116.9	233.7	750	57485	29119	23176	0.333	0.596	1.013
B4	1.138	125.0	249.9	250	28500	17024	10065	0.345	0.617	1.049
B6	0.569	125.0	187.4	1750	9192532	1013778	3246250	0.346	0.620	1.050
B7	0.854	156.2	249.9	125	175520	56448	30063	0.347	0.623	1.056
B8	0.569	187.4	249.9	125	2762191	305749	188072	0.347	0.623	1.057
C2	0.683	75.0	149.9	1250	4710626	1201746	4031757	0.347	0.625	1.057
C3	1.029	112.5	224.9	750	85533	40212	38710	0.360	0.651	1.085
C4	1.138	125.3	250.5	250	27787	16855	10065	0.373	0.673	1.120
C6	0.569	125.3	187.9	1500	8962320	1003699	3246250	0.373	0.675	1.121
C7	0.854	156.6	250.5	125	170812	55887	30063	0.374	0.678	1.127
C8	0.569	187.9	250.5	125	2682417	302709	188072	0.374	0.678	1.128
D2	0.668	73.1	146.1	1250	6025185	1469669	5444514	0.374	0.680	1.128
D3	0.994	109.6	219.2	500	111437	51695	54824	0.381	0.694	1.141
D4	1.138	125.6	251.1	250	27092	16688	10065	0.394	0.715	1.177
D6	0.569	125.6	188.3	250	8738262	993743	3246250	0.394	0.715	1.177
D7	0.854	156.9	251.1	125	166237	55333	30063	0.395	0.719	1.183
D8	0.569	188.3	251.1	125	2605045	299707	188072	0.395	0.719	1.184
E2	0.650	71.7	143.5	1000	7163646	1769343	6770046	0.395	0.720	1.184
E3	0.975	107.6	215.2	500	134307	60309	70564	0.401	0.732	1.194
E4	1.196	126.5	252.9	250	25117	13168	4452	0.415	0.759	1.274
E7	0.897	158.1	252.9	125	153271	43662	281367	0.416	0.763	1.275
E8	0.598	189.7	252.9	125	2386593	236492	2600754	0.416	0.764	1.275

Cont. Table D.7										
	$\Delta\varepsilon_{\max}$ x 10^{-3}	σ_m	$\sigma_{\max}$	n	N_M	N_{SWT}	N_G	F_M	F_{SWT}	F_G
F2	0.676	60.8	121.6	1000	33851781	3004340	37397911	0.416	0.764	1.275
F3	1.011	90.9	181.9	500	725545	104958	508763	0.417	0.771	1.276
F4	1.269	132.1	264.1	250	15818	8588	1661	0.440	0.813	1.491
F7	0.952	165.1	264.1	125	93216	28476	2539410	0.442	0.819	1.491
F8	0.635	198.1	264.1	125	1393762	154238	31138032	0.442	0.820	1.491
G2	0.705	50.5	101.0	1000	186110857	5448922	#	0.442	0.820	1.491
G3	1.060	76.0	152.0	500	4146906	181654	3679460	0.442	0.824	1.492
G4	1.331	140.3	280.6	250	8204	5469	730	0.485	0.890	1.981
G7	0.998	175.4	280.6	125	45839	18134	21839218	0.489	0.899	1.981
G8	0.666	210.5	280.6	125	643764	98222	#	0.490	0.901	1.981
H2	0.735	41.9	83.9	1000	1000710705	9961660	#	0.490	0.901	1.981
H3	1.097	62.6	125.2	500	25780207	353534	27774095	0.490	0.903	1.981
H4	1.386	149.1	298.1	250	4207	3591	353	0.574	1.003	2.993
H7	1.040	186.3	298.1	125	22157	11906	#	0.583	1.018	2.993
H8	0.693	223.6	298.1	125	289993	64485	#	0.583	1.021	2.993
I2	0.756	34.1	68.3	1000	6239902288	20822573	#	0.583	1.021	2.993
I3	1.134	51.2	102.4	500	163993528	709753	#	0.583	1.022	2.993
*I4	1.439	156.5	313.0	250	2431	2506	178	0.730	1.164	5.005

* first failure observed (García 2008)

Table D.8 Config. #18										
	$\Delta\varepsilon_{\max}$ x 10^{-3}	σ_m	$\sigma_{\max}$	n	N_M	N_{SWT}	N_G	F_M	F_{SWT}	F_G
A1	1.138	126.3	252.6	2000	25435	16279	10065	0.112	0.176	0.284
A2	1.138	126.3	252.6	3500	25435	16279	10065	0.309	0.483	0.781
A3	1.138	126.3	252.6	1000	25435	16279	10065	0.365	0.570	0.923
A4	1.138	126.3	252.6	250	25435	16279	10065	0.379	0.592	0.958
A5	0.285	94.7	126.3	2000	4581893072	94297871	#	0.379	0.592	0.958
A6	0.569	126.3	189.5	2000	8203894	969386	3246250	0.379	0.595	0.959
A7	0.854	157.9	252.6	125	155356	53977	30063	0.381	0.599	0.965
A8	0.569	189.5	252.6	125	2421630	292360	188072	0.381	0.599	0.966
B2	0.717	78.9	157.9	2500	2873793	791057	2599950	0.382	0.604	0.967
B3	1.070	118.4	236.8	750	50131	27566	23176	0.403	0.643	1.013
B4	1.138	126.2	252.4	250	25650	16333	10065	0.417	0.664	1.049
B6	0.569	126.2	189.3	1750	8273079	972590	3246250	0.418	0.667	1.050
B7	0.854	157.8	252.4	125	156762	54155	30063	0.419	0.670	1.056
B8	0.569	189.3	252.4	125	2445287	293327	188072	0.419	0.671	1.057
C2	0.683	75.7	151.4	1250	4283296	1152922	4031757	0.419	0.673	1.057
C3	1.029	113.6	227.2	750	77191	38579	38710	0.433	0.700	1.085
C4	1.138	126.5	253.0	250	25012	16172	10065	0.447	0.722	1.120
C6	0.569	126.5	189.8	1500	8067372	963016	3246250	0.448	0.725	1.121
C7	0.854	158.1	253.0	125	152583	53622	30063	0.449	0.728	1.127
C8	0.569	189.8	253.0	125	2375031	290439	188072	0.449	0.729	1.128
D2	0.668	73.8	147.6	1250	5481780	1410099	5444514	0.449	0.730	1.128
D3	0.994	110.7	221.4	500	100656	49600	54824	0.456	0.744	1.141
D4	1.193	126.0	252.0	250	26085	13506	4652	0.470	0.771	1.218
D6	0.597	126.0	189.0	250	8413327	804250	1500592	0.470	0.771	1.218
D7	0.895	157.5	252.0	125	159615	44782	12105	0.471	0.775	1.233
D8	0.597	189.0	252.0	125	2493325	242556	62118	0.471	0.776	1.236
E2	0.682	72.0	144.0	1000	6924514	1431953	3669625	0.471	0.777	1.236
E3	1.023	108.0	216.0	500	129496	48809	34690	0.477	0.791	1.257
E4	1.276	131.9	263.7	250	16077	8447	1508	0.499	0.834	1.494
E7	0.957	164.8	263.7	125	94865	28007	125599	0.501	0.840	1.495
E8	0.638	197.8	263.7	125	1420509	151698	1022624	0.501	0.841	1.495

Cont. Table D.8										
	$\Delta\varepsilon_{\max}$ x 10^{-3}	σ_m	$\sigma_{\max}$	n	N_M	N_{SWT}	N_G	F_M	F_{SWT}	F_G
F2	0.721	61.0	122.0	1000	32744787	2260010	20777085	0.501	0.842	1.495
F3	1.078	91.3	182.5	500	700408	78954	262676	0.502	0.851	1.498
F4	1.352	143.0	286.0	250	6656	4733	555	0.556	0.926	2.142
F7	1.014	178.8	286.0	125	36531	15692	1224105	0.561	0.938	2.142
F8	0.676	214.5	286.0	125	502237	84994	13792369	0.561	0.940	2.142
G2	0.751	50.7	101.4	1000	180139165	4122780	#	0.561	0.940	2.142
G3	1.130	76.2	152.5	500	4007352	137444	1974338	0.561	0.945	2.142
G4	1.418	153.1	306.2	250	3115	2920	232	0.676	1.068	3.679

E4 - visible cracking (García 2008)

Table D.9 Config. #19										
	$\Delta\varepsilon_{\max}$ x 10^{-3}	σ_m	$\sigma_{\max}$	n	N_M	N_{SWT}	N_G	F_M	F_{SWT}	F_G
A1	1.110	113.5	226.9	2000	78109	28240	16622	0.037	0.101	0.172
A2	1.138	129.7	259.3	3500	19251	14597	10066	0.296	0.444	0.669
A3	1.138	129.5	259.0	1000	19490	14667	10066	0.370	0.541	0.811
A4	1.138	129.6	259.2	250	19330	14620	10066	0.388	0.566	0.846
A5	0.285	97.2	129.6	2000	3544579326	84689261	#	0.388	0.566	0.846
A6	0.569	129.6	194.4	2000	6234783	870609	3246626	0.389	0.569	0.847
A7	0.854	162.0	259.2	125	115681	48477	30067	0.390	0.573	0.853
A8	0.569	194.4	259.2	125	1760962	262570	188103	0.390	0.573	0.854
B2	0.717	81.0	162.0	2500	2241152	710451	2600197	0.392	0.578	0.855
B3	1.070	121.5	243.0	750	38277	24758	23178	0.420	0.622	0.901
B4	1.138	129.7	259.3	250	19251	14597	10066	0.438	0.646	0.937
B6	0.569	129.7	194.5	1750	6209151	869211	3246626	0.439	0.649	0.938
B7	0.854	162.1	259.3	125	115169	48399	30067	0.440	0.653	0.944
B8	0.569	194.5	259.3	125	1752539	262148	188103	0.440	0.653	0.945
C2	0.683	77.8	155.6	1250	3308035	1030374	4032136	0.441	0.655	0.945
C3	1.029	116.7	233.4	750	58384	34478	38715	0.459	0.686	0.973
C4	1.165	128.7	257.4	250	20822	13650	6809	0.476	0.712	1.025
C6	0.583	128.7	193.1	1500	6715998	812833	2196121	0.477	0.715	1.026
C7	0.874	160.9	257.4	125	125309	45260	19001	0.478	0.719	1.035
C8	0.583	193.1	257.4	125	1920002	245145	107916	0.478	0.720	1.037
D2	0.683	75.1	150.1	1250	4650636	1190193	3979737	0.479	0.721	1.038
D3	1.017	112.6	225.2	500	84309	41865	38102	0.487	0.738	1.056
D4	1.234	135.1	270.1	250	12418	8787	2669	0.516	0.779	1.190
D6	0.617	135.1	202.6	250	4005333	523274	860746	0.516	0.779	1.191
D7	0.926	168.8	270.1	125	71797	29137	6225	0.518	0.786	1.219
D8	0.617	202.6	270.1	125	1049751	157816	27148	0.519	0.787	1.226
E2	0.650	77.2	154.3	1000	3573061	1305633	2378267	0.519	0.788	1.226
E3	0.975	115.8	231.5	500	63460	44503	20870	0.530	0.804	1.261
E4	1.302	141.4	282.7	250	7561	5812	1067	0.578	0.865	1.595
E7	0.977	176.7	282.7	125	41954	19269	2036	0.582	0.875	1.683
E8	0.651	212.0	282.7	125	584373	104371	6492	0.582	0.876	1.711

Cont. Table D.9

	$\Delta\varepsilon_{max}$ x 10^{-3}	σ_m	σ_{max}	n	N_M	N_{SWT}	N_G	F_M	F_{SWT}	F_G
F2	0.643	65.1	130.2	1000	17866580	2778027	14362266	0.582	0.877	1.711
F3	0.962	97.7	195.3	500	356943	95840	166848	0.584	0.884	1.715
F4	1.370	147.7	295.4	250	4655	3914	435	0.661	0.975	2.537
F7	1.028	184.6	295.4	125	24748	12978	663	0.668	0.989	2.806
F8	0.685	221.6	295.4	125	327540	70297	1452	0.669	0.992	2.929
G2	0.632	54.3	108.5	1000	96693722	6366641	91135018	0.669	0.992	2.929
G3	0.951	81.4	162.8	500	2139699	214724	1328907	0.669	0.995	2.930
G4	1.439	154.1	308.1	250	2906	2676	178	0.792	1.129	4.941
G7	1.079	192.6	308.1	125	14778	8874	209	0.804	1.149	5.793
G8	0.720	231.1	308.1	125	185402	48067	289	0.805	1.153	6.412
H2	0.628	44.8	89.5	1000	556780502	14583254	#	0.805	1.153	6.412
H3	0.938	67.1	134.3	500	13382532	507213	10429728	0.805	1.154	6.412
H4	1.467	158.1	316.1	250	2173	2220	123	0.969	1.315	9.326
H7	1.100	197.6	316.1	125	10740	7360	129	0.986	1.339	10.715
H8	0.734	237.1	316.1	125	130113	39865	141	0.987	1.344	11.978
I2	0.621	36.6	73.3	1000	3351541230	35352069	#	0.987	1.344	11.978
I3	0.931	54.9	109.9	500	86346366	1205309	80604937	0.987	1.344	11.978
I4	1.496	162.1	324.1	250	1633	1844	84	1.206	1.538	16.223
I7	1.122	202.6	324.1	125	7837	6113	78	1.229	1.567	18.518
I8	0.748	243.1	324.1	125	91579	33108	66	1.231	1.573	21.210
J2	0.813	29.8	59.5	1000	#	27305201	#	1.231	1.573	21.210
J3	1.217	44.6	89.3	500	571133133	938931	#	1.231	1.574	21.210
J4	1.525	166.1	332.1	250	1232	1537	58	1.521	1.806	27.361
J7	1.144	207.6	332.1	125	5740	5098	47	1.552	1.841	31.158
J8	0.763	249.1	332.1	125	64625	27610	30	1.554	1.847	37.043
K2	0.821	24.0	48.1	1000	#	#	#	1.554	1.847	37.043
K3	1.234	36.1	72.1	500	#	2155261	#	1.554	1.848	37.043
K4	1.553	170.1	340.1	250	934	1291	40	1.937	2.124	45.962

K - first failure observed (García 2008)

Table D.10 Config. #20										
	$\Delta\varepsilon_{\max}$ x 10^{-3}	σ_m	$\sigma_{\max}$	n	N_M	N_{SWT}	N_G	F_M	F_{SWT}	F_G
A1	1.138	128.9	257.8	2000	20439	14942	1814	0.140	0.191	0.284
A2	1.138	129.9	259.8	3500	18874	14485	1631	0.405	0.536	0.781
A3	1.138	128.9	257.8	1000	18874	14942	1631	0.474	0.632	0.923
A4	1.174	128.5	257.0	250	18874	13305	1631	0.491	0.659	0.977
A5	0.294	96.4	128.5	2000	3466429783	77071741	674296866	0.491	0.659	0.977
A6	0.587	128.5	192.8	2000	6087747	792301	525979	0.492	0.663	0.978
A7	0.881	160.6	257.0	125	112748	44116	3427	0.493	0.667	0.988
A8	0.587	192.8	257.0	125	1712712	238953	12728	0.493	0.667	0.990
B2	0.740	80.3	160.6	2500	2193298	646549	600911	0.495	0.673	0.992
B3	1.104	120.5	240.9	750	37390	22531	4030	0.520	0.720	1.062
B4	1.219	129.3	258.6	250	18874	11085	1631	0.538	0.753	1.152
B6	0.610	129.3	194.0	1750	6087747	660076	525979	0.539	0.756	1.154
B7	0.914	161.6	258.6	125	112748	36754	3427	0.540	0.761	1.171
B8	0.610	194.0	258.6	125	1712712	199075	12728	0.540	0.762	1.175
C2	0.731	77.6	155.2	1250	3249854	782463	949521	0.541	0.764	1.176
C3	1.102	116.4	232.7	750	57273	26183	7006	0.559	0.805	1.242
C4	1.229	130.6	261.2	250	17795	10274	1507	0.579	0.840	1.343
C6	0.615	130.6	195.9	1500	5739707	611804	485989	0.579	0.844	1.345
C7	0.922	163.3	261.2	125	105827	34066	3112	0.581	0.849	1.366
C8	0.615	195.9	261.2	125	1599181	184516	11244	0.581	0.850	1.370
D2	0.721	76.2	152.4	1250	4040711	895837	1221585	0.581	0.852	1.371
*D3	1.073	114.3	228.6	500	72439	31511	9467	0.591	0.874	1.405

* first failure observed (García 2008)

Table D.11 Config. #21										
	$\Delta\varepsilon_{\max}$ x 10^{-3}	σ_m	$\sigma_{\max}$	n	N_M	N_{SWT}	N_G	F_M	F_{SWT}	F_G
A1	1.138	131.4	262.7	2000	16746	13826	10065	0.171	0.207	0.284
A2	1.138	131.4	262.7	3500	16746	13826	10065	0.469	0.568	0.781
A3	1.138	131.4	262.7	1000	16746	13826	10065	0.555	0.672	0.923
A4	1.138	131.5	262.9	250	16610	13782	8714	0.576	0.698	0.964
A5	0.285	98.6	131.5	2000	3076540827	79832560	#	0.576	0.698	0.964
A6	0.569	131.5	197.2	2000	5357362	820682	2810456	0.577	0.701	0.965
A7	0.854	164.3	262.9	125	98255	45697	25393	0.578	0.705	0.972
A8	0.569	197.2	262.9	125	1475615	247512	153424	0.578	0.706	0.973
B2	0.717	82.2	164.3	2500	1954084	669709	2309980	0.580	0.711	0.974
B3	1.070	123.2	246.5	750	32977	23338	20167	0.613	0.757	1.027
B4	1.152	134.7	269.3	250	12822	11848	6144	0.641	0.787	1.086
B6	0.576	134.7	202.0	1750	4135756	705545	1981741	0.641	0.791	1.087
B7	0.864	168.3	269.3	125	74325	39286	16831	0.644	0.795	1.097
B8	0.576	202.0	269.3	125	1089991	212788	93084	0.644	0.796	1.099
C2	0.691	80.8	161.6	1250	2298050	836363	2706747	0.645	0.798	1.100
C3	1.041	121.2	242.4	750	39334	27986	24297	0.672	0.836	1.144
C4	1.151	134.6	269.2	250	12874	11910	6215	0.700	0.866	1.202
C6	0.576	134.6	201.9	1500	4152374	709200	2004458	0.700	0.869	1.203
C7	0.863	168.3	269.2	125	74647	39489	17060	0.702	0.874	1.213
C8	0.576	201.9	269.2	125	1095132	213890	94627	0.703	0.875	1.215
D2	0.675	78.5	157.0	1250	3027048	1038448	3700281	0.703	0.877	1.216
*D3	1.005	117.8	235.6	500	53003	36527	35003	0.717	0.896	1.236

* first failure observed (García 2008)

Table D.12 Config. #24								
	$\Delta\varepsilon_{\max}$ x 10^{-3}	σ_m	$\sigma_{\max}$	n	N_M	N_{SWT}	F_M	F_{SWT}
A1	0.874	118.0	235.9	2000	52189	64893	0.055	0.044
A2	1.138	129.2	258.3	3500	20061	14834	0.304	0.381
A3	1.138	128.9	257.8	1000	20480	14954	0.374	0.477
A4	1.138	129.0	257.9	250	20396	14930	0.391	0.501
A5	0.285	96.7	129.0	2000	3726839595	86482235	0.391	0.501
A6	0.569	129.0	193.4	2000	6578473	889041	0.392	0.504
A7	0.854	161.2	257.9	125	122553	49503	0.393	0.507
A8	0.569	193.4	257.9	125	1874378	268129	0.393	0.508
B2	0.717	80.6	161.2	2500	2352644	725493	0.395	0.513
B3	1.070	120.9	241.8	750	40350	25282	0.421	0.555
B4	1.212	129.6	259.2	250	19330	11245	0.440	0.587
B6	0.606	129.6	194.4	1750	6234783	669610	0.440	0.591
B7	0.909	162.0	259.2	125	115681	37285	0.442	0.596
B8	0.606	194.4	259.2	125	1760962	201950	0.442	0.597
C2	0.727	77.8	155.5	1250	3320306	793764	0.442	0.599
C3	1.096	116.6	233.3	750	58618	26561	0.461	0.639
C4	1.346	144.3	288.6	250	6025	4643	0.520	0.716
C6	0.673	144.3	216.5	1500	1943220	276464	0.521	0.724
C7	1.010	180.4	288.6	125	32778	15394	0.526	0.735
C8	0.673	216.5	288.6	125	445974	83380	0.527	0.738
D2	0.790	84.2	168.3	1250	1544946	404814	0.528	0.742
D3	1.176	126.3	252.5	500	25516	14239	0.556	0.792
D4	1.439	153.8	307.5	250	2970	2698	0.676	0.924
D6	0.720	153.8	230.6	250	958027	160677	0.677	0.927
D7	1.079	192.2	307.5	125	15139	8947	0.688	0.947
D8	0.720	230.6	307.5	125	190417	48459	0.689	0.950
E2	0.822	87.9	175.7	1000	1017396	286083	0.691	0.955
E3	1.233	131.8	263.6	500	16170	9751	0.735	1.029
E4	1.507	163.4	326.7	250	1490	1730	0.975	1.235
E7	1.130	204.2	326.7	125	7080	5735	1.000	1.266
E8	0.754	245.0	326.7	125	81748	31062	1.002	1.272

Cont. Table D.12

	$\Delta\varepsilon_{\max}$ x 10^{-3}	σ_m	$\sigma_{\max}$	n	N_M	N_{SWT}	F_M	F_{SWT}
F2	0.851	74.1	148.3	1000	5247994	502175	1.002	1.275
F3	1.273	111.2	222.4	500	96037	17325	1.010	1.316
F4	1.570	171.8	343.5	250	831	1183	1.440	1.618
F7	1.178	214.7	343.5	125	3704	3923	1.488	1.663
F8	0.785	257.6	343.5	125	39474	21251	1.492	1.672
G2	0.872	61.8	123.6	1000	29169863	970329	1.492	1.673
G3	1.312	92.7	185.3	500	602436	32726	1.494	1.695
*G4	1.630	179.5	358.9	250	494	843	2.217	2.119

- first failure observed (García 2008)

E. Fatigue Damage Results for the Proposed Parameter Estimation Method

Table E.1 Fatigue damage calculated at the middle of the loading sublevel in which failure was observed by García (2008).

Config. #	F_{SWT}	Load level
3	0.964	D4
4	1.000	F3
5	1.035	H
6	1.075	F3
13	1.041	E4
15	0.948	C
17	1.000	I4
18	1.000	~G8
19	1.089	K
20	0.996	D3
21	1.000	D3
24	0.948	G4